VOLTAGE AND REACTIVE POWER CONTROL IN ISLANDED MICROGRIDS

NADER ASHRAF EL-TAWEEL

A THESIS SUBMITTED TO THE FACULTY OF GRADUATE STUDIES IN
PARTIAL FULFILLMENT OF THE REQUIREMENTS FOR THE DEGREE
OF
MASTER OF APPLIED SCIENCE

GRADUATE PROGRAM
IN
ELECTRICAL ENGINEERING AND COMPUTER SCIENCE

YORK UNIVERSITY, TORONTO, ONTARIO

JUNE 2016

© Nader Ashraf El-Taweel, 2016

ABSTRACT

Active distribution systems are moving towards a new paradigm shift, where they can be clustered into microgrids capable of operating in both grid-tied and islanded modes depending on the penetration levels and types of the distributed generation (DG) units. Droop control is a key control method for operating islanded microgrids (IMGs) to share the loading active and reactive power among the DG units. The settings of the droop parameters for DG units can considerably affect the ability of an IMG to satisfy the required voltage tolerance boundary prescribed in steady-state voltage regulation standards. Previous studies put on view lots of advantages and concerns for microgrids operation in islanded mode, whether it is initiated for emergency, intentionally planned or permanent island system purposes. From the concerns that have not been addressed yet, such as: 1) The ability of the DG units to maintain equal reactive power sharing in a distribution system; 2) The ability of the DG units to maintain acceptable voltage boundary beyond their point of common coupling (PCC); 3) The functionality of the existing voltage and reactive power (Volt/Var) controllers when microgrids operate in islanded mode.

Accordingly, this thesis analyzes the complexity of voltage regulations in droop-controlled IMGs. A new algorithm is proposed to satisfy the voltage regulation requirements of IMGs. The proposed algorithm obviates the need for a

centralized secondary controller, where each DG unit updates its own droop parameters, autonomously, via interaction with other DG units, using a low-bandwidth, peer-to-peer communication network.

Similarly, this thesis proposes a complementary distributed control scheme for the primary local droop control of DG units in IMGs in order to improve the accuracy of the reactive power sharing via eliminating the mismatch due to the distribution feeder impedance. The proposed control layer takes the voltage regulation requirements for the entire IMG system into account. It aims to periodically adjust the voltage droop parameter settings based on a peer-to-peer cooperative protocol among the DGs control units.

Also, the operation conflicts between DG units and Volt/Var controllers, such as shunt capacitors (SCs) and load-ratio control transformer (LRT) during the IMG mode of operation, are investigated in this thesis. These operation conflicts have been validated through conducting simulations for different local control schemes. The results show that major voltage regulation and reactive power control problems might arise between droop controlled IMG and the conventional Volt/Var control schemes. Further, a new local control scheme for SCs and LRTs has been proposed to mitigate their operational challenges in IMGs.

ACKNOWLEDGMENTS

All praise is to Allah, the Almighty, the Most Gracious and the Most Merciful, Who empowers me to accomplish this thesis, Alhamdulillah.

I would like to express my truthful gratitude to my supervisor and mentor Dr. Hany Farag for his guidance, valuable advice, care, and patience. I learned a lot and am still learning from him how to think as a researcher, how to come up with a novel research point, how properly to present my work, and improve my writing's especially when we write papers.

I also would like to offer my gratitude to Dr. John Lam. He was my project advisor in one of my M.Sc. program courses. I appreciate your patience and guidance during all the project phases.

No words can describe my gratitude and appreciation to my parents and my brother. My late father who inspires me toward my engineering career. My mother, who sacrifices so much for us, without her encouragement and endless support I never would able to do this master and achieve my goals. My brother, who supports and cheers me in the hard times.

Lastly, I would like to thank electrical power research team in Lassonde, especially Sanjida and Mohamed Zaki, as well as my friend's especially Sayed, Moomen and Fergala.

TABLE OF CONTENTS

LIST OF TABLES

LIST OF FIGURES

ACRONYMS

ADS	Active Distribution System
ANSI	American National Standards Institute
AWC	Asynchronous Weak Commitment
CSP	Constraint Satisfaction Problem
CT	Current Transformer
DCO	Distributed Constraint Optimization
DCS	Distributed Constraint Satisfaction
DG	Distributed Generation
DGA	Distributed Generation control Agent
DMS	Demand Managing System
DNO	Distributed Network Operator
DR	Distributed Resource
ESS	Energy Storage System
EPS	Electric Power System
GHG	Greenhouse Gas

IID	Island Isolation Device
IMG	Islanded Microgrid
LDC	Line Drop Compensator
LRT	Load-Ratio control Transformer
LTC	On-Line Tap Changer
MGCC	Microgrid Central Controller
PCC	Point of Common Coupling
PEV	Plug-in Electrical Vehicle
PT	Potential Voltage Transformer
PZC	Point of Zone Coupling
RDG	Renewable Distributed Generation
SC	Shunt Capacitor
SVR	Step Voltage Regulator
Volt/Var	Voltage and Reactive Power

Chapter 1
THESIS DIGEST

1.1 Motivation

Recently, power distribution systems have been integrated into a level, where all utilities can interconnect with distributed generation (DG). The DG units have been recently introduced into distribution systems as a result of their various benefits to the utility grid and customers such as decreasing the usage of fossil fuels (avoid electricity price fluctuation since it overcomes the dependency on the fossil fuel market), reducing greenhouse gas (GHG) emissions and environmental impacts, liberalization of electricity market, cost reduction and avoidance of construction of new costly transmission lines. In addition to the grid support that improves the power quality, DG units can improve the system reliability (minimize the supply interruption and having backup generations) and help in the peak power shaving [1]. However, integrating DG units in existing distribution networks has significant impacts on the voltage profile, power flow, and system losses and thus they affect the operation of voltage and reactive power (Volt/Var) devices and the coordination of the protection devices installed in the system [2], [3]. Conventional distribution systems were designed to have a unidirectional power flow from the utility side to the customer side. However, with high penetration of DGs into distribution systems, a bi-directional power flow may exist from the customer DG

side to the utility side and vice versa. The bi-directionality of the power flow and the intermittent nature of the renewable DGs confuse the operation of Volt/Var devices that may affect the power quality from the voltage level perspective, increase the system losses and cause wear and tear of the devices due to increasing the switching operation of such devices.

DGs' various advantages and their widespread implementation give the accessibility of introducing the micro-grid concept. True to their name, microgrids are miniature versions of power grids as they are typically implemented in local areas. Microgrids offer improvement in the power system reliability and stability as well as assisting with renewable power integration, where they are capable of operating in two modes of operation: grid-connected and islanded. In the grid-connected mode, microgrids operate in parallel with the main distribution networks. While in the islanded mode of operation, microgrids are completely cut off from the main grid and the DG units become responsible for supporting its local load demand. Moreover, hybrid islanded systems with various types of DG units are viable solutions to supply electricity for remote territories and islands. Such hybrid islanded systems are able to 1) eliminate the need for costly overhead or underwater (marine) transmission lines; 2) reduce the power plant operation and maintenance cost; 3) avoid costly transportation of fuel and its transportation

environment concern (leaking and spilling); and 4) avoid danger of blackout in case of extremely cold territories.

Unlike conventional power grids, the majority of DG units in microgrids are interfaced via voltage-source inverters coupled with passive output filters. As converters lack physical inertia, several technical issues need to be carefully addressed before the real implementation of microgrids. To that end, the IEEE has published a guide for IMGs operation requirements [4]. The IEEE 1547.4 guide stated that "The DR[1] island system should be able to actively regulate voltage and frequency within the agreed upon ranges (e.g., as specified in ANSI/NEMA C84.1-2006 for DR island systems that include the area EPS[2]). Voltage regulation equipment within the DR island system may need to be modified to meet the needs of the DR island system".

The operational characteristics of a typical IMG depend primarily on the applied control scheme(s) of the installed DG units, where DG units become mainly responsible for holding the microgrid frequency and voltage amplitudes when microgrids operate in islanded mode [3], [5]. In microgrid systems, primary local power controllers are usually implemented in the voltage-source inverters of the DG units during the islanded mode to mimic the characteristics of synchronous generators operating in parallel [6], [7]. Droop control enables active and reactive power sharing by using local measurements of the output voltage and frequency of

the DG units. Droop control is the most robust control scheme for the IMG, where the DG is incapable of representing the conventional system reference slack bus to maintain the system frequency, fix the slack bus voltage and supply, or absorb any needed amount of power [6]. The droop parameters of such controllers are conventionally designed so that the DG units forming the IMGs share the load demand in proportion to their rated capacities [8]. Using conventional droop control, DGs change their generated active and reactive power according to the loading condition that is measured at the PCC of each DG unit. However, conventional settings of the droop parameters do not ensure accurate reactive power sharing among the droop-controlled DG units due to the mismatch in the DG output and the feeder impedances. In addition, conventional droop parameter settings do not ensure that appropriate voltage magnitude regulations will be maintained in all loading conditions [9]. Continuous changes for the voltage profile is expected to occur over the IMG distribution feeders due to the high penetration of RDGs and the "plug-and-play" characteristic of the drooped DGs. Such changes in the voltage profile will affect the values and locations of the minimum and maximum voltages, which are considered the most important information for proper voltage regulation. For these reasons, Volt/Var control is identified in the literature as one of the main technical challenges that impede the seamless integration of IMG systems.

Several researchers have proposed low-bandwidth communication-based methods for real-time adjustments of the droop control parameters of DG units in order to enhance the IMG operation [7], [9]–[15]. These methods can be classified according to the control structure into: 1) centralized secondary and tertiary control [7]–[15], and 2) distributed secondary control [16]. Centralized secondary control methods [12], [13] can notably enhance the reactive power sharing accuracy by taking the system impedance mismatch into consideration. Further, centralized tertiary control methods [14], [15] can optimally update the droop parameter settings to satisfy the IMG operational constraints and objectives. Centralized methods, however, may result in undesirable properties with respect to the scalability and reliability of the IMG system, due to complex communication requirements and single point-of-failure [17]. In addition, the operation of IMGs without a central controller is still a desirable solution in a number of conditions, the most critical of which occurs when the microgrid is allowed to operate only in islanded mode during inadvertent events in the upstream network [8], [9]. Distributed secondary control and peer-to-peer multi-agent methods have been recently proposed as a means to provide more reliable, resilient and smart control in IMGs [17]–[20]. The concept of distributed control aligns with the current trend of smart grid structure, which is mainly clustered into microgrids [18].

Based on these considerations, this thesis analyzes the complexities of Volt/Var control in droop-controlled IMG systems. It also provides distributed control solutions in order to alleviate such challenges and facilitate seamless integration of IMG systems. Toward that end, four main objectives have been identified for the work in this thesis as follows:

1) Investigating the Volt/Var challenges of droop-controlled IMG systems without consideration of conventional Volt/Var devices (i.e. line voltage regulators and shunt capacitors);
2) Developing a novel distributed constraint satisfaction approach for Volt/Var control in droop-controlled IMG systems;
3) Incorporation of conventional Volt/Var devices in droop-controlled IMG systems and studying their operation interferences with droop-controlled DG units; and
4) Developing new control schemes to mitigate the operation challenges of conventional Volt/Var devices in droop-controlled IMG systems.

This thesis based on a set of assumption, where the loads are considered to be constant and the system dynamics is not considered, because this work contribute in the steady state analysis of the IMG. Moreover, the communication aspects in the multi-agent environment such as latency are neglected.

1.2 Thesis Layout

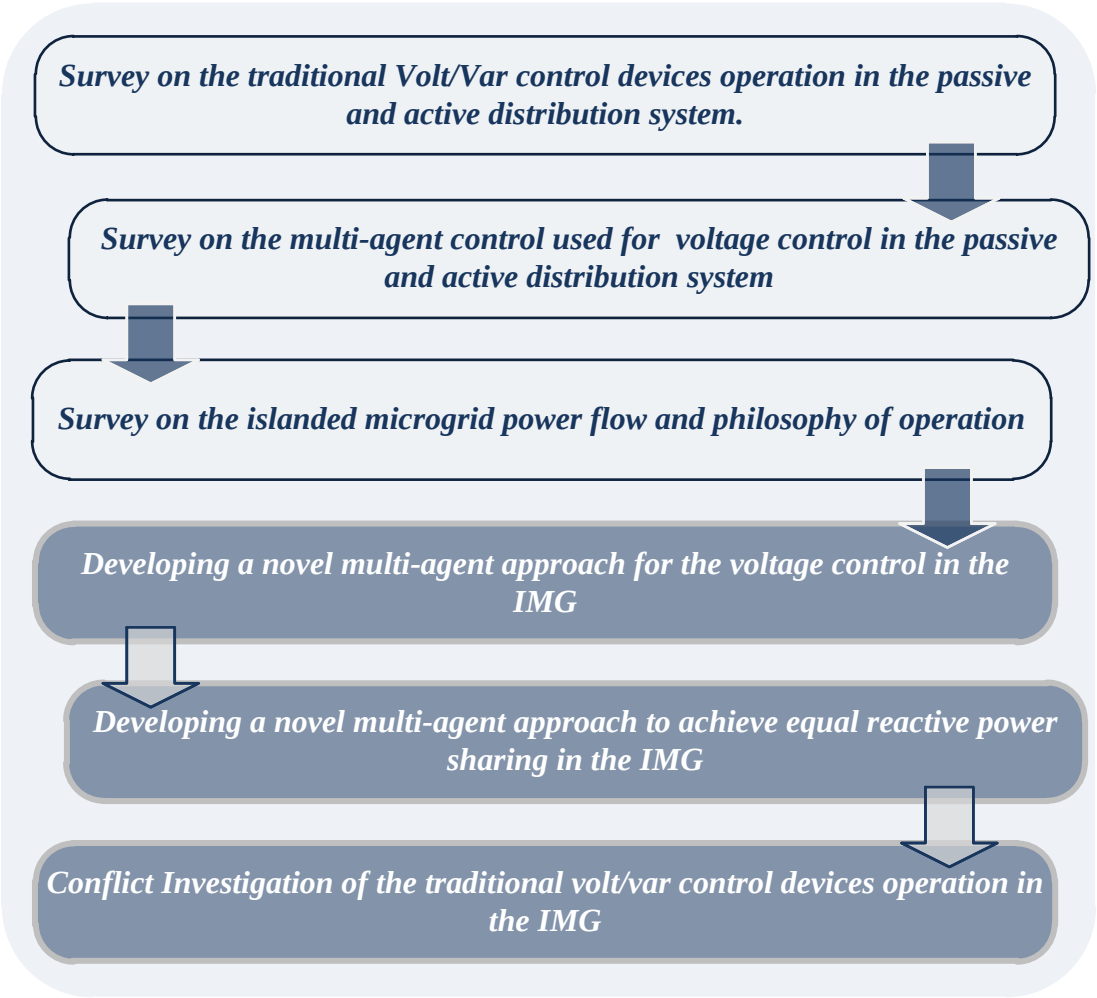

Figure 1.1 Thesis layout schematic diagram

Chapter 2
LITERATURE SURVEY

2.1 Introduction

Power system legacy consists of three inter-connected networks: generation systems, transmission systems, and distribution system [21], [22]. The power flow in conventional distribution systems is unidirectional (passive) from the utility side to the consumer side. In order to ensure the power quality and customer satisfactions, voltage and reactive power (Volt/Var) control devices such as load-ratio control transformers (LRTs) and shunt capacitors (SCs) are located across the system to enhance the voltage profile, guarantee an acceptable voltage range at the consumer load points, and minimize the system losses [23], [24]. The voltage regulator devices can be controlled in either way locally or remotely. Nonetheless, inappropriate voltage regulation may lead to severe problems to the customer, such as affecting the equipment's efficiency, malfunction of the equipment's, tripping of the loads, and huge monetary loss to industrial customer [25], [26]. Voltage quality is one of the main power quality parameters, in which the utilities are responsible for delivering an acceptable voltage range to the customers. The American National Standards Institute (ANSI) in a document number C84.1, which is applied by most of the utilities in North America, gives definitions for three different types of voltages [27]:

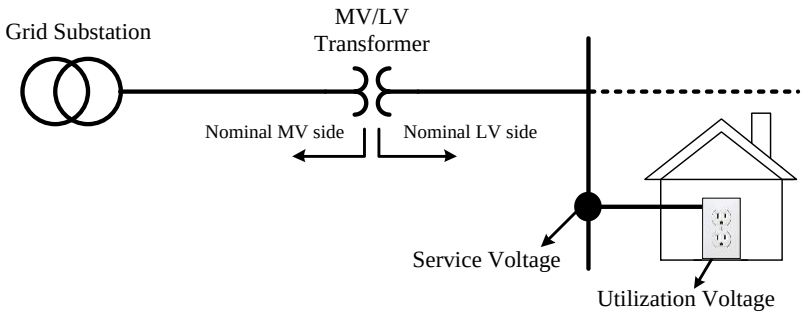

Figure 2.1 ANSI standard voltage rating schematic locations

1. Nominal voltage: The voltage of the system in which it is designated and to which the system parameters characteristics are compared to as a per unit base voltage.
2. Service voltage: The point of common coupling voltage between the utility distribution system and the customer electric system.
3. Utilization voltage: The voltage utilized by the customer electric system.

Figure 2.1 shows a schematic diagram that identifies the locations of these voltages in a typical distribution system. ANSI C84.1 standard defines two ranges for the service voltage given as:

1) *Range A*: describes the normal operating condition of the service voltage provided by the utilities. This range is between ±5% per unit voltage for low-voltage systems and –2.5% to +5% for medium-voltage systems.
2) *Range B*: describes the up-normal operating conditions of the service voltage that should be limited in time duration. However, the system will not be

affected by *Range B* voltage and the equipment should operate at acceptable performance until regulating the voltage back to *Range A*. This range is between –8.3% to +5.8% per unit voltage for low-voltage systems and –5% to +5.8% for medium-voltage systems.

Two main devices are widely used in the distribution system for Volt/Var controlling, which are LRTs, and SCs [23], [28]–[30], in order to maintain the voltage magnitude within its tolerance boundary prescribed in ANSI C84.1: line voltage regulator and shunt capacitors. Without the need for a communication network, distribution network operators used to appropriately control those devices to maintain the Volt/Var requirements. However, recently distribution systems experienced the integration of distributed generation from the customer side. This might in turn convert conventional distributions into active distribution systems (ADS). In ADS, the power flow can be in either direction from the utility to customers and vice versa [22]. For this reason, Volt/Var control devices are strongly affected by the transformation of distribution networks toward ADS. Volt/Var control strategies were originally developed under the strong assumption of unidirectional power flow. Hence, the continuation of using such strategies in ADS will result in significant interferences between the operation of DG units and conventional Volt/Var devices. [31]. Several methods have been recently proposed to mitigate the challenges of Volt/Var control in ADS

Moreover, the widespread implementation of DG units in distribution networks is creating microgrids with enough generation capacity to meet all or most of their local demand. Figure 2.2 shows the transition of the conventional distribution system to the islanded mode systems. In IMGs, DG units are responsible for sharing the system load power demand [8]. Therefore, DG units must be able of holding the IMG voltage and frequency within their prescribed limits. Droop control is a well-known control scheme in IMGs that has been extensively adopted to share the power in IMGs without using microgrid central controllers (MGCC) [8], [9]. In conventional droop-controlled IMGs, a local control unit is utilized in each DG unit that participates in sharing the power demand to mimic the droop characteristics of synchronous generators.

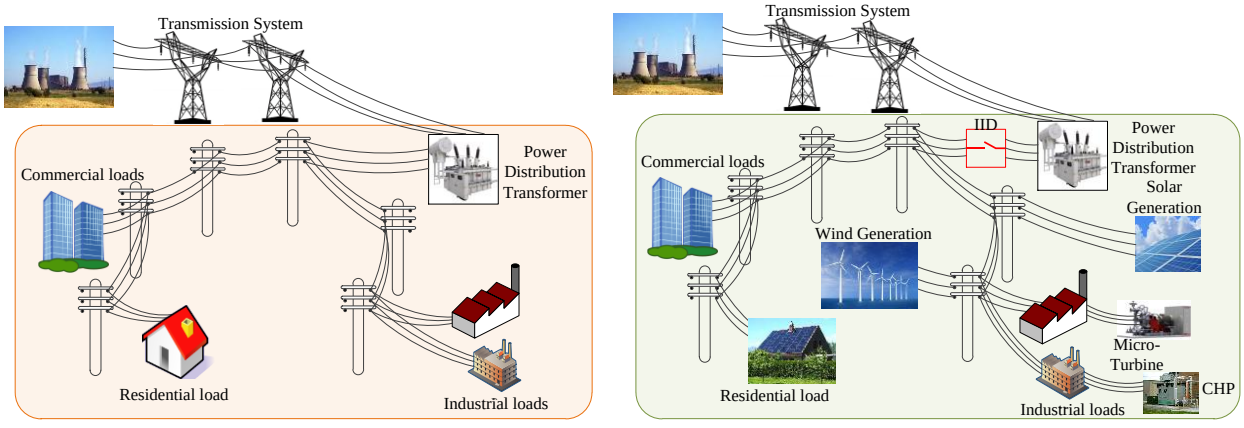

Figure 2.2 (a) Conventional distribution system, (b) Islanded distribution system

However, conventional droop control satisfies the active power sharing, it fails shortly to ensure equal reactive power sharing among the DGs. Moreover, conventional droop settings might ensure voltage regulation at the point of common coupling (PCC) of DG units; however, a voltage violation still might occur at some load points due to voltage drops along the distribution feeders. To that end, several methods have been recently proposed to mitigate the challenges of Volt/Var control in IMG systems.

The remainder of this chapter presents the required background and critical literature survey for the issues and mitigation techniques of Volt/Var control in 1) conventional distribution systems, 2) ADS, and 3) IMGs.

2.2 Voltage and Reactive Power Control in Conventional Distribution Systems.

LRTs can be installed at the substation known as on-line tap changers (LTCs) to maintain the acceptable voltage range on the secondary side of the transformer. Also, LRTs can be installed along the distribution feeder known as step voltage regulators (SVRs) [32], [33]. The SVR is one of the main devices traditionally used in distribution systems to regulate a target point voltage. Usually, the target point is located at the load centre, downstream from the SVR. SCs are installed to compensate the reactive power supplied by the substation and therefore decrease the voltage drop and the system losses [34]–[36]. These Volt/Var devices can be

controlled either locally or centralized using a remote control as described herewith.

2.2.1 Local Voltage and Reactive Power Control

In a local control scheme, Volt/Var devices usually aim to hold an electrical quantity at their designed set points [23]. For example, LRTs hold the desired voltage bandwidth at a certain targeted bus along the distribution feeder. Similarly, SCs can use several electrical quantities as set points such as voltage, reactive power, power factor, or current [35]. Another criterion of local control of SC is based on a pre-specified time or temperature setting. For example, SCs can switch its capacitor banks to consider weekdays, weekends, holidays, and different seasons. Furthermore, SCs can control their banks locally based on the temperature at areas where the temperature is directly related to reactive load such as air conditioning [35]. The superiority of the local control scheme is that it depends on local information and autonomously it takes the decision to regulate the system.

2.2.1.1 Load-Ratio Control Transformer Local Control

Conventionally an LRT consist of an auto-transformer with a mechanical load tap changer, most of the autotransformer are 32 steps with ±10% tap range [37]–[40]. Each step of transformer affects the distribution system by $20\% \div 32 = 0.00625$ pu. The main objective of the LRTs devices is to hold the voltage at

certain targeted bus within an acceptable voltage bandwidth. Where the bandwidth is allowance range of voltage variation of the target bus around the voltage set point, which means the voltage will be hold within ±one-half of the bandwidth given as (2.1)-(2.3) [37], [39].

$$V_{lb} \le V_T \le V_{ub} \tag{2.1}$$

where

$$V_{lb} = V_{set} - \frac{1}{2} BW \tag{2.2}$$

$$V_{ub} = V_{set} + \frac{1}{2} BW \tag{2.3}$$

where V_T is the target point voltage, V_{lb} is the bandwidth lower boundary limit, V_{ub} is the bandwidth upper boundary limit, V_{set} is the voltage set point, and BW is the allowable bandwidth.

The local voltage regulation strategy of the LTC is usually much easier compared to the SVR, given that the regulated target point is the secondary side of the autotransformer and can be measured locally. Therefore, the regulation of the LTC is performed as follows:

$$Tap = \frac{V_S - V_P}{0.00625} \tag{2.4}$$

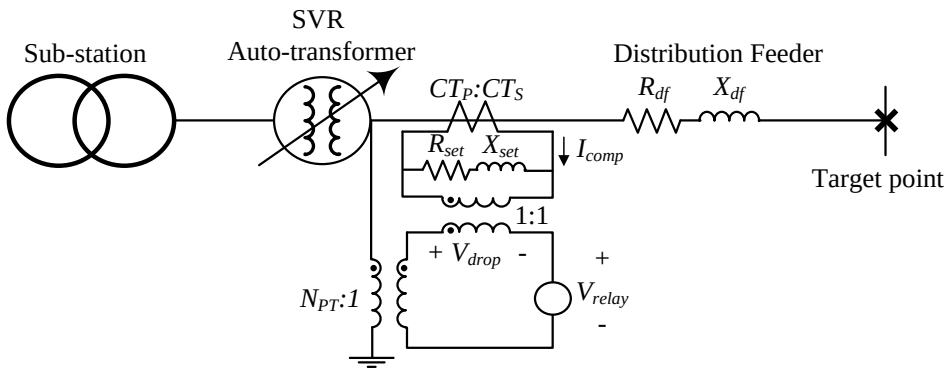

Figure 2.3 Line drop compensator circuit

where V_S and V_P are the secondary and primary side voltage of the autotransformer. Nonetheless, in some cases the LTC controlled a remote point such as the SVR tap, which is controlled locally using a compensation circuit called line drop compensator (LDC).

Figure 2.3 shows a schematic diagram of the LDC circuit [37]. As shown in the figure, the LDC circuit tends to simulate the voltage drop between the SVR and its target point in a secondary circuit by modelling the distribution feeder impedance. Using the LDC circuit, the SVR estimates the voltage at the target point to take an appropriate tap setting decision. The LDC circuit consists of step-down current transformer to reduce the current of the distribution system with a ratio of $CT_P : CT_S$. Usually, the current is reduced to 5 amperes in the control circuit [37]. Also, the LDC circuit consist of a potential transformer to step down the voltage to 120 volts with a N_{PT} turns ration. Therefore, one tap setting of the auto-transformer corresponds to a change of 0.00625×120 volts $= 0.75$ volts in

the LDC control circuit. The tap setting Tap_t at any t is given as follows (2.5)-(2.10) [37], [39]:

$$Tap_t = Tap_{t-1} \qquad if \;\; V_{lb} \le V_{relay} \le V_{ub} \tag{2.5}$$

$$Tap_t = Tap_{t-1} + Round\left(\frac{V_{set} - V_{relay}}{0.75}\right) \qquad if \;\; V_{relay} \le V_{lb} \tag{2.6}$$

$$Tap_t = Tap_{t-1} - Round\left(\frac{V_{relay} - V_{set}}{0.75}\right) \qquad if \;\; V_{relay} \ge V_{ub} \tag{2.7}$$

where

$$V_{relay} = V_{reg} - V_{drop} \tag{2.8}$$

and V_{drop} represents the voltage drop between the SVR location and the target bus point and V_{relay} represents the measured voltage at the target bus on a 120-volt basis and is given as follows:

$$V_{relay} = V_{reg} - V_{drop} \tag{2.9}$$

and,

$$V_{drop} = I_{comp}\left(R_{set} + jX_{set}\right) \tag{2.10}$$

where, R_{set} and X_{set} represents the LDC circuit settings that simulate the distribution feeder impedance (R_{df} and X_{df}) until the target point.

2.2.1.2 Shunt Capacitor Local Control

Shunt Capacitors (SCs) are one of the traditional elements in distribution system that are implemented to minimize the system losses, improve the voltage profile, correct the power factor, and relax the system capacity [41]–[43]. SCs inject reactive power at their location, and compensate injected portion of reactive power generated by the substation. Thus, SCs eliminate the losses and voltage drop accompanied by the transmission of the same amount toward the SCs location, which leads to the system power capacity relaxation and enhance the system voltage profile. Several optimization methodologies have been proposed to size and allocate the SCs in distribution networks [36], [44], [45].

The SC stand-alone controller automatically monitors and switches based on real-time network conditions. There are several types of local SC control mechanisms; they can be based on voltage, VAR, current, or temperature local measurement. The common local SC Control types are briefly discussed as following [35]:

I. ***Voltage Control***: in this type of control, the capacitor performs the switching operation ON and OFF depending on the measured voltage to ensure its node within the predetermined acceptable voltage limit.
II. ***VAR Control***: in this type of control, the capacitor measures the incoming amount of VARs to the capacitor bus, which indicates the reactive power

demand downstream the SC node. The local controller determines the number of banks that will compensate the amount of reactive power. Another phase of the VAR control is the power factor control that targets the unity power factor.

III. ***Temperature Control***: this type of control is used when the type of inductive loads is related to the temperature. By increasing the temperature to a certain limit, the capacitors are switched on to compensate for the highly inductive load.

IV. ***Intelligent control***: Capacitors manufacturer produced several type of intelligent standalone SCs that can perform more than control type at once to ensure the acceptable limits for the power quality.

2.2.2 Centralized Voltage and Reactive Power Control

Centralized control for the Volt/Var aims to increase the system efficiency, by solving a mathematical optimization problem forecast for 24 hours ahead [35], [46]. The output of this optimization problem is hourly remote dispatching of the Volt/Var control devices tap setting. The optimization objective tends to minimize the system losses, cost, and the mechanical tap switching of the Volt/Var devices, while considering the voltage and generation limit [44], [45]. The disadvantage of the centralized Volt/Var control is the inability to modify its setting under any critical not forecasted situation, such as load variation.

2.3 Challenges of Voltage and Reactive Power Control in ADS

The authors in [31], [47] show that the impact of the DG units on the regulator devices that use LDC control rely on the size and location of the DG, as well as the loading condition. That is a result of the interaction between the DG and the LDC control circuit. For instance, if the DG unit is located between the SVR and target bus, the LDC control circuit will inappropriately estimate the voltage at the target bus due to the unseen (unmeasured by the current transformer of the LDC circuit) current injected by the DG towards the target bus, which may cause undervoltage [31], [47]. Another conflict scenario is when the DG is implemented downstream the SVR target bus and during low load demand the DG generation will exceed the load demands and reverse the power to the substation. Thus, the SVR auto-transformer will operate in reverse mode and regulate the substation voltage. In a situation, when the substation voltage is higher than the SVR set point, the SVR will tends to regulate the voltage and tap down its setting. However, the substation side voltage is rigid, thus the overall effect will raise the voltage on the DG side. Furthermore, this sequence will continue until the regulator tap reach its minimum tap setting causing +10% overvoltage on the DG side [48].

The interaction between the SC and the DG depends on the SC control type [35]. For instance the author in [35] points to the possibility of overvoltage occurrence near the capacitor node, when the SC is time or temperature controlled. Because the load demand is reduced, due to the DG power generation and the SC controllers do not monitor the system changes that typically occur due to the injected power of DG units. This might in turn causes system overvoltages, undervoltages and significant increase in the system losses [8], [44]. Excessive reactive power generation might also occur if the DG units operate at non-unity power factor. Also, VAR-controlled SCs are usually confused with the reverse power flow due to high DG penetration. If the DG injects power with unity power factor and the flow of reactive remains the same, the SC will work on compensating the reactive power as prior to the DG installation causing an overvoltage.

In [31], the authors shows the possibility of the three-phase SC capacitor hunting due to overvoltage at single-phase DG location. In such situation, the SC will sense an overvoltage at the DG phase and will decide to switch off its capacitor banks. However, after switching off, an undervoltage may occur at the other two phases, thus the SC will decide to switch on again, and so on until the malfunction of the SC.

It is worth noting that centralized remote control will be a hard choice to control the voltage regulator devices in ADS due to the uncertainty of intermittent renewable DGs alongside “plug and play” DGs characteristics, unless there is an accurate short-term forecast method for load and power generation [31].

2.4 Mitigation of Voltage and Reactive Power Control Challenges in ADS

Several control topologies have been proposed in the literature to overcome the influence of the DGs’ penetration upon the voltage profile and the conflicts between the DG units and the voltage regulators in the ADS. The control topologies are classified as follows

2.4.1 Local Control for Voltage and Reactive Power Control in Active Distribution Systems

In local control topology, the voltage and reactive power control devices and DGs take decision based on local measurement without any communication links. In [33] the authors proposed a local daily basis coordination between the SVR and the SC and the synchronous generator based on the operation time delay. Nonetheless, the coordination is a base case specific that requires the DGs to be located far away from the SVR and only the synchronous generator that operates at constant voltage is involved in the coordination. The authors in [49]–[53] discussed the capability of the DGs to absorb reactive power to mitigate the

voltage rise at the end of the feeder, for example, when a high PV generation exists at light load condition and reverse power flow exists. However, controlling the reactive power may result in more losses in the system, especially in low voltage systems where the system feeder R/X ratio is high and voltage less sensitive to reactive power. DGs active power curtailment to mitigate the voltage rise at the DGs location is proposed in [54]–[58] even by reducing the generated power or storing the excessive power in energy storage systems (ESS). The authors in [59] utilized the DGs as a voltage controller support by controlling them in terms of the line voltage sensitivity and they recommend a significant distance between the voltage support DGs. In [60] the authors utilized two local intelligent controllers to mitigate the influence of the DG on the voltage profile, the first controller based on a set of rules to change between power factor correction (i.e. controlling the injected and absorbed reactive power to regulate the DG PCC) and voltage control mode, and the second control relying on fuzzy logic equations that set the reference setting of the power factor response to the DG PCC voltage. In [61] local intelligent controllers were used to regulate the voltage in ADS based on fuzzy logic relations and system sensitivity analysis.

However, the limitations of the local control are:

1. Interaction conflict between the voltage controller devices and the DGs;

2. High stress (number of switchings) on voltage controller devices particularly in case of renewable DG penetration;
3. Possibility of increasing the system power losses;
4. DGs benefits and power generation are not guaranteed to be maximized due curtailment.

2.4.2 Centralized Control of Voltage and Reactive Power Control in ADS

In the centralized control all the system data are sent via communication links to the distributed network operator (DNO), which runs an optimization power flow problem. The DNO assigns the tap setting for each voltage controller and the setting of the system DGs. In [62]–[64], the authors formulate an optimization problem to dispatch the SVRs and the SCs using a day-ahead forecast for the load and the renewable generation profile. However, they didn't consider the interaction conflict between the DGs and SVRs. The authors in [65] presents an optimal Volt/Var planning by controlling the DGs reactive power injection, nonetheless they didn't consider the coordination between the Volt/Var devices and minimization of the curtailed active power. In [66] the authors considered the penetration of PV generation and propose a coordination between the SVR and the static var compensator in an unbalanced three-phase distribution system to minimize the losses and the tap switching. Nonetheless, they didn't consider the

DGs reactive power contribution to the voltage regulation. In [67] the authors proposed a centralized demand managing system (DMS) based on two scheduling stages: the first stage is the day-ahead forecast for system optimization condition, while the second stage is a complementary stage that adjust the system schedule every 15 min to satisfy the system constraints. A centralized coordination between a genetic algorithm reactive power control and SVR tap setting control is proposed in [68] to regulate the voltage in active distribution system and reduce the SVR stress. In [69] a multi-objective optimization problem based on a genetic algorithm is solved to minimize the voltage deviation and system losses. In [70] the authors perform a multi-objective reactive power optimization problem considering the dynamic reactive power reserves to enhance the voltage profile. The authors in [71] consider the high penetration of plug-in electrical vehicle (PEVs) and DGs. They proposed a centralized real-time optimization problem divided into three stages: the first stage aims to maximise the PEVs customer satisfaction and delivered power, the second stage aims to maximize the energy captured by the DGs (minimize the curtailed power), and the third stage aims to relax the operation of SVR and minimize the system voltage deviation.

However, the drawbacks of the centralized control methods are:

1. The uncertainty problem of the load demand and the renewable DGs forecasting;

2. The required high bandwidth at each node, and device is not practical;
3. The unreliable single point of failure of the centralized communication;
4. The required fast and accurate optimization and power flow solution at each time step.

2.4.3 Multi-Agent Control of Voltage and Reactive Power Control in ADS

In the multi-agent (decentralized) control, Volt/Var devices and DGs are coordinated via low-bandwidth, peer-to-peer communication, in order to regulate the voltage and minimize the system losses. In [72], SVR and load points have been defined as control agents. Each load agent sends its measurement to the SVR agent. Based on a fuzzy logic controller, the SVR mitigates the received maximum voltage deviation. Nonetheless, assigning an agent for the loads seems to be costly and unpractical. Further, the proposed control scheme is somehow similar to the centralized scheme, as the SVR agent receives the data from all the other agents in the system. In [73], the authors present a multi-agent approach for DG reactive power dispatching to regulate the voltage. However, the work in [69] didn't consider the SVR coordination in the problem formulation. In [38], the authors rely on a voltage estimation method to estimate the minimum and maximum node voltage at a multiple feeders. They allocated a remote terminal unit across the feeders to measure the voltage and help improving the voltage profile estimation.

The work in [34] relies only on SVR in the voltage regulation problem by assigning each SVR a control zone. This will in turn increase the SVR devices stress. A multi-agent approach has been proposed in [74] to coordinate between PVs and LTC in order to minimize the reverse power flow. The work in [70] assumed the existence of an energy storage system for each PV unit, which is costly and unpractical in case of fully charged ESS. The authors in [16], [75] proposed a coordination between the DGs and the voltage control devices such as SVR and the SC, in which each agent has its own objective; for instance, the SVR objective is to minimize the tap switching operation and the voltage deviation while the DG agent objective is to maximize the capture of energy. In [76], [77] the authors adopted a multi-agent fuzzy controller to mitigate the effect of high renewable DG penetration upon the voltage profile. They also consider the SVR that feed multiple feeders. In [73], the authors modified their algorithm to contain DGs reactive power control take place as a first solution stage. Then, if the first stage fails shortly to minimize the voltage deviation, an active power curtailment of the DGs output power will take place.

The multi-agent control model reduces the communication requirement and computational burden, and tackles the single-point of failure of centralized control. Using multi-agent control, it is much easier to modify and upgrade the model of the control system. However, the decentralized model might not provide an

optimal solution for the systems as each agent has only partial information about the system.

2.5 Challenges of Voltage and Reactive Power Control in IMGs

The droop control parameters are usually designed to be pre-specified in order to share the loads in proportion to the ratings of DGs [7], [78]. Nonetheless, such settings are not able to achieve the desired reactive power sharing [7]. This might in turn lead to reactive power circulation in the system due to the different impedances seen by each DG inverter [7], [10], [79]–[82]. Further, fixed settings of droop parameters might fail short in satisfying the IMG operation requirements under all operating conditions. Previous works showed that conventional settings of droop parameters ensure voltage regulation at the point of common coupling (PCC) of DG units; however, a voltage violation might occur at some load points due to voltage drops along distribution feeders [9]. Moreover, the authors in [9] have shown that voltage and reactive power requirements have a significant impact on the successful operation of droop-controlled IMGs.

In [83] an optimization planning problem was formulated to determine the optimal sizing and allocation of SC in islanded microgrids. The objective was to minimize the total system losses. Nonetheless, the authors represented one of the DG units as a slack bus, which does not accurately model the characteristics of

islanded microgrids. Recently, the authors in [45] proposed a new algorithm for optimal planning of SCs in multi-microgrid systems with consideration of droop-controlled islanded microgrids. However, the previous works did not investigate the real-time operational challenges of SC during islanded mode of operation. In [8] the authors proposed an optimization problem for optimum droop parameter considering the voltage regulation within the system; however, they didn't consider the operation of the voltage regulator.

Nonetheless, the step voltage regulator and the shunt capacitor are the workhorse of the distribution systems voltage regulation and are mainly required to maintain the customer's voltages within the specified limits; operation of the regulators in the IMG mode hasn't been addressed yet in the literature.

2.6 Mitigation of Voltage and Reactive Power Control Challenges in IMG

Various modified local control methods have been presented in the literature to enhance the accuracy of reactive power sharing in droop-controlled IMG systems [79], [81]. The concept of virtual impedance has been proposed in [10], [80], [82] to mend the accuracy of reactive power sharing and improve the system control stability. Modified local droop control methods are capable of eliminating the mismatch of the output impedances of the DG units, thus enhancing the reactive power sharing accuracy. However, the reactive power sharing is still not

exact and the satisfaction of voltage regulation tolerance boundary in the entire IMG system is not ensured. To overcome the limitations of these methods, a secondary control layer with a low bandwidth communication has been widely presented in the literature [13], [17], [20], [84]–[90]

Given the reactive power sharing problem in IMG, communication based methods have been proposed in the literature in order to enhance the operation of droop-controlled IMGs. The proposed methods can be classified based on the control structure into 1) centralized secondary and/or tertiary control [8], [12]–[15], and 2) distributed secondary control [17]–[20]. Centralized secondary control methods [12], [13] can notably enhance the reactive power sharing accuracy by taking the line impedance mismatch into consideration. Further, centralized tertiary control methods [14], [15] are able to optimally update the droop parameter settings to satisfy the IMG operational constraints and objectives. However, centralized methods may result in undesirable properties with respect to the scalability and reliability of the IMG system due to the complex communication requirements and the single point-of-failure [17]. In addition, the operation of IMGs without a central controller is still a desirable solution in a number of conditions, the most critical of which occurs when the microgrid is allowed to operate only in islanded mode during inadvertent events in the upstream network [7], [9].

In [17]–[20], consensus-based multi-agent algorithms were utilized to restore the system voltage and frequency of IMGs. Also, the proposed algorithms in [17]–[20] achieved accurate reactive power sharing and proper voltage regulation at the PCC of droop-controlled DG units. However, to the best of this author's knowledge, the studies in [17]–[20] have a common shortfall regarding the IMG system scalability; where these studies are exclusive for very small-scale IMG systems with a set of parallel DG units connected to a single common bus. The IEEE 1547.4 standard has extended the definition of IMGs to include area electric power systems [4]. In such systems, issues related to undervoltages might occur at some load points due to voltage drops along distribution feeders [9]. Moreover, the uncertainty and variability associated with intermittent renewable DG (RDG) units make distribution feeders in IMG susceptible to dynamic changes of power flows, which might in turn alter the system voltage profile and interfere with the pre-specified droop parameter settings causing voltage limit violations [16].

Chapter 3
ANALYSIS OF VOLTAGE AND REACTIVE POWER CHALLENGES IN IMG

3.1 Introduction

This chapter presents the analysis of the dynamic changing in the voltage profile in IMGs, and analyzes the impact of distribution feeder impedances on the accuracy of reactive power sharing. To that end, a steady-state model of three-phase system is presented to verify the challenges of the three phases IMG in a simulation case study. Several case studies have been carried out to address the challenges of IMG voltage and reactive power control.

3.2 Analysis of Voltage violation in IMG

A variety of microgrid formations can be identified in a distribution network that includes high penetration of DGs. The formations are based on the locations of the island isolation devices (IIDs) [4]. In islanded mode, droop control, which enables active and reactive power sharing through the introduction of droop characteristics to the output voltage frequency and magnitude of dispatchable DG units, is usually applied. Droop control is the most powerful control scheme for the islanded mode, where there is no DG that is able to act as a reference slack bus by holding the system frequency, fixing the slack bus voltage and supplying or absorbing any excessive amount of power.

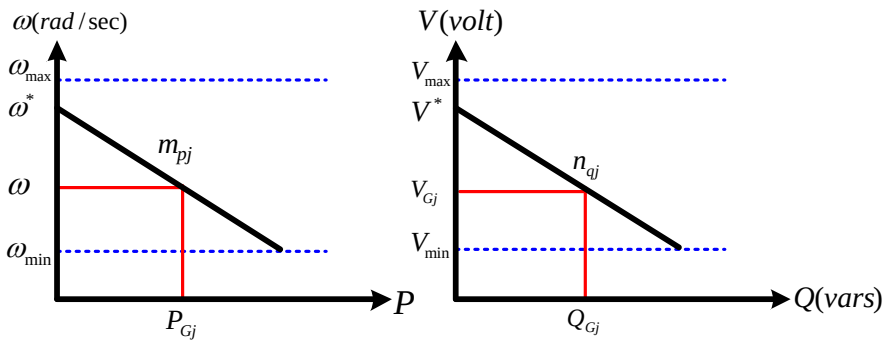

Figure 3.1 Droop curve characteristics

The philosophy of droop control is derived from the synchronous generator droop characteristics shown Figure 3.1 [2], [8]. As shown in the figure, when the real power demand increases, the frequency decreases. Consequently, when the frequency decreases, the local droop controller injects more active power according to its setting in order to compensate the increase of the of load demand. Similarly, when the reactive power demand increases, the voltage magnitude decreases. In consequence, the droop controller injects more reactive power to supply the increase in the reactive power demand. The generated active and reactive power from the drooped controlled dispatchable DG units can be given as follows:

$$P_{Gj} = \frac{1}{m_{pj}}\left(\omega_j^* - \omega\right) \quad \forall j \in B_{droop} \tag{3.1}$$

$$Q_{Gj} = \frac{1}{n_{qj}}\left(V_{Gj}^* - V_{Gj}\right) \quad \forall j \in B_{droop} \tag{3.2}$$

where B_{droop} is the set of all droop buses; ω is the system steady-state frequency; ω_{Gj}^{*} and V_{Gj}^{*} are the pre-specified DG unit output frequency and voltage magnitude at no-load, respectively; ω is DG j operating frequency; and V_{Gj} is the voltage at DG j. m_{pj} and n_{qj} are the static droop gains of active and reactive power, respectively. P_{Gj} and Q_{Gj} are the injected active and reactive power by the DG unit, respectively. It is noteworthy that the droop equations expressed by (3.1) and (3.2) are usually justified when the output impedance of the droop-controlled DG unit is mainly inductive due to the coupling inductor used at the DG interface converter output, the X/R ratio of the network feeders, or the use of virtual inductive output impedance [81].

The settings of the droop parameters for the individual DG units have a significant impact on their proportion of active and reactive power sharing. Conventionally, the droop parameters are designed so that the DG units within the IMG share the load demand in proportion to their rated capacities as follows [12], [34]:

$$m_{p1} S_{\max,1} = \cdots = m_{pj} S_{\max,\,j} = \cdots = m_{pn_g} S_{\max,\,n_g} \tag{3.3}$$

$$n_{q1} S_{\max,1} = \ldots = n_{qj} S_{\max,\,j} = \ldots = n_{qn_g} S_{\max,\,n_g} \tag{3.4}$$

where $S_{\max,j}$ is the maximum apparent power of DG j and n_g is the number of drooped DGs in the entire IMG system. In order to ensure equal power sharing between DG units, the static droop coefficients are usually calculated as follows [79]:

$$m_{pj} = \frac{\omega_{\max} - \omega_{\min}}{S_{\max,j}} \tag{3.5}$$

$$n_{qj} = \frac{V_{\max} - V_{\min}}{S_{\max,j}} \tag{3.6}$$

where $\omega_{\max}$, $\omega_{\min}$, $V_{\max}$, and $V_{\min}$ are the frequency and voltage magnitude specified limits.

Figure 3.2 depicts an example for a section of distribution feeder in microgrid systems connected with upstream and downstream networks that can together or individually form IMG system(s). The section has distributed load buses, droop-controlled DG units, and RDG unit(s) that might be located at any bus within the section.

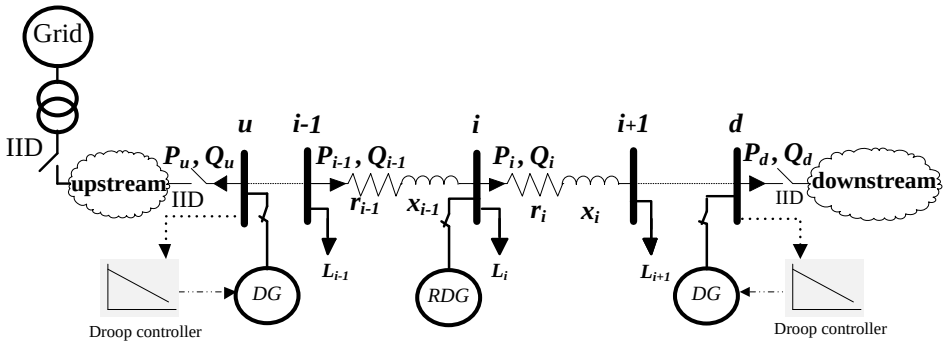

Figure 3.2 A typical segment of distribution feeder in IMG systems

Intermittent RDGs like solar and wind are locally controlled in order to track their maximum power operating point and are therefore represented as PQ buses in the steady-state modeling of IMGs [9]

In general, a set of recursive equations can be used to model the droop-based power flow that reflects the steady-state operation of the section between the upstream and downstream parts shown in Figure 3.2. The upstream and downstream networks are lumped at their connection points with the section and they are assumed to operate in islanded mode together with the studied section. The active and reactive power at branch i and the voltage magnitude at any bus i between buses u and d, where $u < d$ can be expressed as [16]:

$$P_i = P_{Gu} - P_u - \sum_{n=u+1}^{n=i} \left(P_{L,n} - P_{RDG,n}\right) \tag{3.7}$$

$$Q_i = Q_{Gu} - Q_u - \sum_{n=u+1}^{n=i} \left(Q_{L,n} - Q_{RDG,n}\right) \tag{3.8}$$

$$V_i^2 = V_{Gu}^2 - 2\sum_{n=u}^{n=i-1} \left(r_n P_n + x_n Q_n\right) \tag{3.9}$$

where P_u and Q_u are the active and reactive power flow of the upstream branch of the section; r_n and x_n are the branch impedance; P_n and Q_n are the branch active and reactive power; $P_{L,n}$ and $Q_{L,n}$ are the active and reactive power demand; and $P_{RDG,n}$ and $Q_{RDG,n}$ are the active and reactive power of each RDG unit. By substituting the DG active and reactive power from (3.1) and (3.2), the steady-state

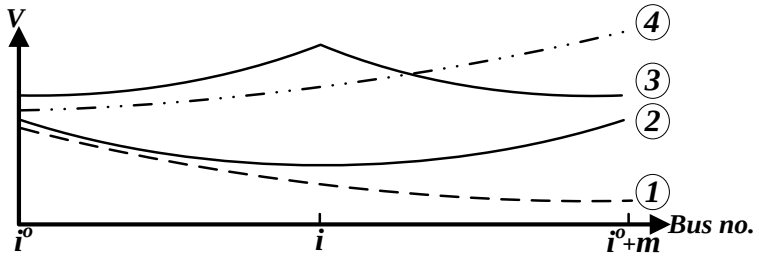

Figure 3.3 Voltage profiles of a typical distribution feeder in IMG systems

power flow at branch *i* and the voltage magnitude at bus *i* can be represented as follows:

$$P_i = \frac{1}{m_{Pu}}\left(\omega_u^* - \omega\right) - P_u - \sum_{n=u+1}^{n=i}\left(P_{L,n} - P_{RDG,n}\right) \tag{3.10}$$

$$Q_i = \frac{1}{n_{qu}}\left(V_{Gu}^* - V_{Gu}\right) - Q_u - \sum_{n=u+1}^{n=i}\left(Q_{L,n} - Q_{RDG,n}\right) \tag{3.11}$$

$$V_i^2 = \left(V_{Gu} - Q_{Gu} n_{qu}\right)^2 - 2\sum_{n=u}^{n=i-1}\left(r_n P_n + x_n Q_n\right) \tag{3.12}$$

As shown in (3.7)–(3.12), the changes of the magnitude and direction of the branch power flow and in consequence the voltage profile in IMGs depend on several factors including the droop parameter settings of DG units, the variability of local loads, and the distribution feeder parameters. In addition, with high penetration of RDGs and the "plug-and-play" characteristic, it is expected that such changes will significantly increase. Figure 3.3 shows the possible voltage profiles along the typical section of distribution feeders in droop-controlled IMG systems.

As depicted in the figure, voltage profile (1) is identical to conventional distribution systems, which indicates a dominant power flow from upstream to downstream networks. Voltage profile (4) is the opposite of (1), where it indicates a reverse power flow from downstream toward upstream. Voltage profile (2) occurs when the local loads in the feeder are supplied from both sides, and voltage profile (3) occurs when RDG units generate enough power to supply neighbor loads.

Droop-controlled DG units are currently the only available devices to maintain the voltage regulation requirements in the entire IMGs. In local droop control, without communication, a DG unit located at node *j* changes its reactive power generation with the change of the voltage magnitude at its PCC at pre-set voltage droop parameters (i.e. V_{Gj}^{*} and n_{qj}) as follows:

$$\Delta Q_{Gj} = \frac{-1}{n_{qj}} \times \Delta V_{Gj} \tag{3.13}$$

Equation (3.13) implies that each droop-controlled DG unit autonomously changes its reactive power generation only when a change on the system loading occurs. Yet, since almost no information is available for DG units beyond the local measurement of the voltage magnitude at the PCCs, a proper voltage regulation in the entire IMG might be unreachable using pre-set droop parameters as explained earlier in the previous section.

3.3 Analysis of Reactive Power Sharing problem in IMG

In this section, the issue of reactive power sharing accuracy in droop-controlled IMGs due to the distribution feeder impedance mismatch is analyzed. Figure 3.2 depicts an example for a typical section of MV radial distribution feeder in IMG systems. The section consists of distributed load buses and upstream/downstream drooped DG units. Each DG in the MV feeder might also represent the equivalence of parallel DG units connected to a single PCC. As shown in the figure, droop characteristics provide a measure of negative proportional feedback that controls the active and reactive power sharing as shown in (3.1) – (3.2). Also, the voltage magnitude at any bus *i* can be represented as given in (3.9). From (3.8) and (3.9), the change of the voltage magnitude ΔV_i due to the change of its load demand can be expressed as a function of the change of reactive power and voltage magnitude of its upstream DG unit *j* as follows:

$$\Delta V_i = \frac{1}{V_i}\left(V_{Gj}\Delta V_{Gj} - \Delta Q_{Gj} X_{i,j}\right) \tag{3.14}$$

where $X_{i,j}$ is the feeder reactance between DG *j* and load *i*. It is worth noting that (3.14) equation is a differentiation of (3.12) with respect to Q_{Gj}. Similarly, ΔV_i can be also expressed as a function of the changes of its downstream DG unit *j*+1 as follows:

$$\Delta V_i = \frac{1}{V_i}\left(V_{Gj+1}\Delta V_{Gj+1} - \Delta Q_{Gj+1} X_{i,j+1}\right) \tag{3.15}$$

where $X_{i,j+1}$ is the feeder reactance between DG *j+1* and load *i*.

It is noted that ΔQ_{Gj} for each drooped DG unit at a pre-specified voltage droop parameter setting can be obtained from (3.2) as shown in (3.9). In consequence, from (3.13), (3.14), and (3.15), the change of the reactive power sharing in response to the change of load demand can be formulated as follows:

$$\frac{\Delta Q_{Gj+1}}{\Delta Q_{Gj}} = \frac{\Delta V_{Gj+1}}{\Delta V_{Gj}} = \frac{n_{qj} V_{Gj} + X_{i,j}}{n_{qj+1} V_{Gj+1} + \lambda X_{i,j+1}} \tag{3.16}$$

where λ is the ratio of the feeder reactance at bus *i* that is seen by DG *j+1* and DG *j*, respectively. Since the voltage magnitude is close to unity, (3.16) can be represented approximately as:

$$\frac{\Delta Q_{Gj+1}}{\Delta Q_{Gj}} \cong \frac{n_{qj} + X_{i,j}}{n_{qj+1} + \lambda X_i} \tag{3.17}$$

Figure 3.4 shows the change of the reactive power sharing with respect to λ at per

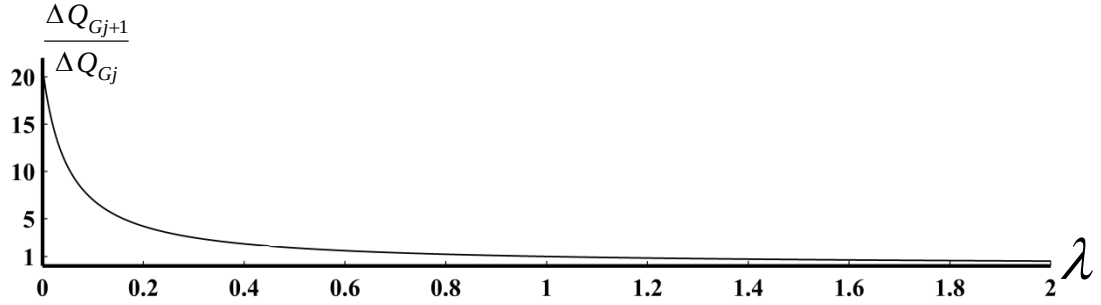

Figure 3.4 Impact of feeder impedance on the reactive power sharing

unit $X_{i,j}$ and $n_{qj} = n_{qj+1} = 0.05$ per unit. As depicted in the figure, the accuracy of the reactive power sharing is highly dependent on λ. As shown, with pre-specified droop parameter settings, an equal reactive power sharing occurs only when λ equals unity.

3.4 Exact Modelling of Power Flow In IMG

As shown in Figure 3.5, a section of a three-phase feeder model is presented between bus *u* and *d*. The impedance matrix that considers the variation of the frequency, self and mutual impedance can be given as follows:

$$\left[Z_{ud}^{abcn}(\omega)\right] = \begin{bmatrix} Z_{ud}^{aa} & Z_{ud}^{ab} & Z_{ud}^{ac} & Z_{ud}^{an} \\ Z_{ud}^{ba} & Z_{ud}^{bb} & Z_{ud}^{bc} & Z_{ud}^{bn} \\ Z_{ud}^{ca} & Z_{ud}^{cb} & Z_{ud}^{cc} & Z_{ud}^{cn} \\ Z_{ud}^{na} & Z_{ud}^{nb} & Z_{ud}^{nc} & Z_{ud}^{nn} \end{bmatrix} \tag{3.18}$$

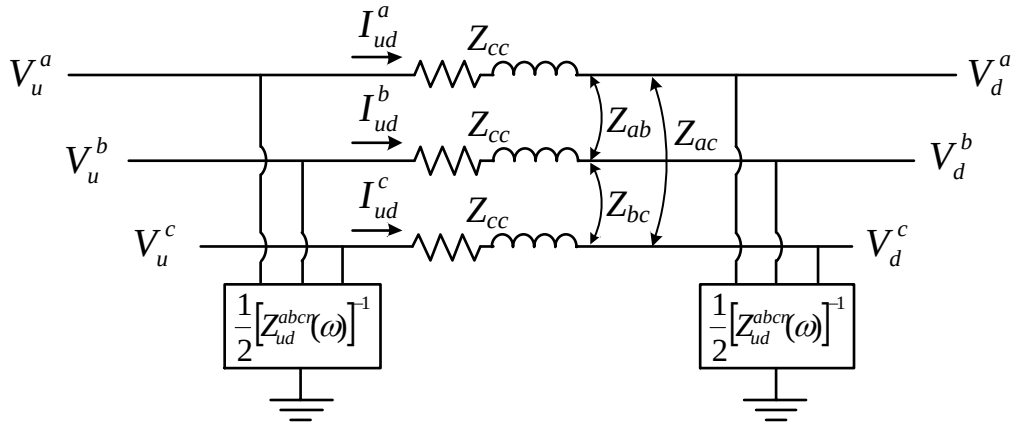

Figure 3.5 Three-phase feeder section model

since any efficiently grounded distribution system will have zero voltage at the ground. By applying Kron's reduction, which still include the effect of the ground wire [7], [91], the three-phase feeder model will be reformulated as given:

$$\left[Z_{ud}^{abc}(\omega)\right]=\begin{bmatrix} Z_{ud}^{aa,n} & Z_{ud}^{ab,n} & Z_{ud}^{ac,n} \\ Z_{ud}^{ba,n} & Z_{ud}^{bb,n} & Z_{ud}^{bc,n} \\ Z_{ud}^{ca,n} & Z_{ud}^{cb,n} & Z_{ud}^{cc,n} \end{bmatrix} \tag{3.19}$$

The relation between the branch voltage V_{ud} and current I_{ud} between two buses u and d as shown in Figure 3.5 can be given as follows:

$$\begin{bmatrix} V_d^a \\ V_d^b \\ V_d^c \end{bmatrix}=\begin{bmatrix} V_u^a \\ V_u^b \\ V_u^c \end{bmatrix}-\begin{bmatrix} Z_{ud}^{aa,n} & Z_{ud}^{ab,n} & Z_{ud}^{ac,n} \\ Z_{ud}^{ba,n} & Z_{ud}^{bb,n} & Z_{ud}^{bc,n} \\ Z_{ud}^{ca,n} & Z_{ud}^{cb,n} & Z_{ud}^{cc,n} \end{bmatrix}\begin{bmatrix} I_{ud}^a \\ I_{ud}^b \\ I_{ud}^c \end{bmatrix} \tag{3.20}$$

The branch current between nodes u and d can be given as follows:

$$\begin{bmatrix} I_{ud}^a \\ I_{ud}^b \\ I_{ud}^c \end{bmatrix}=\begin{bmatrix} Y_{ud}^{aa,n} & Y_{ud}^{ab,n} & Y_{ud}^{ac,n} \\ Y_{ud}^{ba,n} & Y_{ud}^{bb,n} & Y_{ud}^{bc,n} \\ Y_{ud}^{ca,n} & Y_{ud}^{cb,n} & Y_{ud}^{cc,n} \end{bmatrix}\begin{bmatrix} V_u^a & V_d^a \\ V_u^b & -V_d^b \\ V_u^c & V_d^c \end{bmatrix} \tag{3.21}$$

where

$$\begin{bmatrix} Y_{ud}^{aa,n} & Y_{ud}^{ab,n} & Y_{ud}^{ac,n} \\ Y_{ud}^{ba,n} & Y_{ud}^{bb,n} & Y_{ud}^{bc,n} \\ Y_{ud}^{ca,n} & Y_{ud}^{cb,n} & Y_{ud}^{cc,n} \end{bmatrix}=\begin{bmatrix} Z_{ud}^{aa,n} & Z_{ud}^{ab,n} & Z_{ud}^{ac,n} \\ Z_{ud}^{ba,n} & Z_{ud}^{bb,n} & Z_{ud}^{bc,n} \\ Z_{ud}^{ca,n} & Z_{ud}^{cb,n} & Z_{ud}^{cc,n} \end{bmatrix}^{-1} \tag{3.22}$$

Load modelling of different load behaviour such as constant impedance, constant current and constant power, and different load category such as residential, commercial and industrial are considered in the IMG power flow. The active and reactive power required by the different load models is affected by the change of the voltage of their nodes and system frequency. The relation between the load active and reactive power and the voltage and frequency is presented as follows:

$$P_{Lu}^{ph} = P_{Nu}^{ph}\left|V_u^{ph}\right|^{\alpha}\left(1+N_{pf}\Delta\omega\right) \tag{3.23}$$

$$Q_{Lu}^{ph} = Q_{Nu}^{ph}\left|V_u^{ph}\right|^{\beta}\left(1+N_{qf}\Delta\omega\right) \tag{3.24}$$

where P_{Lu}^{ph} and Q_{Lu}^{ph} represent the load active and reactive power at each of the three phases $ph = a, b \text{ or } c$ at node u; P_{Nu}^{ph} and Q_{Nu}^{ph} represent the nominal load active and reactive power; V_u^{ph} is the node voltage at phase ph; $\Delta\omega$ is the deviation of the angular frequency from the nominal per unit angular frequency. N_{pf} and N_{qf} are the frequency deviation parameter and can be represented by 1 and –1 respectively [7]. α and β are the exponents of active and reactive power, respectively. The exponential parameters for constant power, constant current, and constant impedance can be selected as 0, 1, and 2 respectively [92]. Furthermore, different load categories can be found in [93].

Let $P_u^{a,b,c}$ and $Q_u^{a,b,c}$ denote the calculated real and reactive power injected to the IMG system at each of the three phases *ph* at node *u*. The calculated active and reactive power for phase *a*, P_u^a, and Q_u^a can thus be given as follows [8]:

$$P_u^a = \sum_{\substack{d=1 \\ d\neq i}}^{n_{br}} \sum_{ph=a,b,c} \left[\begin{array}{l} V_u^a V_u^{(ph)} Y_{ud}^{a(ph)} \cos\left(\theta_{ud}^{a(ph)} + \delta_u^{(ph)} - \delta_u^a\right) - \\ V_u^a V_d^{(ph)} Y_{ud}^{a(ph)} \cos\left(\theta_{ud}^{a(ph)} + \delta_d^{(ph)} - \delta_u^a\right) \end{array} \right] \tag{3.25}$$

$$Q_u^a = \sum_{\substack{d=1 \\ d\neq i}}^{n_{br}} \sum_{ph=a,b,c} \left[\begin{array}{l} V_u^a V_d^{(ph)} Y_{ud}^{a(ph)} \sin\left(\theta_{ud}^{a(ph)} + \delta_d^{(ph)} - \delta_u^a\right) - \\ V_u^a V_u^{(ph)} Y_{ud}^{a(ph)} \sin\left(\theta_{ud}^{a(ph)} + \delta_u^{(ph)} - \delta_u^a\right) \end{array} \right] \tag{3.26}$$

where n_{br} is the number of branches; Y_{ud} and θ_{ud} are the branch admittance magnitude and angle for branch ud, respectively; V_u and δ_u are the voltage magnitude and angle at bus u, respectively. Similar equations can be extracted for the calculated active and reactive power for phases *b* and *c*. For each phase *ph* of each bus *i* within the IMG, there are two power flow mismatch equations represented as follows [45]:

$$P_u^{ph} = 1_A \times P_{Gu,droop}^{ph} + P_{Gu,spec}^{ph} - P_{Lu}^a \tag{3.27}$$

$$Q_u^{ph} = 1_A \times Q_{Gu,droop}^{ph} + Q_{Gu,spec}^{ph} - Q_{Lu}^a \tag{3.28}$$

where 1_A is a binary variable; it equals zero for PQ buses and one for droop buses; $P_{Gu,droop}^{ph}$ and $Q_{Gu,droop}^{ph}$ represent the calculated active and reactive generated power of droop-controlled DG units; $P_{Gu,spec}^{ph}$ and $Q_{Gu,spec}^{ph}$ are the pre-specified active and

reactive generated power of non-droop controlled DG units. For each droop bus *i*, the system steady-state frequency ω and bus voltage magnitude V_u^{ph} are dependent on the generated three-phase active and reactive power that are governed by the static droop parameter settings as:

$$\omega = \omega_u^{\ *} - m_{pu} \times \sum_{ph=a,b,c} P_{Gu,droop}^{ph} \tag{3.29}$$

$$V_u^{ph} = V_u^{\ *} - n_{qu} \times \sum_{ph=a,b,c} Q_{Gu,droop}^{ph} \tag{3.30}$$

At its point of common coupling, it is assumed that the three-phase droop-controlled DG unit is able to maintain balanced voltage waveforms, represented in the power flow as:

$$V_u^a - V_u^b = 0 \& V_u^a - V_u^c = 0 \tag{3.31}$$

$$\delta_u^a - \delta_u^b = \left(2\pi/3\right) \& \delta_u^a - \delta_u^c = -\left(2\pi/3\right) \tag{3.32}$$

As shown in the above equations, the droop-based three-phase power formulation of IMGs is made up of *N* equations comprising *N* unknown variables to be calculated given as [8]:

$$N = 6 \times n_{PQ} + 12 \times n_{droop} \tag{3.33}$$

where n_{PQ} and n_{droop} are the number of PQ and droop buses in the IMG, respectively.

3.5 Case studies

Two case studies are presented in this section to study the challenges of voltage and reactive power control in IMG using for both three-phase balanced and unbalanced system i.e. case 33 bus system and the unbalanced IEEE 34 distribution system.

3.5.1 The 33-bus balanced distribution test system

In this case study five identical DGs are located across the 33-bus distribution test system operate in islanded mode, the system and its data are shown in the Appendix in Figure A.1 and Table A-1. The rating, location, and the coupling impedance of the penetrated DG units to the test system are shown in Table 3-1. The droop parameter was designed to have equal active and reactive sharing as shown in (3.3)–(3.6).

Table 3-1 DGs Droop parameters and bus location

	Rating (MVA)	**Bus connection, Bus location**	**Connection-location Impedance** [93]
DG 1	1.5	Bus 5, Bus 34	0.012453+0.012453j
DG 2	1.5	Bus 9, Bus 35	0.012453+0.012453j
DG 3	1.5	Bus 12, Bus 36	0.012453+0.012453j
DG 4	1.5	Bus 18, Bus 37	0.003113+0.003113j
DG 5	1.5	Bus 25, Bus 38	0.003113+0.003113j

Where the case study base MVA was considered as 1 MVA; active and reactive power static droop gains, m_p and n_q, are designed to be 0.0018 and 0.0333 per unit for each droop-controlled DG unit, respectively. V^* and ω^* are set to be 1.02 and 1.0 per unit for all DG units, respectively. Figure 3.6 and Figure 3.7 show the DGs generation sharing of the system active and reactive power. As is depicted in the figures, the active power sharing is exact among the five DGs; however, the reactive power sharing is not achieved.

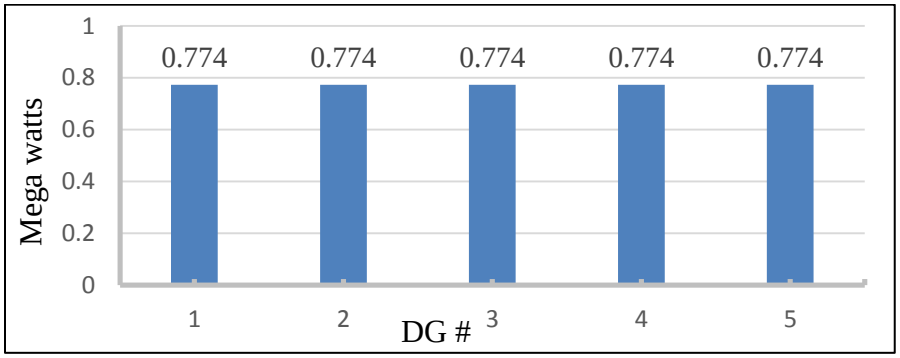

Figure 3.6 DGs active power generation

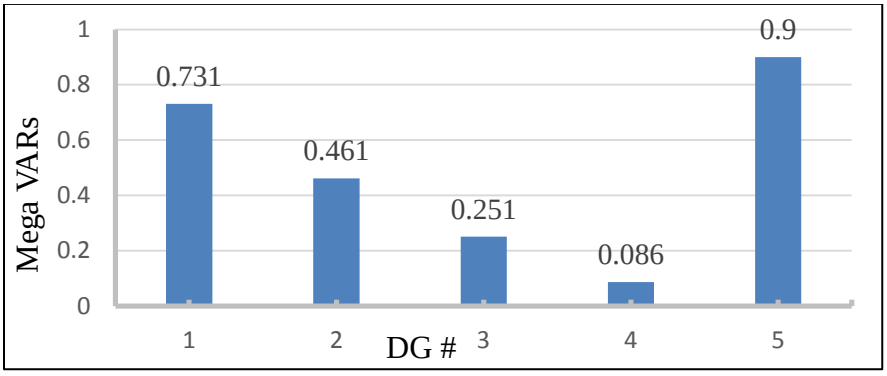

Figure 3.7 DGs reactive power generation

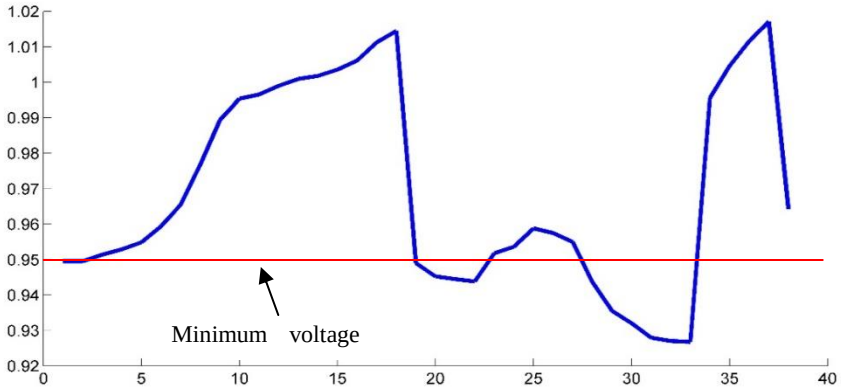

Figure 3.8 Voltage profile during the islanded mode

Moreover, as shown in Figure 3.8, an undervoltage might occur during the islanded mode.

3.5.2 Three-phase unbalanced 34-bus test system

This case study was simulated without considering any Volt/Var devices to avoid any conflict interaction between those devices and the droop-controlled IMG. The system base MVA was considered to be 0.5 MVA, and the DGs are assumed to be identical, of equal 2 MVA rating capacity with minimum power factor of 0.7. The DG units are connected at busses 2, 10, and 14, respectively, with interconnection impedance of $0.003113 + 0.003113j$. The active and reactive power static droop gains m_p and n_q are designed to be 0.05 and 0.5, respectively, thus, achieve the equal power sharing among the DGs. The no-load reference voltage V_{Gj}^* and frequency ω^* is set at 1.02 and 1.0 per unit, respectively.

As shown in Table 3-2, the reactive power sharing in the system is not equal, which is main challenge of the droop control in the islanded microgrid that may lead to circulating reactive power and increase the losses. Moreover, as depicted in Figure 3.9, undervoltage may occur without propoer incorporation of the Volt/Var devices in the IMG.

Table 3-2 DGs output voltage, active and reactive power

DG #	Voltage (p.u.)	Reactive power generation (p.u.)	Active power generation (p.u.)
DG 1	1.0055	0.29	1.15
DG 2	0.9850	0.7	1.15
DG 3	0.9679	1.04	1.15

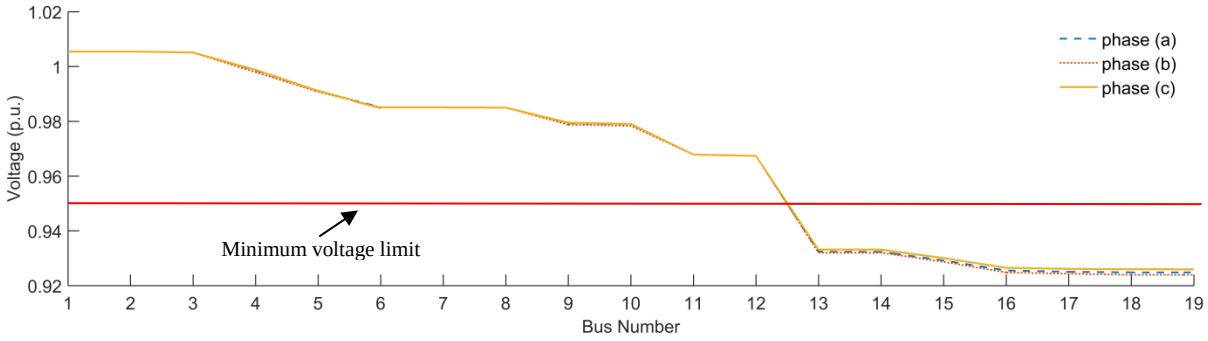

Figure 3.9 Voltage profile of the 34-bus system backbone during islanded mode

Chapter 4

MITIGATION OF VOLT/VAR CONTROL CHALLENGES USING A CONSTRAINT SATISFACTION APPROACH

This chapter is divided into two sections. In the first section, a distributed control scheme is proposed to mitigate the voltage regulation challenges. In the second section, a distributed control scheme is proposed to enhance the accuracy of DGs' reactive power sharing, while considering the IMG acceptable voltage boundaries. The proposed schemes utilize a low-bandwidth communication, which are a complementary process to either local droop or distributed secondary control to achieve fully distributed control in IMGs. To that end, a distributed constraint satisfaction (DCS) approach is adopted to formulate the problem of voltage regulation and reactive power sharing of IMGs in a multi-agent environment. In the formulated problem, DG units interact together via peer-to-peer communication to autonomously adjust their own voltage droop parameter settings. An asynchronous weak commitment (AWC) technique has been proposed to solve the formulated problem. Several case studies are presented to validate the proposed control scheme.

4.1 Impact of Droop Paramter Settings on the Voltage and Reactive Power sharing

Since almost no information is available for DG units beyond the local measurement of the voltage magnitude at the PCCs, a proper voltage regulation and equal reactive power sharing in the entire IMG might be unreachable using a pre-set droop parameters as explained in chapter 3. Hence, with adequate knowledge of the current state of the network, appropriate adjustments of the droop parameter settings can be utilized to regulate the voltage and achieve equal power sharing in the entire IMG. Here it is worth noting that previous studies showed that the settings of n_{qj} affect the stability of the IMG system [4], [7]–[9]. For this reason, n_{qj} is assumed to be pre-set and thus the no load reference voltage V_{Gj}^{*} in (3.2) is identified as the controlled setting for steady-state voltage regulation and achieving proper reactive power sharing. In this work as depicted in Figure 4.1, three possible scenarios are introduced for the participation of each droop- controlled DG unit in

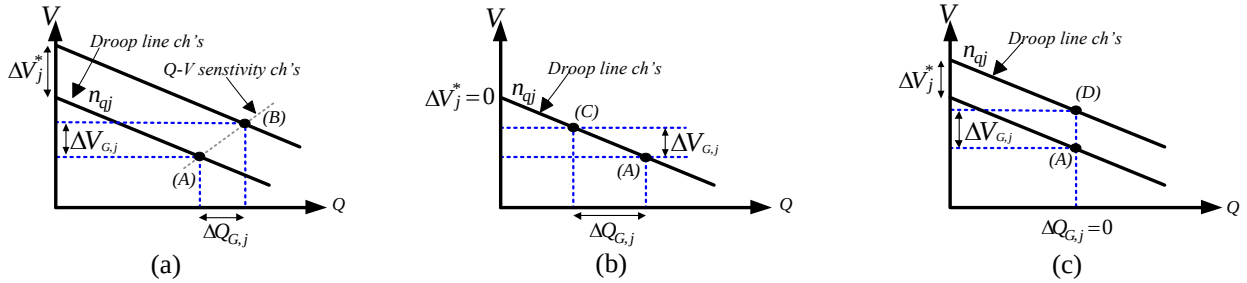

Figure 4.1 DGs participate in voltage regulation via (a) sensitivity characteristics, (b) response to settings update of other unit(s), and (c) specified reactive power generation

the process of voltage regulation. A detailed description of the three scenarios is presented hereunder.

4.1.1 Impact of Droop Parameter Settings on Voltage Regulation

Figure 4.1shows the voltage droop characteristics of a DG unit located at node *j* and operates originally at steady-state point *A*. In order for such DG to participate in regulating the voltage at any node *i* within the IMG, it requires moving to a new steady-state operating point. The new operating point depends on the adjustment of no-load reference voltage ΔV_{Gj}^{*} taken by such DG unit along with other DG units in the IMG. Such dependency can be illustrated in the three possible scenarios of DGs participation depicted in Figure 4.1. In the *first scenario*, as shown in Figure 4.1 (a), DG unit *j* regulates the voltage at a remote node *i* within the IMG by calculating the required change of its local voltage and in consequence the generated reactive power (i.e. from *A* to *B*) according to the power flow sensitivity characteristics represented as:

$$\Delta Q_{Gj}^{(A,B)} = SF_j \times \Delta V_{Gj}^{(A,B)} \tag{4.1}$$

where SF_j is the partial derivative of the reactive power flow given in (3.11) with respect to the nodal voltage [73]. In order for DG *j* to move from *A* to *B*, while preserving the droop control, a change of the no-load specified reference voltage

ΔV_{Gj}^{*} is required. Toward this end, the change of the droop reactive power generation in (3.13) is reformulated as follows:

$$\Delta Q_{Gj} = \frac{-1}{n_{qj}} \times \left(\Delta V_{Gj} - \Delta V_{Gj}^{*} \right) \tag{4.2}$$

Without loss of generality, it is assumed that the load change during steady-state voltage regulation process is neglected. As such, the change of voltage magnitude and reactive power generation at DG *j* can be given as follows:

$$\Delta V_{Gj} = \Delta V_{Gj}^{(A,B)} \quad , \forall V_{Gj}^{Min} \le V_{Gj}^{B} \le V_{Gj}^{Max} \tag{4.3}$$

$$\Delta Q_{Gj} = \Delta Q_{Gj}^{(A,B)} \quad , \forall Q_{Gj}^{B} \le Q_{Gj}^{Max} \tag{4.4}$$

where, Q_{Gj}^{B} and V_{Gj}^{B} are the output reactive power and voltage magnitude at the target operating point *B*; V_{Gj}^{Min} and V_{Gj}^{Max} are the minimum and maximum acceptable voltage limits at the PCC, respectively. Q_{Gj}^{Max} is the maximum generated reactive power of DG *j*, where Q_{Gj}^{Max} is determined using [94]:

$$Q_{Gj}^{Max} = \min \left\{ Q_{Gj,PF}^{Max}, Q_{Gj,C}^{Max} \right\} \tag{4.5}$$

where $Q_{Gj,PF}^{Max}$ and $Q_{Gj,C}^{Max}$ are the reactive power generation limits due to the DG minimum power factor $\left(PF_{\min} \right)$ and the maximum current capability level of the DG inverter, respectively, given as follows:

$$Q_{Gj,PF}^{Max} = P_{Gj} \tan\left(\cos^{-1}\left(PF_{\min}\right)\right) \tag{4.6}$$

$$Q_{Gj,C}^{Max} = \sqrt{\left(S_{Gj}^{Cap}\right)^2 - P_{Gj}^2} \tag{4.7}$$

and S_{Gj}^{Cap} is the maximum capacity limit of DG *j*. From (4.1)-(4.4), the required change of the no-load pre-specified voltage ΔV_{Gj}^{*} as well as the new reference voltage at no load V_{Gj}^{*new} can be calculated as:

$$\Delta V_{Gj}^{*} = \Delta V_{Gj}^{(A,B)} \times \left(1 + SF_j n_{qj}\right) \tag{4.8}$$

$$\Delta V_{Gj}^{*new} = V_{Gj}^{*} + \Delta V_{Gj}^{*} \tag{4.9}$$

One can observe that the steady-state operating points of other droop-controlled DG unit(s) within the IMG that maintain their reference voltages (i.e. $\Delta V_{Gj}^{*} = 0$) are changed according to their own droop characteristics in response to the action of DG unit(s) that actively regulate the voltage by (4.9). Accordingly, Figure 4.1 (b) shows the *second operation scenario* of DG unit *j* when it is affected by the active voltage regulation of other droop-controlled DG units.

As shown in the figure, DG *j* in this scenario moves from point *A* to *C* in response to other DG unit(s) that updates their voltage droop parameter settings. Such change in the operating point aims to update the reactive power sharing in order to maintain the reactive power balance in the entire IMG.

In another word, if DG *j* is the only DG that does not actively regulate the voltage (i.e. $\Delta V_{Gj}^{*} = 0$), the change in its reactive power generation can be given as follows:

$$\Delta Q_{Gj} = \Delta Q_{Gj}^{(A,C)} = \frac{-1}{n_{qj}} \times \Delta V_{Gj}^{(A,C)} = -\sum_{k \neq j} \Delta V_{Gk}^{(A,C)} \tag{4.10}$$

The two operating scenarios described in Figure 4.1 (a) and (b) can be utilized to derive a generalized formula for calculating the required change of the no-load reference voltage to achieve the reactive power change from point *A* to a target point *A** as shown in Figure 4.2 for each droop-controlled DG unit *j* as follows:

$$\Delta V_{Gj}^{*} = \Delta V_{Gj}^{(A,A^*)} \times \left(1 + \frac{\Delta Q_{Gj}^{(A,A^*)}}{\Delta V_{Gj}^{(A,A^*)}} \times n_{qj} \right) \tag{4.11}$$

where $\Delta Q_{Gj}^{(A,A^*)}$ is calculated using (4.1) and (4.10) in the first and the second scenarios, respectively. Also, $\Delta Q_{Gj}^{(A,A^*)}$ might have a specified setting due to certain local constraints or preferences. Figure 4.1 (c) shows an example of such *scenario*, where DG unit *j* aims to participate in the voltage regulation process without changing its reactive power generation via moving from *A* to *D* (i.e., $\Delta V_{Gj}^{*} = \Delta V_{Gj}^{(A,D)}, \Delta Q_{Gj} = \Delta Q_{Gj}^{(A,D)} = 0$).

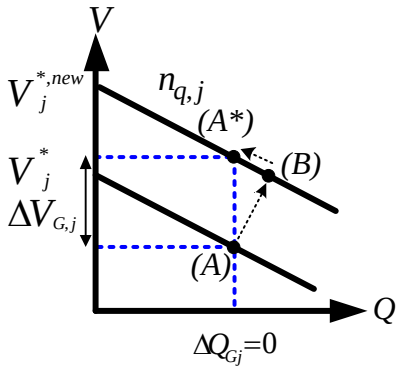

Figure 4.2 Generic droop parameter control relation between voltage and reactive power

In another word the *third scenario* shown in Figure 4.1 (c) can be described as a combination of the first two scenarios. As depicted in Figure 4.2, the Q–V operating point moves from *A* to *B* using the *first scenario* ; then it moves from *B* to *A** via the *second scenarios*.

The described operation scenarios are incorporated in the solution algorithm of each droop-controlled DG unit in the proposed distributed voltage regulation scheme in order to generate feasible solutions (i.e. adjustments of the no-load reference voltages) as will be described in the following sections.

4.1.2 Impact of Droop Parameter Settings on the Reactive Power Sharing

By considering the change of the no-load reference voltage as a control parameter, the change of reactive power sharing in (3.17) can be reformulated by considering the adjustment of ΔV_{Gj}^* as:

$$\frac{\Delta Q_{Gj+1}}{\Delta Q_{Gj}} = \frac{n_{qj} + \left[X_{i,j} - \dfrac{\Delta V_{Gj}^{*}}{\Delta Q_{Gj}} \right]}{n_{qj+1} + \left[\lambda X_{i,j} - \dfrac{\Delta V_{Gj+1}^{*}}{\Delta Q_{Gj+1}} \right]} \tag{4.12}$$

As can be seen in (4.12) ΔV_{Gj}^{*} can be utilized to correct the reactive power sharing between the drooped DG units via eliminating the mismatch of the distribution feeder reactance.

Based on the aforementioned discussions, let's assume that DG unit *j* was originally operating at stead-state point *A* at which inaccurate reactive power sharing occurs. Also, let's assume that DG unit *j* requires changing its reactive power by $\Delta Q_{Gj}^{(A,A^*)}$ to correct its reactive power sharing (i.e. via moving to a new steady-state operating point A^*). To do so, while preserving the droop characteristics, ΔV_{Gj}^{*} can be obtained using (4.11). As shown in (4.11), ΔV_{Gj}^{*} is determined based on the required change of the reactive power generation as well as the change in the voltage magnitude at the DG's PCC (i.e. $\Delta V_{Gj}^{(A,A^*)}$). It is noteworthy that in droop-controlled IMGs, the new operating point A^* that is required to correct the reactive power by $\Delta Q_{Gj}^{(A,A^*)}$ for each DG unit *j*, depends on the desired control action(s) taken by such DG unit along with other DG units in the IMG. Figure 4.1 show the possible methods that can be used to change the

reactive power generation of DG unit *j* in steady-state. These methods are modeled in this work in the form of three possible actions a_1, a_2 and a_3 for each DG unit *j* given as:

$$\Delta Q_{Gj}^{(A,A^*)} = \begin{cases} SF_j \Delta V_{Gj}^{(A,B)} , & \forall a_1 \\ \dfrac{-1}{n_{qj}} \times \Delta V_{Gj}^{(A,C)} , & \forall a_2 \\ \Delta Q_{Gj}^{Spec} , & \forall a_3 \end{cases} \tag{4.13}$$

where ΔQ_{Gj}^{Spec} is DG *j* specified reactive power change. As illustrated in Figure 4.1(a), DG unit *j* determines its target point *B* and in consequence sets $\Delta V_{Gj}^{(A,B)}$ in a_1 according to its local sensitivity characteristics. One can observe that the steady-state operating points of the droop-controlled DG unit(s) within the IMG that do not actively adjust their voltage droop setting (i.e. $\Delta V_{Gj}^{(A,A^*)} = 0$) are changed in response to the action a_1 of other DG unit(s). Such reaction is represented in this work as a_2, which might be a preference for some DG units. Accordingly, Figure 4.1 (b) shows the second possible action a_2 of DG unit *j* in response to a_1 of other droop-controlled DG units. As depicted in the figure, DG *j* in this scenario adjusts its reactive power generation via moving from *A* to *C* without changing its droop parameter settings in response to the reactive power adjustments of other DG unit(s) via a_1. Such change in the operating point aims to maintain the reactive power

balance in the entire IMG. It is noteworthy that a_1 and a_2 might do not ensure appropriate voltage regulation in the entire IMG system. Hence, a third action a_3 is proposed in this work to set $\Delta V_{Gj}^{(A,A^*)}$ at a specified value $\Delta V_{Gj}^{Spec.}$ in order to satisfy the voltage regulation requirements.

Detailed description of the problem formulation of reactive power sharing and voltage regulation is presented hereunder in the following sections.

4.2 Distributed Communication Model

In order to implement a distributed control scheme, a two-way communication network needs to be deployed to facilitate the exchange of messages among the local control agents of the DGs. The communication network is modeled in this paper as a directed graph given as [90]:

$$G = (v, E, \Lambda) \tag{4.14}$$

where $v = \{v_1, \dots v_j \dots, v_{n_{DG}}\}$, is a set of nodes at which control agents (i.e. DG units) are connected in the IMG, and $E \subseteq v \times v$ is the set of directed edges that describes the communication links between the control agents. An edge $(v_j, v_k) \in E$ denotes that control agent j can obtain information from control agent k, but not necessary vice versa. Λ is an $n_{DG} \times n_{DG}$ adjacency matrix; where $\Lambda = [\Lambda_{jk}] \in \Re^{n \times n}$ with Λ_{jk} equals one if $(v_j, v_k) \in E$, and zero otherwise. Also, in order to

align with the literature, self-loops is not counted in E, i.e., $\Lambda_{jj}=0$. The in-neighbors of control agent j are those eligible to send data to j and are represented as $\mathcal{N}_j^{in} = \{l \in \mathcal{V}: (l,j) \in E \; and \; l \neq j\}$. Further, the out-neighbors of control agent j are those eligible to receive data from j and are represented as $\mathcal{N}_j^{out} = \{l \in \mathcal{V}: (j,l) \in E \; and \; l \neq j\}$ [90]. Given that a two-way communication is deployed, it is assumed in this work that $\mathcal{N}_j^{in} = \mathcal{N}_j^{out}$. It is noteworthy that the communication model is totally independent of the IMG system and the DGs locations; however a communication optimization problem can be adopted to minimize the exchanged messages path and the duration of the solution set points of the drooped DGs [89], [95]. In such a way, every specified periodic time interval or when a violation occurs, the control agents initiate a *synchronization of process* to determine the required correction for the reactive power sharing and maintain the voltage regulation requirements. Once the synchronization of process is initiated, the control agents exchange their information to determine the required adjustments of their reactive power generation. In such a way, every specified periodic time interval, the control agents initiate a *synchronization of process* to determine the required correction for the reactive power sharing and maintain the voltage regulation requirements. The synchronization of process is a collaboration process among the control agents that continues until a general agreement for the new settings to satisfy the operation requirements is reached [16], [20]. However,

during the periodic time interval, any control agent can trigger a *synchronization of process* in case of any constraint violation. Once the synchronization of process is initiated, the control agents exchange their information to determine the required adjustments of their voltage and reactive power generation.

4.3 Distributed Constraint Satisfaction Problem Defination and Formulation

A constraint satisfaction problem (CSP) is a problem that consists of a finite set of control variables associated with finite domains and comprises a set of constraints that limits the values each variable can choose [96], [97]. CSP has been widely used in various applications such as resource allocation, scheduling problem, operation research problem, and graphic systems [96], [97]. The mathematical formula of the CSP can be expressed as a function that is mainly dependent on three parameters: variables, domains and constraints given as follows [96]–[98]:

$$CSP = f\left(X, D, C\right) \tag{4.15}$$

where, X is the set of finite control variables $\{X_1, X_2, ..., X_n\}$, D is the set of non-empty solution domain $\{D_1, D_2, ..., D_n\}$ that is a range or a group of each variable feasible solution; C is the set of constraints $\{C_1, C_2, ..., C_n\}$ that limit the satisfaction values of the variables assigned from each variable domain D. The problem of voltage and reactive power control in droop-controlled IMGs can be

formulated as a CSP to ensure system allowable voltage limits and the desired reactive power sharing. The variables are the reference no load voltages of the DG units given as:

$$X = \left\{ V_{Gj}^{*}, \forall j \in B_{droop} \right\} \tag{4.16}$$

Similarly, the domain of the control variables can be defined as follows:

$$D = \left\{ D_{Gj} \in \left\{ V_{Gj}^{*,Min} \rightarrow V_{Gj}^{*,Max} \right\}, \forall j \in B_{droop} \right\} \tag{4.17}$$

where, D_{Gj} represents a domain range of V_{Gj}^{*}. In this work, the value assignment of the control variable V_{Gj}^{*} for each DG unit *j*, aims to satisfy the system constraints.

The formulation presented in (4.15)-(4.17) is a centralized CSP that requires a central controller in order to be solved in its existing arrangement. In order to obviate the need for a central controller, the problem described in (4.15)-(4.17) must be reformulated as a distributed CSP (DCS). DCS is a problem in which the variables and constraints are distributed among intelligent automated agents [96]–[98]. Where, each agent searches in its own domain for a value assignment of its variable, which satisfies its own constraints, as well as other agents' constraints. Fortunately, the distributed nature of the droop-controlled DG units in IMGs make them behave intrinsically as distributed control agents (DGA). To that end, each DGA has its own variable V_{Gj}^{*}, domain D_{Gj}, and local constraint Q_{Gj}^{Max}.

Further, in order to distribute the voltage and reactive power of the entire IMG system among the DGAs, a local zone is defined for each DGA (i.e. the IMG system is divided into a number of zones that are equal to the number of DGAs). In addition to the droop-controlled DG unit that acts as the volt/var agent, each zone *z* may contain local loads and/or RDGs. Accordingly, the DCS problem of each DGA can be mathematically formulated as follow:

$$DCS_Z = f\left(V_{Gj}^{*}, D_{Gj}, C_Z, C_C\right) \quad , \forall j \in B_{droop}^{Z} \tag{4.18}$$

where, C_Z represents the zone constraints, including the voltage magnitude and the DG reactive power limits, C_C is a common IMG system constraint for the reactive power balance among the droop-controlled DG units, and B_{droop}^{Z} is the location set of the droop-controlled DG unit in zone *z*. Figure 4.3 shows a schematic diagram of the proposed IMG distributed control structure.

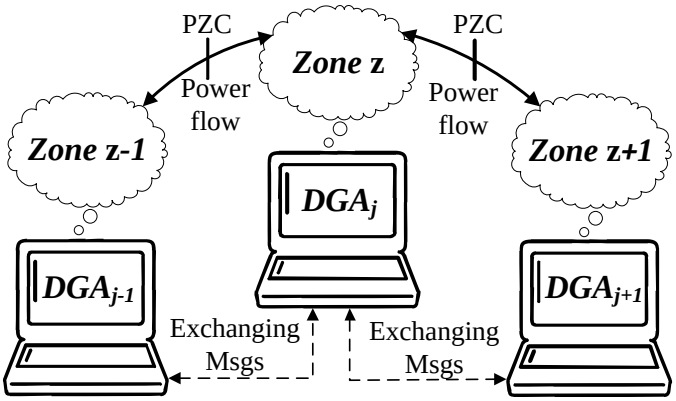

Figure 4.3 Schematic diagram for the proposed DCS structure in IMGs

As shown in the figure, each zone is connected with its adjacent zone(s) (e.g. upstream and downstream) at the point of zone coupling (PZC). In steady-state operating conditions, droop-controlled DGAs interact together via a low-bandwidth peer-to-peer communication network to determine the value assignments for their variables in order to satisfy the constraints in (4.18). However, appropriate value assignments of the DGAs to their variables cannot be taken without adequate knowledge of the current state of the IMG system (i.e. state estimation). In local droop-controlled IMG systems, since almost no information is available for each DGA beyond the voltage magnitude and power of its droop-controlled DG unit, proper detection and thus mitigation of the voltage violation could be unreachable. In order to enhance the state estimation capability of the DGAs, it is assumed in this work that voltage and branch power meters are placed at three different locations in the IMG system: 1) droop-controlled DG units, 2) PZCs, and 3) remote load points at the end of the feeder laterals. Such places are sufficient to provide adequate observation of the system state [16], [99].

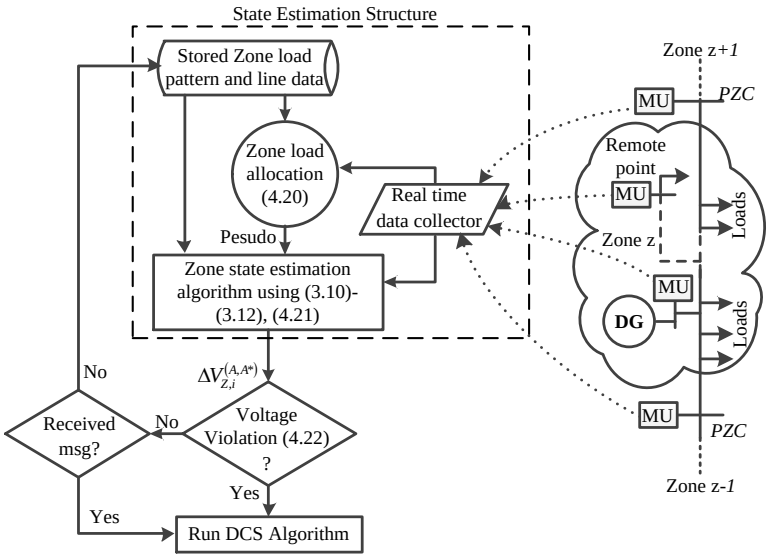

Figure 4.4 Zone voltage profile state estimation algorithm of each DGA

Figure 4.4 shows a flowchart of the developed state estimation algorithm of each DGA. As shown in the figure, each DGA receives real-time measurements of its zone (i.e. local measurements at the DG location and remote measurements at PZCs and/or end of feeder laterals). Then, it allocates the load demand within its assigned zone to provide pseudo measurements in order to obtain a complete observation of the zone.

A real-time load modeling technique that incorporates the customer class curves and provides the uncertainty in the estimates is used in the state estimation algorithm [16]. For any zone *z* at time *t*, the real-time load estimates of load point *i*, can be obtained as follows:

$$P_{Li}^{Z}(t) = \left(\left|P_u^Z - P_d^Z\right| - P_{loss}^Z\right) \left[\frac{\sum_{m=1}^{M} LMF_k(t) \times ADC_{i,m}}{\sum_{\forall i \in B^Z} \sum_{m=1}^{M} LMF_k(t) \times ADC_{i,m}} \right] \tag{4.19}$$

where, P_u^Z, P_d^Z and P_{loss}^Z are the upstream, downstream and real power loss of zone z; M is the number of load classes, $ADC_{i,m}$ is the average daily customer demand at load point i, belonging to class m, at time t and LMF_m is the class-specific load model factor, belonging to class m, at time t. The power factor of each load point, at time t, is obtained by accessing historical information [99]. The solution for the voltage state estimation problem for each zone z is obtained by minimizing the performance index J given by [16]:

$$Min \quad J = \sum_{l=1}^{L} w_l \left(y_l - h_l(x)\right)^2 \tag{4.20}$$

where l denotes the vector containing the measurements; w_l and $h_l(x)$ represent the weight and the measurement function associated with measurement y_l, respectively; L is the number for real-time and pseudo measurements of the zone. A branch-based estimation method is utilized in this work to solve the problem in (4.20). The method estimates the node voltages using backward-forward sweep calculations via running the droop-based power flow equations described in (3.10)-(3.12) [16], [99].

Once the voltage profile in the zone is estimated, the DGA determines the minimum and the maximum voltages in its zone and compares them with the allowed limits to determine the maximum overvoltage or undervoltage deviation and its location, if any, given as:

$$\Delta V_{z,i}^{(A,A^*)} = \begin{cases} \max\left(V_i - V_{ub}\right) \ \forall i \in B^z, \& \, V_i > V_{ub} \\ \min\left(V_i - V_{lb}\right) \ \forall i \in B^z, \& \, V_i < V_{lb} \\ 0 \qquad\quad \forall i \in B^z, \& \, V_{ub} \geq V_i \geq V_{lb} \end{cases} \tag{4.21}$$

As depicted in Figure 4.4, once a voltage violation is detected by the state estimation algorithm of each DGA within its zone and/or it receives a message of voltage violation from neighbor DGAs, the DGAs interact together in order to satisfy the DCS formulated problem. A detailed description of the proposed solution algorithm of the DCS voltage regulation problem is presented in the following section.

4.4 Solution Algorithms for distributed Constraint Satisfaction Problems

In a DCS environment, each agent has its own *agent-view*, which stores its variable assignment, domain, constraints and algorithm procedures. The solution philosophy of the DCS problems adopts a multi-stage negotiation protocol among the automated agents via peer-to-peer communication channels. *ok?* message is the main type of message communicated among agents. It is sent by one agent to learn

if its proposed variable assignment is consistent with other agents' constraints. Further, using *ok?* messages, each agent evaluates the variable value of other agents from its *agent-view*. Each recipient agent responds to *ok?* messages with either: 1) *good* message to indicate that the proposed variable assignment of the sender agent is consistent with its own constraints; or 2) *no-good* message to communicate an inconsistent variable assignment [97].

In order to reach a consensus and satisfy the constraints of the whole IMG system, an appropriate communication algorithm is required among the DGAs to solve the DCS problem described in the previous section. Several methods are proposed in the literature to solve DCS problems, such as synchronous backtracking, asynchronous backtracking and asynchronous weak commitment search (AWC) [97]. Each method has its own merits and disadvantages. For instance, in the synchronous backtracking method at any time instance, there is only one agent that assigns a value to its variable and forwards it to the next agent, according to a pre-specified priority order via an *ok?* message (i.e. typically from higher to lower). When a lower priority agent cannot find a solution that satisfies its constraint, it sends a backtracking *no-good* message to the higher priority agent to assign another value to its variable. As such, the synchronous backtracking method requires a sequential delay between different agents. This might, in turn, requires a heavy computational time to reach a solution. In contrast, in the asynchronous

backtracking method, all agents operate concurrently and evaluate their assigned variable by sending an *ok?* message to its adjacent agents. Then, each agent waits for a *good* or *no-good* message response, like the synchronous algorithm. Receiving *good* messages from other agents indicates that the assigned variable is consistent with other agents' constraints. Otherwise, a multiple negation process is performed between the violated constraint agent and its higher priority agent. Whereas, the higher agent should find another assignment for its variable and send it back to the violated constraint agent to search for a consistent variable.

The drawback in the asynchronous backtracking method is that the agents have a fixed, assigned priority order. Hence, in the case of a poor priority ordering, the lower priority agent performs an exhaustive search to assign its variable each time it receives a variable from the poor priority ordered agent. To mitigate the drawback of asynchronous backtracking, the AWC method, with dynamic priority ordering, is proposed. In AWC, when an agent fails to find a suitable assignment for its variable, 1) it sends a *no-good* message; 2) it increases its priority order; and; 3) it sends an *ok?* message containing a variable solution according to the *min-conflict heuristic* that minimize the constraints violation [98].

4.5 Forrmulation of IMG Voltage Regulation as DCS

The voltage regulation problem in IMG can be formulated as a CSP as shown in (4.15)-(4.17), where the system constraint *C*, which includes the voltage tolerance boundary at each node *i* within the IMG, the DG reactive power capacity limits and the IMG reactive power mismatch defined as:

$$C = \begin{cases} V_{lb} < V_i < V_{ub} \\ Q_{Gj} \le Q_{Gj}^{Max} \quad ,\forall j \in B_{droop} \\ \sum_j \Delta Q_{Gj} = 0 \quad ,\forall j \in B_{droop} \end{cases} \tag{4.22}$$

However, to reformulate the problem in a DCS environment as given in (4.18), C_Z is given as follows:

$$C_Z = \begin{cases} V_{lb} < V_i < V_{ub} \quad ,\forall i \in B^Z \\ Q_{Gj} \le Q_{Gj}^{Max} \quad ,\forall j \in B_{droop}^Z \end{cases} \tag{4.23}$$

and C_C is a common IMG system constraint for the reactive power balance among the droop-controlled DG units given in (4.22); where B^Z is the set of all buses within zone *z*, and B_{droop}^Z is the location set of the droop-controlled DG unit in zone *z*.

Using (4.21), the inequality voltage constraints described in (4.23) can be converted into a single inequality constraint to regulate the voltage at the location of the maximum voltage deviation represented as follows:

$$\left|\Delta V_{z,i}^{(A,A^*)} - \frac{1}{V_i}\left(V_{Gj}\Delta V_{Gj}^{(A,A^*)} - \Delta Q_{Gj}^{(A,A^*)}\sum_{n=j}^{i-1} x_n\right)\right| \le \varepsilon \tag{4.24}$$

It is worth noting that equation (4.24) is a differentiation of (3.9) with respect to ΔQ_{Gj}, where $\Delta Q_{Gj}^{(A,A^*)}$ and $\Delta V_{Gj}^{(A,A^*)}$ are the required change of reactive power generation and voltage magnitude of the droop-controlled DG unit located at bus *j* $\forall j \in B_{droop}^{Z}$to regulate bus *i* with the required $\Delta V_{z,i}^{(A,A^*)}$; ε is the acceptable bandwidth of voltage deviation to avoid excessive updates of ΔV_{Gj}^{*} in response to the dynamic changes of RDG output power generation.

4.5.1 Proposed Asynchronous Weak Commitment Algorithm

In this work, an AWC algorithm is adopted for distributed voltage regulation in droop-controlled IMGs. In the adopted algorithm, all DGAs have the same priority order during normal operating conditions. The DGA that detects voltage violation within its zone using its state estimation algorithm will increase its priority and collaborate with other adjacent DGAs to regulate the voltage. When there is more than one zone having voltage violation in the IMG system, the DGA with the maximum voltage deviation will increase its priority to be the highest priority. Therefore, any DGA that detects voltage violation within its zone will calculate the required $\Delta V_{z,i}^{(A,A^*)}$ using (4.21) to regulate its zone voltage, unless it receives different update for $\Delta V_{z,i}^{(A,A^*)}$ requested by a higher priority DGA.

According to the determined $\Delta V_{z,i}^{(A,A^*)}$, the DGA will search for the possible value assignment of its variable V_{Gj}^{*} to achieve the required $\Delta V_{z,i}^{(A,A^*)}$. As described previously, the participation of each DGA in the process of voltage regulation and in consequence the value assignment of its V_{Gj}^{*} can be modeled in the form of three possible scenarios. Hence, instead of the arbitrary value assignment of the DGA variable as well as the random search direction for the solution in the multi-agent DCS environment, those operation scenarios can be stored in the agent *view* to represent the set of possible search directions of value assignments for each DGA. As such, in order to satisfy the constraint in (4.24), a set of possible assignments $a = \{a_1, a_2, a_3\}$ for $\Delta Q_{Gj}^{(A,A^*)}$ and thus ΔV_{Gj}^{*} can be taken by the DGA given in (4.13).

where a_1, a_2 and a_3 indicate the assignment of active voltage regulation via sensitivity, response to active voltage regulation, and active voltage regulation with specified reactive power generation limits, respectively.

Based on the above premises, the highest priority DGA begins by searching the feasible value assignment(s) for voltage regulation among its agent *view*. If more than one-value assignments are feasible, the initial assigned value is selected to minimize the voltage deviation in the buses within the zone. This will in turn enforces the search direction to implicitly take the loss minimization into

consideration while searching for a feasible solution to satisfy the voltage constraints. However, optimal solution for loss minimization requires a distributed constraint optimization (DCO) algorithm, which is outside the scope of this work [98]. Based on the initial assigned value, the change of the voltage magnitude at the PZC between the highest priority DGA and its adjacent zone(s) can be estimated as follows:

$$\Delta V_{PZC}^{Z,Z_{adj}} = \frac{1}{V_{PZC}^{Z,Z_{adj}}}\left(V_{Gj}\Delta V_{Gj}^{(A,A^*)} - \Delta Q_{Gj}^{(A,A^*)} \sum_{n=j}^{PZC-1} x_n \right) \tag{4.25}$$

Similarly, the estimated required change in the reactive power flow between the highest priority DGA and its adjacent zone(s) to maintain the reactive power balance can be given as follows:

$$\sum_{Z_{adj}} \Delta Q_{PZC}^{Z,Z_{adj}} = -\Delta Q_{Gj}^{(A,A^*)} \quad , \forall j \in B_{droop}^{Z} \tag{4.26}$$

Equations (4.25) and (4.26) represent the coupling constraints that need to be met between the highest priority DGA and its adjacent DGAs. Once (4.25) and (4.26) are determined, the highest priority DGA sends *ok? message* to its adjacent DGAs with the required changes. The message contents are defined as follows:

$$\left[ID^{Z}; \Delta V_{PZC}^{Z,Z_{adj}}; \Delta Q_{PZC}^{Z,Z_{adj}}; \rho^{Z}; Ok? \right] \tag{4.27}$$

where ID^z and ρ^z are the identification number and the priority order of the sender DGA z, respectively. The recipient DGAs check the consistency of the assigned values of (4.25) and (4.26) on their zone constraints defined in (4.18)-(4.22). Toward that end, the recipient DGAs might initiate communication acts with their own adjacent DGAs in the IMG system via *ok?* messages. Then all DGAs that received *ok?* message reply to their sender DGA with either a *good* message or a *no-good* message. The *good* message means that the assigned action of the sender DGA is consistent with the adjacent DGAs' constraints. On the other hand, *no-good* message means that the adjacent DGA can't satisfy the requested changes. In the latter case, a multi-negotiation will take place. Where, the inconsistent adjacent DGAs will send back a *no-good* message then raise its priority order to send an *ok?* message with its possible value assignment based on its *min-conflict heuristic* technique, which satisfies its own constraints and minimize the voltage deviation of the sender agent. The sender DGA will search among the possible variable assignments received from the adjacent DGAs and choose the one that is consistent with its own constraints as well as the constraints of adjacent DGAs. However, in the worst-case scenario, the sender DGA will choose from the received possible assignments the one that minimizes the voltage violation of its zone based on its *min-conflict heuristic* technique. When the DGA receives back *good* messages from all its adjacent DGAs, it will send them an execute order as a confirmation that a

constraint satisfaction is reached. An *execute* order is added in this work to the AWC algorithm to terminate the voltage regulation process and avoid the execution of any further actions. The *execute* order is sent by highest priority DGA.

Figure 4.5 summarizes the main procedures of the AWC algorithm implemented in each DGA during the solution process.

when *Agent View* and *current value* are not consistent
1. **if** no value in D_{Gj} is consistent with *Agent View*
2. **then backtrack**;
3. **else check_agent_view**
6. **if** no **ok?** message is received
7. **then** ρ^z (i.e. current priority) $\leftarrow 1 + \rho_{max}^{z,z_{adj}}$
   # $\rho_{max}^{z,z_{adj}}$ is the maximal priority value over all neighbors;
8. send [ID^z; $\Delta V_{PZC}^{z,z_{adj}}$; $\Delta Q_{PZC}^{z,z_{adj}}$;$\rho^z$; **ok?**] to all neighbors;
9. **else** send [ID^z; $\Delta V_{PZC}^{z,z_{adj}}$; $\Delta Q_{PZC}^{z,z_{adj}}$;$\rho^z$; **ok?**] to $Z_{adj} \notin ok?\ sending\ ZA$;
end if; **end if**;

- procedure **check_agent_view**
  1. select $V^* \in D_{Gj}$ (i.e. Using (31)-(32)) where *Agent View* and V^* are consistent **and** V^* minimizes the violated constraints
  2. $V_{Gj}^* \leftarrow V^*$;
  3. determine effect of ΔV_{Gj}^* on $\Delta V_{PZC}^{Z,Z_{adj}}$
- procedure **backtrack**
  1. send *no-good* to the agents with inconsistent variables
  2. $\rho^z \leftarrow 1 + \rho_{max}^{z,z_{adj}}$
  3. **check_agent_view**
  4. send [ID^z; $\Delta V_{PZC}^{z,z_{adj}}$; $\Delta Q_{PZC}^{z,z_{adj}}$;$\rho^z$; **ok?**] to all neighbors;

Figure 4.5 The proposed AWC algorithm implemented in each DGA

4.6 Forrmulation of DCS for Equal Reactive Power Sharing in IMGs

Figure 4.6 shows an example of the directed graph communication model as discussed earlier in section 4.2 for reactive power between three DG control agents. As shown, the information flow is designed based on a specific priority order scheme. The priority order ρ is assigned in a way that each control agent l or a group of control agents (e.g. parallel DG units share a common PCC) has a direct edge with a higher priority control agent j. Such control agent with the higher priority operates as an aggregator agent. It collects the generated reactive power in the current operating point, Q_{Gl}^{A}, and the specified units of sharing (h_l) from its lower priority in-neighbors. Then, it calculates the average reactive power per sharing unit ($Q_{sh,j}$) and the total number of sharing units (h_{Tj}) for the aggregation including itself, as follows:

$$Q_{sh,j} = \frac{Q_{Gj}^{A}}{h_j} + \sum_{\forall l \in N_j^{in}} \frac{\Lambda_{jl} \times Q_{Gl}^{A}}{h_l} \tag{4.28}$$

$$h_{Tj} = h_j + a_{jl} \sum_{\forall l \in N_j^{in}} h_l \tag{4.29}$$

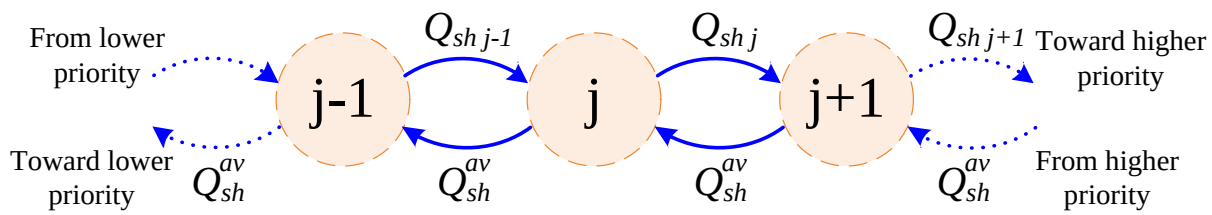

Figure 4.6 A directed graph communication model for the synchronization process

As shown in the figure, the information flow continues until the highest priority agent in the entire IMG is reached. Next, the highest priority agent determines the overall average reactive power per unit sharing Q_{Gj}^{av} and the overall number of sharing units for the entire IMG h_T using (4.28)-(4.29). Using such information, each control agent can determine the required change in its reactive power generation to correct the sharing as follows:

$$\Delta Q_{Gj}^{(A,A^*)} = h_j \times Q_{Gj}^{av} - Q_{Gj}^{A} \tag{4.30}$$

where Q_{Gj}^{A} is the steady-state reactive power generation of DG *j* prior to the sharing correction.

To that end, the reactive power sharing problem in IMG can be formulated as a CSP as shown in (4.15)-(4.17), where the system constraint *C* that contains the reactive power sharing correction, the DG reactive power capacity limits, the IMG reactive power mismatch, and the voltage tolerance boundary at each node *i* within the IMG, defined as follows:

$$C = \begin{cases} \Delta Q_{Gj} = \Delta Q_{Gj}^{(A,A^*)} & ,\forall j \in B_{droop} \\ Q_{Gj} \le Q_{Gj}^{Max} & ,\forall j \in B_{droop} \\ \sum_j \Delta Q_{Gj} = 0 & ,\forall j \in B_{droop} \\ V_{lb} < V_i < V_{ub} & \end{cases} \tag{4.31}$$

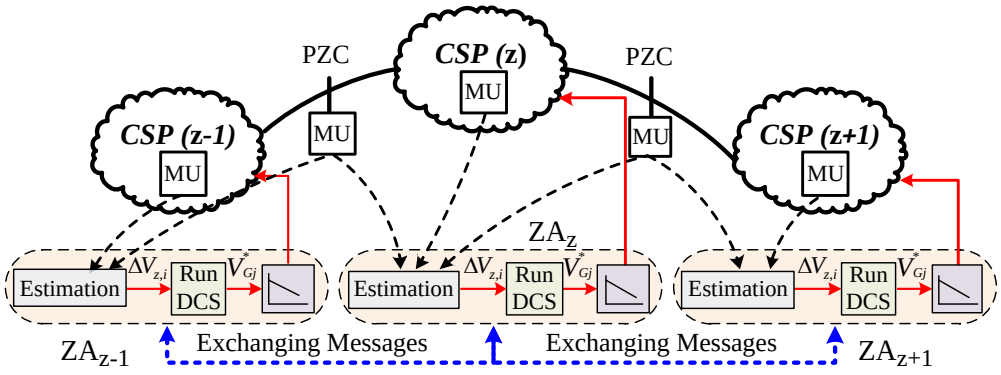

Figure 4.7 A schematic diagram of the proposed DCS problem formulation

However, the problem can be converted to a decentralized environment by clustering the IMG to a set of zones as discussed previously in this chapter in section 4.3, where each control agent is assigned to a zone to satisfy its constraint.

Figure 4.7 shows a schematic diagram of the proposed distributed control structure for IMG systems. As shown in the figure, each zone is connected with its adjacent zone(s) (e.g., upstream and downstream) at the point of zones coupling (PZC). Each DGA updates its agent-view by estimating the voltage profile of its zone each time it receives real-time measurements (i.e. from local measurements at the DG location and remote measurements at PZCs and load points). Each DGA_z located at bus j has a control variable V_{Gj}^{*} with a defined domain D_{Gj} to satisfy its zone network constraints. Therefore, reformulate the problem in a DCS environment as given in (4.18), C_Z is given as follows:

$$C_Z = \begin{cases} Q_{Gj}^{av} h_j - Q_{Gj}^{A} - \Delta Q_{Gj}^{(A,A^*)} = 0 \quad , \forall j \in B_{droop}^{Z} \\ Q_{Gj} \le Q_{Gj}^{Max} \quad , \forall j \in B_{droop}^{Z} \\ V_{lb} < V_i < V_{ub} \quad , \forall j \in B_{droop}^{Z} \end{cases} \tag{4.32}$$

It is worth noting that the inequality voltage constraints described in (4.32) can be converted into a single inequality constraint to regulate the voltage at the location of the maximum voltage deviation within the zone represented mathematically as given (4.24). Similarly, the system reactive power balance constraint C_C is represented as distributed voltage constraints at the PZCs between the identified zones will be given as (4.25).

4.6.1 Reactive Power Sharing Proposed Algorithm

In this work, a modified AWC algorithm is adopted for appropriate reactive power sharing in droop-controlled IMGs. First, at each specified time interval, the synchronization of process described in section III is triggered for the correction of reactive power sharing with the a specified ordering heuristic (i.e. the specified priority order is chosen in such a way that each DGA has only one higher DGA to send its calculated sharing of the reactive power and the total sharing ratio of its lower priority DGA neighbors). Once the system highest priority DGA determines the average reactive power sharing (Q_{Gj}^{av}), it calculates the required change of its reactive power generation $Q_{Gj}^{(A,A^*)}$ to correct its reactive power sharing using

(4.30). Next, it arbitrary chooses one of the actions given in (4.13) to determine its initial value assignment V_{Gj}^{*}. The assigned value must satisfy its own constraints given in (4.32). Then, it calculates the required change of the voltage magnitude at its PZCs according to the value assignment and sends an *ok?* message to is adjacent DGAs with the following contents:

$$\left[ID^{Z};\rho^{Z};\Delta Q_{PZC}^{av};h_{T};\Delta V_{PZC}^{Z,Z_{adj}};Ok?\right] \tag{4.33}$$

Based on (4.33), the recipient DGAs search for their values assignment that satisfy their own zone constraints defined in (4.32) as well as the new PZC constraint defined by the sender DGA. Toward that end, the recipient DGAs might initiate communication acts with their lower priority adjacent DGAs in the IMG system via *ok?* messages. All DGAs that received *ok?* message reply to their sender DGA with either a *good* message or a *no-good* message. The *good* message indicates that the value assignment of the sender DGA is consistent with the recipient DGAs' constraints. On the other hand, *no-good* message means that the recipient DGA cannot satisfy the specified PZCs constraint. In the latter case, a multi-negotiation process among the DGAs takes place; where, the inconsistent adjacent DGA sends back a *no-good* message then moves its propriety order to the top place among its adjacent DGAs. Next, it sends an *ok?* message with its possible value assignment based on its *agent-view*. Such backtracking procedure is continued until a solution

is found. Here it is worth noting that a solution, at which the satisfaction of both reactive power sharing and voltage constraints occurs, might be infeasible. Hence, in order to avoid the termination of the AWC algorithm when no solution is found, a *min-conflict heuristic* technique is implemented in this work. In this regard, each DGA can update its sharing ratio h_j based on its *min-conflict heuristic* to satisfy its voltage constraints as follows:

$$h_{j,new} = \frac{Q_{Gj,new}^{A*}}{h_T Q_{sh}^{av} - Q_{Gj,new}^{A*}} \left(h_T - h_j \right) \tag{4.34}$$

where $Q_{Gj,new}^{A*}$ is the new target point of the reactive power generation to satisfy the voltage constraints. In this case, the DGA recalculates the average system reactive power sharing to ensure the satisfaction of its constraints as follows:

$$Q_{sh,new}^{av} = \frac{h_T Q_{sh}^{av} - Q_{Gj,new}^{A*}}{h_T - h_j} \tag{4.35}$$

Using (4.34)-(4.35), the DGA sends an *ok?* message that contains $Q_{sh,new}^{av}$ and $h_{j,new}$ as in (31) to its adjacent DGAs. When the DGA receives back *good* messages from all its adjacent DGAs, it sends them an *execute* order as a confirmation that a solution is reached. The *execute* order is added in this work to the AWC algorithm to terminate the general agreement of the reactive power sharing process between the DGAs and avoid the execution of any further actions. The *execute* order is sent

by the highest priority DGA, and after executions all DGAs reset their priority to their pre-specified order and operate in the idle state.

4.7 Performance Measurment of the Proposed AWC

Evaluating the computational efforts of an algorithm is typically inspired by the need to calculate the running time from starting until it returns with a satisfying solution. However, there are many factors that might affect the running time of an algorithm; among which the most prominent are the machine (e.g. computer) characteristics and the way the algorithm is implemented [100]. To alleviate this issue, standard CSP algorithms are normally measured by the number of constraints checks (CC) they perform while searching for a solution [98]. From this perspective, the number of performed CCs can be defined as a machine and implementation independent measure for CSP algorithms, where it counts the main computing operation of all backtracking algorithms [101].

Unlike CSP algorithms, counting the CCs is not a viable metric for evaluating the performance of DCS problems as it does not consider: 1) the simultaneous constrained checks that occur when the agents run concurrently, 2) the time intervals in which agents wait for other agents to complete their computations, and 3) the time required for sending, receiving, and delivering a message [98]. For these reasons, a cycle-based performance evaluation method

has been proposed in [97] for DCS algorithms. In such method, the process time of the DCS and delivering a message [98]. For these reasons, a cycle-based performance evaluation method has been proposed in [97] for DCS algorithms. In such method, the process time of the DCS algorithm is divided into cycles, where one cycle of computation corresponds to a set of actions performed by at least one agent starting by receiving the incoming messages, processing its calculations and actions then sending back messages with its decision. The cycle-based method creates a discrete event simulation model for measuring the performance of DCS algorithms. Each agent maintains its own simulated clock and its time is incremented by one simulated time unit whenever it performs one cycle of computation. Hence, the performance of a DCS algorithm is evaluated in terms of the number of cycles required to solve the problem [97], [102]. It is noted that the number of counted cycles in DCS algorithms is utilized as a combined measure of both communication and computational costs as there is no standard way for measuring them individually [97], [98], [100]. One drawback of the cycle-based method is that it does not take into account the impacts of message delay on the algorithms performance. However, the study in [98] showed that asynchronous-based DCS algorithms (e.g. AWC) are less affected to messages delays compared to synchronous-based DCS algorithms. Furthermore, the application of DCS algorithm in this work requires a non-critical low-bandwidth communication. As

such, the operational message delay can have a negligible effect on the latency when an appropriate medium access control for low-bandwidth communication exists [95].

The number of cycles in a DCS problem is mainly dependent on its scale (i.e. the number of agents, variables and constraints) and the applied DCS algorithm. Several studies have been conducted in the literature to evaluate the performance of a variety of DCS algorithms in both small and large-scale DCS problems [97], [102]. These studies proved the superiority, robustness and scalability of AWC over other DCS algorithms. The authors in [97] showed that an average of 42 cycles is required for an AWC algorithm to solve a DCS problem that consists of 10 agents, 1 variable and 1 constraint. The authors also showed that the number of cycles of asynchronous search is approximately linearly proportional to the number of agents [102], [103]. Based on the aforementioned discussion, the number of cycles is utilized in this work as an indicator for the performance of the proposed AWC algorithm as will be illustrated in the simulation results.

4.8 Case Studies

4.8.1 Voltage Regulation in IMG Using DCS

In this section, simulation studies have been carried out in a MATLAB environment to validate the effectiveness and performance of the proposed

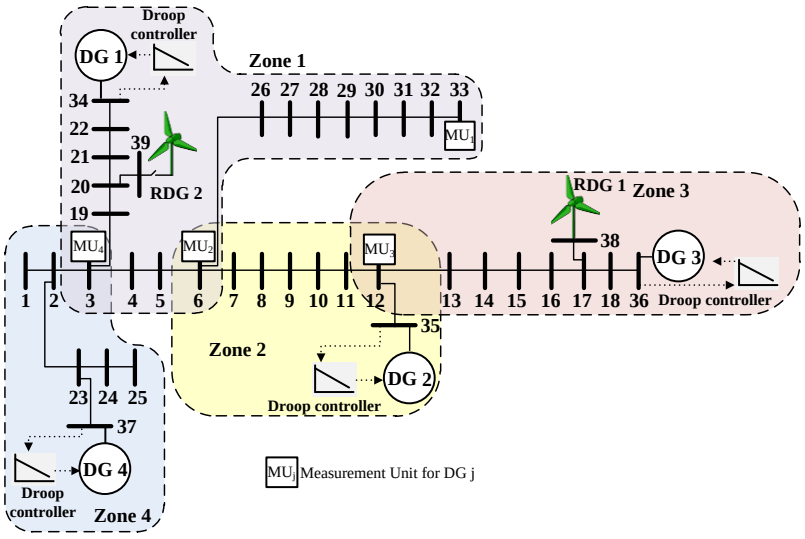

Figure 4.8 The 38-bus distribution test feeder configured to operate in islanded mode

distributed voltage regulation scheme. A 38-bus distribution test feeder has been used in the case studies to simulate an IMG [7]. Figure 4.8 shows a single line diagram of the test system. As shown in the figure, the test system has four dispatchable DG units, located at buses 34, 35, 36 and 37, with interconnection impedance of *0.003113+0.003113j*. The DG units are assumed to be identical, of equal size, consisting of 3 MVA and a minimum power factor of 0.7. The active and reactive power static droop gains, m_p and n_q, are selected to be $9x10^{-4}$ and *0.0333* per unit for each droop-controlled DG unit, respectively [7]. ω^* is set at 1.0 per unit for all DG units.

The IMG system is divided into four zones. Each zone is assigned for a droop-controlled DG unit. Remote measurement units are placed at the PZCs and

the end of the feeder laterals. An intelligent agent (DGA) is defined for each zone and located at the droop-controlled DG unit. Here, it is worth noting that several technical factors might affect the choice of the zone boundaries of each DGA (e.g. supply adequacy, protection, and communication) [16], [16], [95], [104], [105]. Similar to the work in [16], the zone boundaries are chosen in this paper to balance the parallel computation burden among the DGAs during the distributed state estimation process of the voltage profile, described in this chapter in Section 4.3. In this regard, each DGA should be able to continuously monitor the voltage profile and detect any voltage violation within its assigned zone, in comparable time with other DGAs [16]. However, other factors, such as those presented in [95], [104], [105] can still dominate the choice of zone boundaries, without a considerable impact on the performance of the proposed algorithm, as proven in this section.

Three case studies have been carried out in this section. The first and second case studies test the effectiveness of the proposed AWC algorithm under different loading conditions and penetration levels of RDGs. The third case study tests the performance of the AWC when different zone configurations are chosen.

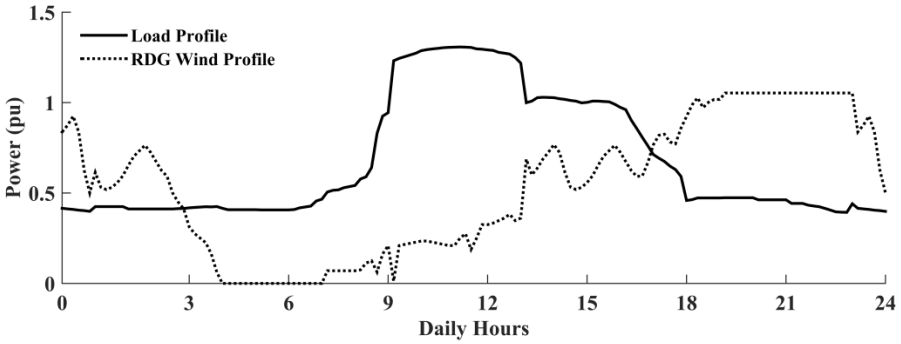

Figure 4.9 Normalized load and wind power generation for the day under study

I. First Case Study: Voltage Violation Occurs at Adjacent Zones

In this case study, a 1.5 MVA wind-based RDG_1 is installed at bus 38, as shown in Figure 4.8. Figure 4.9 shows the normalized load and wind power generation profile for a typical studied day in 10-minute time intervals. Two operation scenarios have been conducted to show the effectiveness of the proposed scheme. The first scenario represents the base case scenario, without the proposed scheme, at which the no-load reference voltage for all droop-controlled DG units is set at a fixed value of 1.02 p.u., during the studied day. In the second scenario, the proposed voltage regulation scheme is implemented. Figure 4.10 and Figure 4.11 show the minimum and maximum bus voltages in the IMG test system for the studied day, with and without the proposed voltage regulation scheme. As shown in the figures, both undervoltages and overvoltages occurred in the first scenario when a fixed setting of the no-load reference voltage is applied during the periods of 1) peak loading; and 2) light loading and high generation, respectively.

The figures also show that the proposed DCS approach is able to satisfy the voltage constraints in all operating conditions. A detailed description of the AWC iterative solution for the formulated DCS problem is presented herewith.

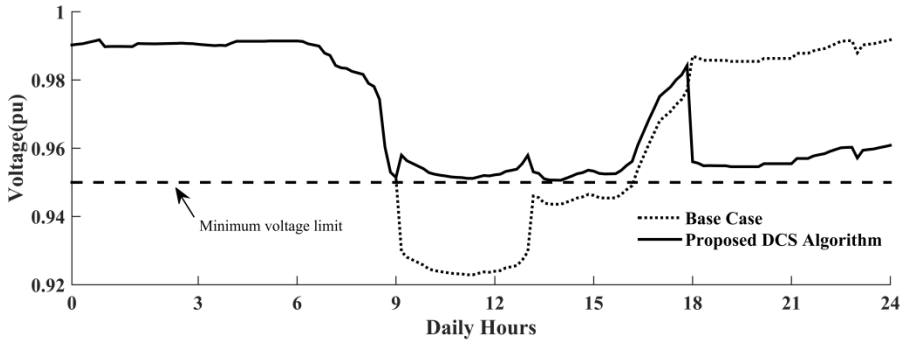

Figure 4.10 Minimum bus voltage without and with using the DCS algorithm

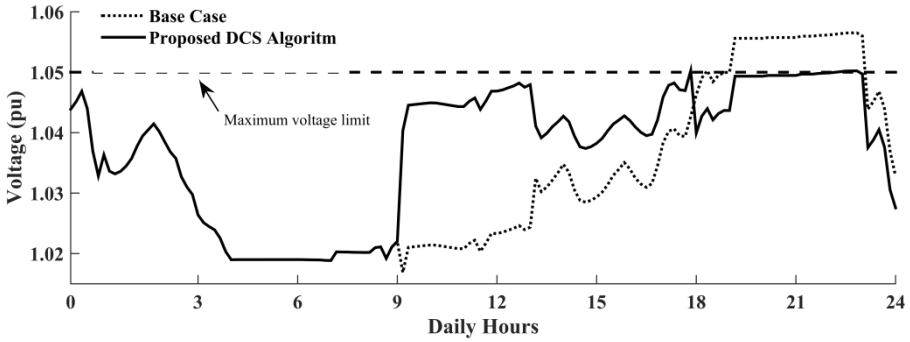

Figure 4.11 Maximum bus voltage before and after using the DCS algorithm during the day under study

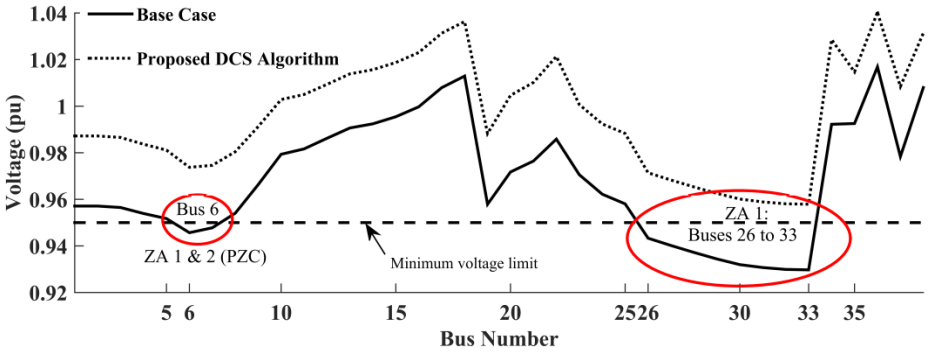

Figure 4.12 System voltage profile at the time of undervoltage occurrence

Figure 4.12 shows the voltage profile at 10:10 am, i.e., the time instant at which undervoltages started to occur with fixed settings. As shown in the figure, buses 26 to 33 located in zone one and bus 6 (a PZC between zones one and two), suffered from undervoltages. Figure 4.13 shows the AWC exchanging messages between the DGAs to regulate the voltage at that time. First, using the state estimation algorithm described in (4.19)-(4.21), DGA_1 detected an undervoltage violation at that time with a maximum voltage deviation of 0.02 p.u., located at bus 33. At the same time instant, DGA_2 detected an undervoltage only at bus 6, with 0.005 p.u. According to the proposed AWC approach, once DGA_1 and DGA_2 detected undervoltages in their zones, they increased their priority orders. Based on its view, DGA_1 aimed to increase the voltage at bus 6 by 0.03 p.u. using (4.13) so that bus 33, at which the maximum deviation occurred, could reach 0.96 p.u with $\varepsilon = 1\%$. However, from *DGA_2-view*, the voltage at bus 6 is required to be boosted with 0.015 p.u. For this reason, DGA_1 and DGA_2, that updated their priority orders,

exchanged the required voltage change at their PZC via *inform* messages in order to update their views and adjust their priority orders accordingly, as shown in Fig. 12. After the message exchange, DGA_2 updated its view to increase the voltage at bus 6 with 0.03, instead of 0.015 p.u. Also, DGA_1 raised its priority in order to be higher than DGA_2, where it had a higher voltage deviation compared with DGA_2. It is noted that the priority orders of DGA_3 and DGA_4 were still set at zero. At step S3, DGA_1, the highest priority agent, assessed the set of feasible assignments in (4.25) to satisfy the voltage constraint within its zone. Table 4-1 shows that a_2 and a_3 are feasible, while a_1 is infeasible in this scenario. As illustrated in the proposed AWC algorithm, the initial assignment is the one that minimizes the voltage deviation in the buses within the zone. As such, DGA_1 assigned a_1 and then calculated: 1) the required change for the voltage magnitude at the PZCs with its adjacent DGAs using (4.26), and; 2) the required change of the reactive power generation within its zone (ΔQ_{G1}), as shown in Table 4-1.

Table 4-1 Possible value assignments of DGA_1 in S3

View of DGA_1	a_1	a_2	a_3
ΔV_{G1}	Generation limit Infeasibility	0.0154	0.0286
ΔV_{G1}^{*}		0	0.0286
ΔQ_{G1}		-0.463	0
ΔV_3		0.026	0.0297
$(\Delta V_6 - \Delta V_{G1})$		0.0145	1.42e-3

At *S4*, DGA_1 sends *ok?* message to its adjacent DGAs to achieve the required change of the voltage magnitude at their PZCs. It also requested a reactive power generation change of +0.463 MVar and zero from DGA_2 and DGA_4, respectively, to maintain the reactive power balance in the IMG system. At *S5*, both DGA_2 and DGA_4 started parallel processing, from their views, to check the feasibility of the new variable assignments of DGA_1 from their own constraints. DGA_4 found that the value assignment of DGA_1 was consistent with its assigned variable, thus it sent a *good* message to DGA_1. The assessment of DGA_2 can be undertaken by calculating the required change of its ΔV_{G2}^{*} to set $\Delta V_6 = 0.03$ p. u. and $\Delta Q_{G2} = 0.463\ MVar$. First, the required voltage change at the location of DG2 can be calculated at the specified ΔV_6 and ΔQ_{G2} using (4.25) as ΔV_{G2}=0.03736 p.u. Then, (4.11) is used to calculate ΔV_{G2}^{*}. The calculation showed that the assignment of DGA_1 is consistent with DGA_2. However, before sending a *good* message to DGA_1, DGA_2 sent an "*ok?*" message to its downstream adjacent agent DGA_3, containing the expected changes of their PZC, due to its new variable assignment, i.e., $\Delta V_{12} = 0.03617$. At *S6*, DGA_3 viewed that at $\Delta V_{12} = 0.03617$ and $\Delta Q_{G3} = 0$, its zone constraints would be violated due to an overvoltage at the PCC of DG3. Hence, DGA_3 sent a *no-good* message to DGA_2 and then raised its priority order to be higher than DGA_2. Using the *min-conflict heuristic*, DGA_3 calculated the required variable assignment in order to: 1) minimize the deviation from the

required ΔV_{12} and; 2) maintain the voltage magnitude at DG3 PCC within the allowed maximum limits. DGA_3 viewed that this action could be achieved when $\Delta V_{G3} = \Delta V_{G3}^* = 0.0237$ at $\Delta Q_{G3} = 0$. As such, DGA_3 sent an *ok?* message to DGA_2 with the required changes to $\Delta V_{12} = 0.0237$.

At *S7*, DGA_2 viewed that in order to be consistent with the value assignments of DGA_3, it had to achieve the following changes: $\Delta Q_{G2} = -0.31713$ MVar,$\Delta V_{G2} = 0.012$, and $\Delta V_{G2}^* = 0.02254$. However, this value is inconsistent with DGA_1 *ok?* message at *S4*. For this reason, DGA_2 raised its priority order to be higher than DGA_1 and responded to DGA_1 with a *no-good* message, followed with an *ok?* message with the required $\Delta Q_{G1} = 0.31713$ at $\Delta V_6 = 0.03$ in order to 1) achieve the reactive power balance, and; 2) satisfy the voltage regulation requirements. Then, at *S8*; DGA_1 performed its calculation process to set $\Delta Q_{G1} = 0.31713$ and $\Delta V_6 = 0.03$, and found using (4.26) and (4.2) that it should show $\Delta V_{G1} = 0.0373$, and $\Delta V_{G1}^* = 0.0478$. DGA_1 sent an "*ok*" message to DGA_4 containing the new required change of their PZC at bus 3 (i.e. $\Delta V_3 = 0.0319$ and $\Delta Q_{G4} = 0$). At *S9*, DGA4 viewed that it can satisfy the requested change by setting $\Delta V_{G4}^* = 0.031183$ and thus it sent a *good* message to DGA_1. By consequence, DGA_1 also sent a *good* message to DGA_2, the highest priority agent. Once the highest priority agent received a *good* message, it broadcasted an *execute*

order for all DGAs to regulate the voltage, using the assigned variables. This message indicated that all DGAs converged to a consensus for their variable assignments to satisfy the constraints.

As shown in Figure 4.13, the proposed AWC algorithm converged in 9 cycles. Similar exchanging messages occurred during the overvoltages at 14:10 and 19:00, but are not shown to avoid duplication.

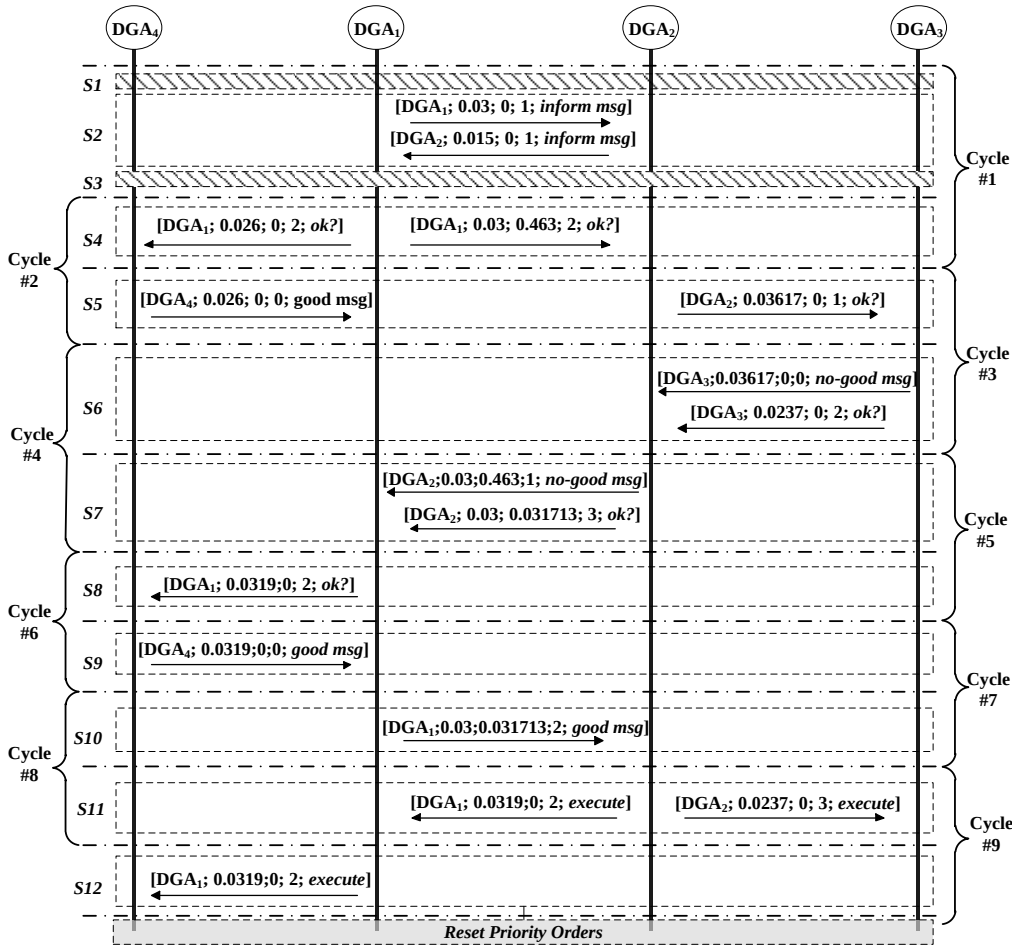

Figure 4.13 AWC exchanging messages among the DGAs at 10:10

Table 4-2 Summary of the DGA variable assignments for first case study

Event	*At 10:10*			*At 14:10*			*At 19:00*		
	ΔV_G*	ΔQ_{Gj}	ΔV_{Gj}	ΔV_G*	ΔQ_{Gj}	ΔV_{Gj}	ΔV_G*	ΔQ_{Gj}	ΔV_{Gj}
DGA_1	0.0478	0.317	0.0373	-0.0195	0	-0.019	-0.0812	-0.7	- 0.058
DGA_2	0.012	-0.317	0.0225	-0.031	-0.24	0.024	-9.9e-3	+0.45	0.025
DGA_3	0.0237	0	0.0237	-8.7e-3	0.24	-0.016	1.9e-3	+0.4	1.9e-3
DGA_4	0.0312	0	0.0312	-0.02	0	-0.02	-0.0512	-0.15	- 0.048

The solution for the DCS problem for both undervoltage and overvoltage scenarios are shown in Table 4-2.

II. Second Case Study: Voltage Violation Occurs at Non-Adjacent Zones

This case study aims to test the performance of the proposed AWC algorithm when voltage violation occurs at non-adjacent zones, simultaneously. To simulate this case study, two wind-based RDGs are installed at buses 38 and 39, with a capacity of 0.6 and 1.2 MVA, respectively. Both the load and generation profiles are assumed to be the same as the first case study. At 10:10, similar to the first case study, an undervoltage at high load demand and low wind generation occurred where, Table 4-3 shows the solution for the DCS problem at that time. After, applying the new DCS settings (i.e.V_{Gj}^{*}) at 10:10, an overvoltage occurred at 19:00 in two non-adjacent zones (zones 1 and 3) due to high wind generation for both RDG_1 and RDG_2.

Table 4-3 Summary of the DGA variable assignments for second case

	At 10:10			*At 19:00*		
	ΔV_G*	ΔQ_{Gj}	ΔV_{Gj}	ΔV_G*	ΔQ_{Gj}	ΔV_{Gj}
DGA_1	0.0373	0.186	0.031	- 0.0189	0	- 0.01899
DGA_2	0.016	-0.186	0.0225	-0.0193	0	-0.0193
DGA_3	0.023	0	0.023	-0.01905	0	-0.01905
DGA_4	0.0274	0	0.0274	- 0.01932	0	- 0.01932

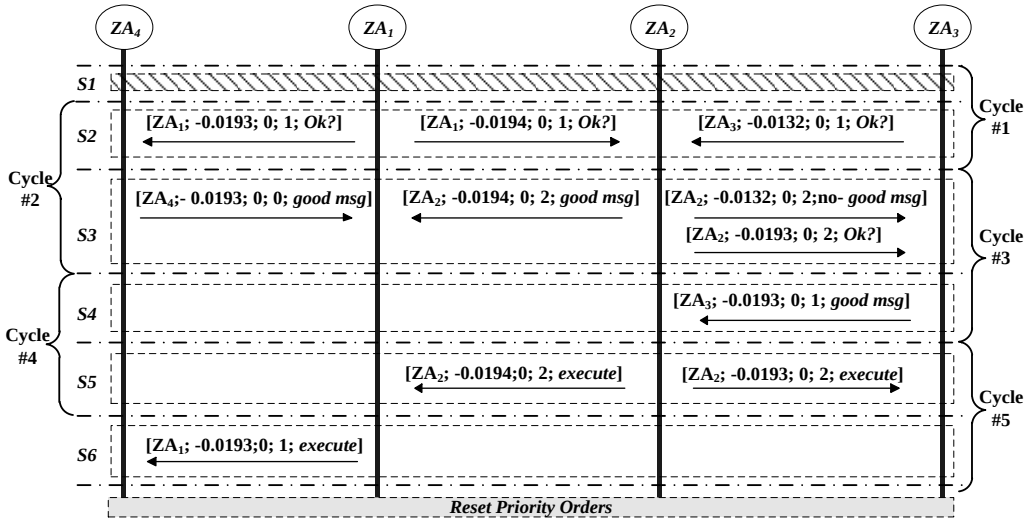

Figure 4.14 AWC exchanging messages among the DGAs at 19:00

Figure 4.14 shows the AWC exchanging messages among the DGAs to regulate the voltage at that time. As depicted in the figure, at *S1* both DGA_1 and DGA_3 detected overvoltages at buses 39 and 38, with 1.059 and 1.053 per unit voltage, respectively. Then, both of them raised their priority orders to *1*, and chose a regulation action that enhanced their own zone voltage profiles and reduced the overvoltage value with $\varepsilon = 1\%$. In the solution process, it was found that DGA_1 chose to reduce its own node voltage with $\Delta V_{G1} = \Delta V_{G1}^{*} = -0.01899$ at $\Delta Q_{G1} = 0$,

then sent an *ok?* message to its adjacent zones, using the expected changes of their PZC due to its new variable assignment, i.e. $\Delta V_3 = -0.0193$ and $\Delta V_6 = -0.0194$. Similarly, DGA_3 chose assignment a_3 with $\Delta V_{G3} = \Delta V_{G3}^* = -0.013$ at $\Delta Q_{G3} = 0$, which affected its adjacent zone (Zone 2) with $\Delta V_{12} = -0.0132$. At *S2*, both DGA_1 and DGA_3 sent an *ok?* message with the required change at the PZC of their adjacent zones. At *S3*, DGA_4 processed its calculation and found that it could satisfy the DGA_1 requirement at $\Delta V_{G4}^* = -0.0193$ and thus responded with a *good* message. However, at the same step, DGA_2 failed to satisfy both requirements from DGA_1 and DGA_3. Consequently, DGA_2 chose an assignment that satisfied the DGA_1 assignment, and sent a *no-good* message to DGA_3. After DGA_2 sent a *no-good* message and raised its priority order, it sent an *ok?* message with the change needed at their PZC that satisfied DGA_1 constraints i.e. $\Delta V_{12} = -0.0193$. At *S4*, DGA_3 found that it could satisfy the DGA_2 assignment as it still reduced the overvoltage value within $\varepsilon = 1\%$ range at $\Delta V_{G3}^* = -0.019$, and thus it sent a *good* message to the highest priority agent, DGA_2. Once the highest priority agent received a *good* message from all of its neighbours at *S6*, it broadcasted an *execute* order for all adjacent DGAs to regulate the voltage using the assigned variables. It has been noted from this case study, that the number of agents that detected voltage violation simultaneously, even if they were non-adjacent, had no significant impact on the performance of the algorithm. As shown in Figure 4.14 the number of

executed cycles to reach a solution was found to be 5; which is fewer than the number of cycles found for the first case study.

4.8.2 Performance Evaluation of the Algorithm and the Impact of zoning

The performance of the proposed algorithm for voltage and reactive power control is carried out by evaluating the previous case study (i.e. Voltage regulation in IMG using DCS). In this case study, the first and second case studies have been carried out for three different zone configurations in order to evaluate the impact of the zone boundaries on the performance of the proposed AWC algorithm. Zone configuration #1 is the original configuration shown in Figure 4.8. In the second zone configuration, the distribution feeder lateral from buses 26 to 33 is assigned to DGA_2 (i.e. zone 2) with the same *PZC* between the DGAs. The difference between the second and third configurations is that in the latter configuration, the lateral from bus 4 to 6 is assigned to DGA_2 instead of DGA_1 (i.e. reallocated to be in zone 2). Table 4-4 presents the violated zones and number of executed cycles for each operation scenario in each case study at different zone configurations. As shown in the table, the impact of zone boundaries on the performance of the proposed AWC is almost neglected. The reason is that zone a configuration affects only the initial guess of the solution (i.e. depending on which DGA(s) that detect the voltage violation and hence has higher priority as well as the adjacent DGAs).

Such change in the initial guess might change the direction of the search in the solution space and thus the number of cycles and the reached solution in the constraint satisfaction problems. However, changing the initial guess (i.e. zone configurations) has limited impact in the number of cycles for small scale multi-agent systems [34]. Table 4-4 shows that for the same event and by changing the zone configuration from 1 to 2, a different assignment for ΔV_{Gj}^{*} might be found. Also, the table shows that configuration 3 gives the same results as 2, where the DGAs that detected the violation in both aforementioned configurations are the same. The only different between configuration 2 and 3 is that at configuration 2, DGA_1 is between DGA_2 and DGA_4 and is able to communicate with both of them, while at configuration 3, DGA_4 is between DGA_1 and DGA_2. Given that, at zone configuration 2 and 3, DGA_1 and DGA_4 did not send any no-good message.

Table 4-4 Cycles number

	First Case study			*Second Case Study*	
Event Time	10:10	14:10	19:00	10:10	19:00
Type of violation	UV	OV	OV	UV	OV
Zone Configuration #1	9	7	9	9	5
Zone Configuration #2	8	7	9	8	6
Zone Configuration #3	8	7	9	8	6
Violated zones #	2	1	1	2	2

i.e UV=undervoltage and OV=Overvoltage

Table 4-5 Variable assignments

	First Case study	*Second Case Study*	
Time	*At 10:10*	*At 10:10*	*At 19:00*
DGA_1	0.0623	0.0562	-0.0245
DGA_2	0	0	-0.0253
DGA_3	0.02	-0.01811	-0.0249
DGA_4	0.031	0.02936	-0.025

The same cycles will be maintained regardless of which DGA passed the information to whom, as long as there is no DGA will go to any further negotiation (i.e. accept the assignment and send good message). Although the exchanging messages are different, the results in Table 4-5 show that the numbers of cycles for the three configurations are almost the same.

4.8.3 Reactive Power sharing in IMG Using DCS

In this section, simulation studies have been carried out in MATLAB environment to validate the proposed approach. A 37-bus distribution test feeder has been used in the case studies to simulate an IMG [16]. Figure 4.15 shows a single line diagram of the test system. As shown in the figure, the test system has four dispatchable DG units located at buses 34, 35, 36 and 37, with interconnection impedance of *0.003113+0.003113j*. All DG units are assumed to have a minimum power factor of 0.7. The IMG system is divided into four zones. Each zone is assigned for a droop-controlled DG unit. Remote measurement units are placed at

the PZCs and the end of the feeder laterals. An intelligent agent is defined for each zone located at the droop-controlled DG unit. Table 4-6 shows the ratings of DGs, the droop parameters that are designed to share the loads according to the DG ratings using (3.3)-(3.6), the specified DGs priority order when the proposed algorithm is applied, and the PZCs between the adjacent zones.

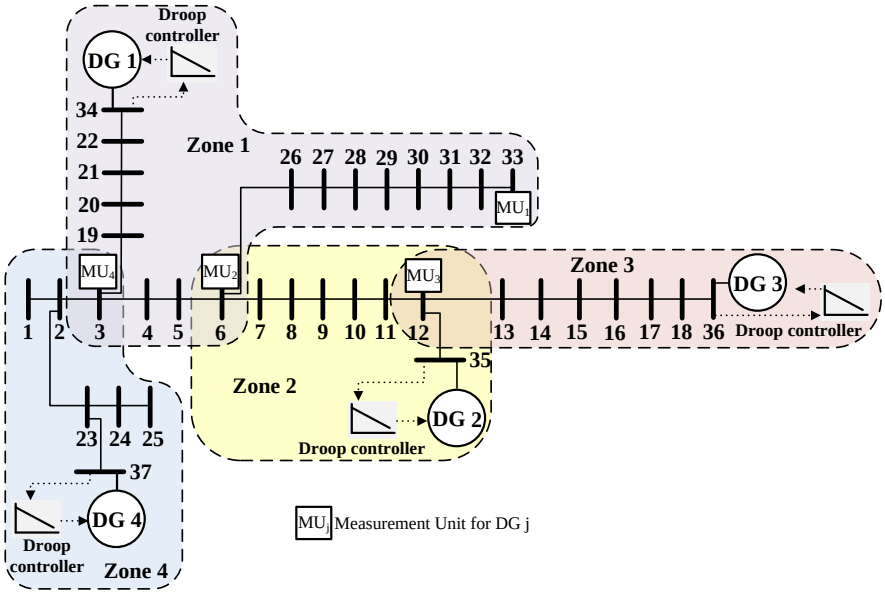

Figure 4.15 The 37-bus distribution test feeder configured to operate in islanded mode

Table 4-6 DGs location and parameters

	location	*Rating*	V_j^*	ω_j^*	m_{pj}	n_{qj}	*priority order*	*(PZC bus,DG#)*
DG 1	34	4 MVA	1.03	1	$6.7561e^{-4}$	0.025	3	(3,4)-(6,2)
DG 2	35	4 MVA	1.03	1	$6.7561e^{-4}$	0.025	2	(6,1)-(12,3)
DG 3	36	2 MVA	1.03	1	0.0014	0.05	1	(12,2)
DG 4	37	2 MVA	1.03	1	0.0014	0.05	1	(3,1)

Four consecutive operating scenarios were simulated to test the effectiveness of the proposed approach. In the first, second and third operating scenarios, the loading levels were assumed to be 65%, 85% and 100% of full load, respectively. In the fourth operating scenario, an outage of DG 3 occurred at a 90% loading level. Table 4-7 and Table 4-8 show the settings of the no-load reference voltages of the DGs and the voltage magnitudes at their PCCs for the four operating scenarios, respectively.

Table 4-7 DGs reference no-load voltage for the studied scenarios

V_G*	*Case #1*	*Case #2*	*Case #3*	*Case #4*
DG 1	1.0395	1.0475	1.0785	1.0785
DG 2	1.0425	1.05	1.074	1.051
DG 3	1.06	1.0744	1.0549	Null
DG 4	1.002	0.99928	1.02128	1.016537

Table 4-8 DGs voltage magnitude at the studied scenarios

V_{PCC}	*Case #1*	*Case #2*	*Case #3*	*Case #4*
DG 1	1.02	1.022	1.044	1.044
DG 2	1.023	1.026	1.039	1.017
DG 3	1.04	1.049	1.049	null
DG 4	0.982	0.973	0.986	0.985

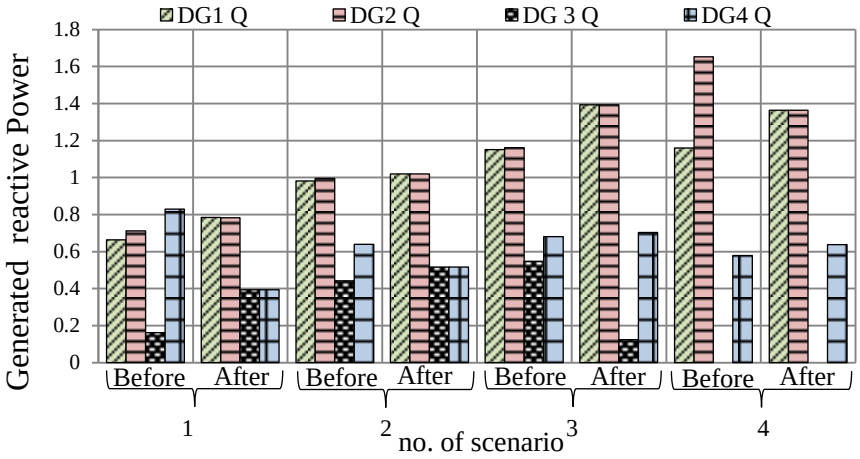

Figure 4.16 DG reactive power generation before and after applying the DCS

Figure 4.16 shows the generated reactive power of each DG unit before and after applying the proposed DCS approach for the four scenarios. As shown in the figure, with the pre-specified settings of V_G^* in Table 4-6, inexact reactive power sharing occurred in the first operation scenario at 65% loading level. When the synchronization of process was triggered, each DGA sent its information (i.e. h_j and $Q_{G,j}$) to its higher priority DGA as described in this Chapter in Section 4.2. Once the information was received by the agent with highest priority order (i.e. DGA_1), it determined the total sharing units of the system (i.e. $h_{T,f} = 12$) and the average reactive power per unit sharing (i.e.$Q_{sh}^{av} = 0.197\ MVA$) using (20)-(21), respectively. DGA_1 then determined the required change of its reactive power generation (i.e. $\Delta Q_{G1}^{(A,A^*)} = 0.126\ MVA$) and chosen action a_1 in (17) as an initial assignment for its control variable V_{DG1}^*. Using a_1 in (17), it determined the

required change of the voltage at 1) its PCC (i.e.$\Delta V_{G1}^{(A,A^*)} = 0.00635\, p.u$), and 2) its PZCs with zones 2 and 4. It also determined the required change in its no-load reference voltage (i.e. $\Delta V_{G1}^{*} = 9.525e^{-3}$). Next, DGA_1 sent an *ok?* message containing Q_{sh}^{av} and $\Delta V_{PZC}^{Z,Z_{adj}}$ using (31) to its adjacent DGAs. Using Q_{sh}^{av}, DGA_2 and DGA_4 determined the required changes to their generated reactive power to satisfy the desired reactive power sharing. Also using $\Delta V_{PZC}^{Z,Z_{adj}}$, they calculated the required changes to the voltage magnitude at their PCCs using (30). Since DGA_2 and DGA_4 were constrained by the required changes of both reactive power and voltage magnitudes, their variables assignments are determined using action a_3 in (17), which were found to be $\Delta V_{G2}^{*} = 0.0125$ and $\Delta V_{G4}^{*} = -0.028$, respectively. Given that the value assignment of DGA_4 satisfied its constraints and it did not have other adjacent DGAs, it sent a *good* message to DGA_1. Regarding DGA_2, it sent an *ok?* message containing Q_{sh}^{av} and $\Delta V_{PZC}^{Z,Z_{adj}}$ (i.e. $\Delta V_{12}^{2,3} = 0.0104$) to its adjacent agent DGA_3 to determine its consistency. To this end, DGA_3 calculated its value assignment that satisfies its constraints (i.e. $\Delta V_{DG3}^{*} = 0.03$) similar to DGA_2 and DGA_4. Then, it sent back a *good* message to DGA_2. After DGA_2 received a *good* message from DGA_3, it sent a *good* message to DGA_1. Once the highest priority agent received a *good* message, it broadcasted an *execute* order for all DGAs to apply their assigned values.

In the second operation scenario, when the load increased to 80%, again the reactive power sharing deviated from the desired sharing as shown in Figure 4.16. The DCS negotiation process for this scenario was similar to the first scenario procedures. In the third operation scenario, at full loading condition, DGA_1 estimated undervoltages in its zone buses with a maximum deviation of 0.017 p.u. located at bus 33. Hence, in addition to the reactive power sharing correction, DGA_1 was required to regulate the voltage within its zone using (29). In order to determine the required change in its reactive power generation, DGA_1 triggered a synchronization process to calculate the total reactive power sharing, which was found to be $Q_{sh}^{av} = 0.2952\ MVA$. In consequence, DGA_1 calculated the required change of its reactive power generation as $\Delta Q_{G1}^{(A,A^*)} = 0.029\ MVA$. Given that DGA1 had specified changes for both reactive power generation and voltage magnitude, it assigned its variable using a_3 in (17) (i.e. $\Delta V_{G1}^{*} = 0.0172$). Also, it calculated the required changes for the voltage magnitudes at its PZCs (i.e. $\Delta V_3^{1,4} = 0.01643$ and $\Delta V_6^{1,2} = 0.017$). Then DGA_1 sent and *ok?* message to its adjacent DGAs. DGA_2 and DGA_4 determined their variables assignments that satisfy their constraints. DGA_2 sent an *ok?* message to DGA_3 with $\Delta V_{12}^{2,3} = 0.0169$. However, DGA_3 could not find a value assignment with the defined domain to satisfy the required changes of $\Delta Q_{G3}^{(A,A^*)}$ and $\Delta V_{12}^{2,3}$ due to an overvoltage

occurrence at its PCC. As such, DGA_3 increased its priority to 3 to be higher than DGA_2 and sent a *no-good* message. To search for a feasible assignment, a *min-conflict heuristic technique* was initiated. Where, DGA_3 changed its sharing units and the average reactive power per unit sharing using (32)-(33) to satisfy its voltage constraints. The new average reactive power generation per unit sharing was found to be $Q_{sh}^{av,new} = 0.34192\ MVA$, and $h_{T,new} = 10.35$ sharing units. Also, its variable assignment was determined as $\Delta V_{G3}^{*} = -0.0195$ at the same $\Delta V_{12}^{2,3}$. DGA_3 then sent an *ok?* message with the contents of its value assignments. DGA_2 searched among its domain to satisfy DGA_3 assignment and then determined the required change of the voltage at its PZC with zones 1 (i.e. $\Delta V_{6}^{2,1} = 0.0215$ p.u). It also determined the required change in its control variable (i.e. $\Delta V_{DG1}^{*} = 0.0225$). Then, DGA_2 increased its priority to 4 in order to be higher than DGA_1 and sent an *ok?* message with the new assignments. DGA_1 founds that it its constraints can be satisfied at $\Delta V_{G1}^{*} = 0.031$ and $\Delta V_{3}^{1,4} = 0.02286$. At the next step of the algorithm procedures, DGA_1 sent an *ok?* message to DGA_4 with the new assignments and DGA_4 found that its constraints can be satisfied at $\Delta V_{G4}^{*} = 0.022$. To that end, DGA_4 sent a *good* message to DGA_1 followed by a *good* message from DGA_1 to DGA_2. Once the highest priority agent received a *good* message, it broadcasted an *execute* order for all DGAs to use the assigned variables.

Figure 4.17 summarizes the exchanging messages among the DGAs in the third scenario. As shown, the AWC reached a solution in seven steps of messages exchange.

In the fourth operation scenario, the loading decreased by 10% compared with the third scenario and DG 3 was tripped out. First, DGA_3 triggered a synchronization of process to communicate its new state. Next, DGA_1, the highest propriety agent, recalculated the system average reactive power and total sharing units (i.e. $Q_{sh}^{av} = 0.3388\ MVA$ and the total system sharing ratio $h_T = 10$), after it received all information from its adjacent DGAs. DGA_1 found that action a_1 is infeasible because of overvoltage occurrence at its PCC.

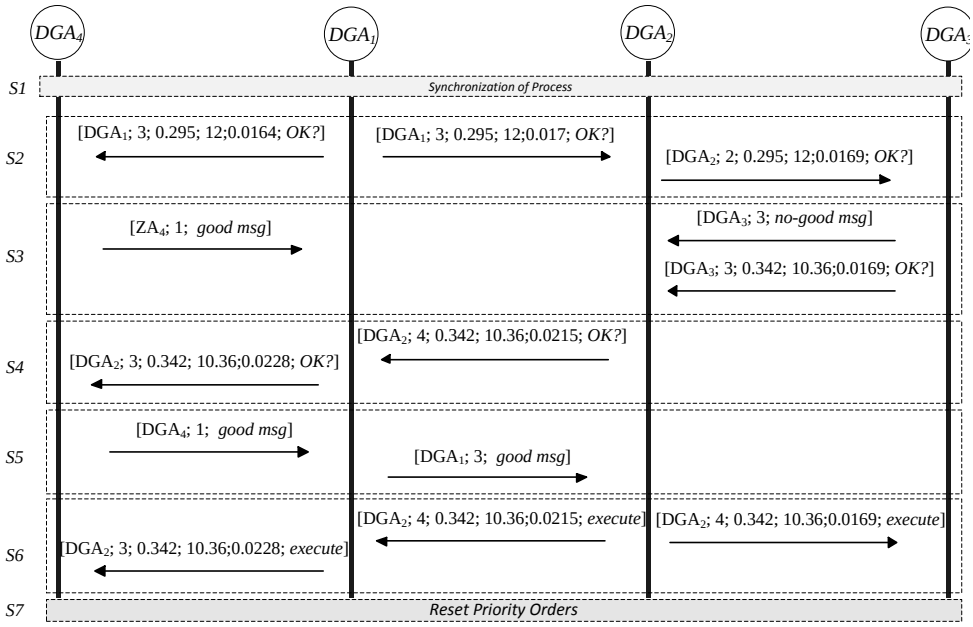

Figure 4.17 Exchanging messages of the proposed AWC in the third scenario

Hence, it selected action a_2 in (17) to determine its initial value assignment (i.e. $\Delta V_{G1}^{*} = 0$). Accordingly, its PZCs assignments were found to be $\Delta \mathrm{V}_{6}^{1,2} = -0.0116$ and $\Delta \mathrm{V}_{3}^{1,4} = -9.42e^{-3}$ at $\Delta V_{G1}^{(A,A^{*})} = -4.9e^{-3}$. Then, similar to the procedures discussed in the previous operation scenarios, DGA_2 and DGA_4 determined their values assignments as $\Delta V_{G2}^{*} = -0.023$ and $\Delta V_{G4}^{*} = -4.74e^{-3}$, respectively. The exchange messages continued until the solution shown in Figure 4.16 was reached. In this operation scenario, it was observed that the choice of appropriate initial value assignment for DGA_1 among the possible set of actions, significantly reduced the required steps of exchanging messages to reach a solution.

Chapter 5
CONFLICT INVESTIGATION OF LOCAL SC OPERATION IN IMG

In this chapter, the operational conflicts between SCs and DG units in microgrids are discussed in detail. Furthermore, a droop-based control is proposed for the operation of the SC in Islanded mode.

5.1 Conflicts of SCs in Islanded Mode

In islanded microgrids, there is no slack bus that can be represented as a reference such that the SC can compensate the reactive power of the downstream network as the case in conventional distribution systems. Moreover, by using the local droop control, DG units tend to change their output power and the point of common coupling voltage, continuously reacting to any change in the system overall power. This might include employing a new DG to the system, releasing a DG from service (i.e. Plug-and-Play) besides the continuously changing of load demand. In consequence, there will be no specific direction at which the SC can detect the change of the system loading. Furtheremore, when a SC is switched on, the droop controlled DG units detect a reduction in the reactive power demand in the distribution system. As such, the DG units share the amount of reduction according to their reactive power droop characteristics.

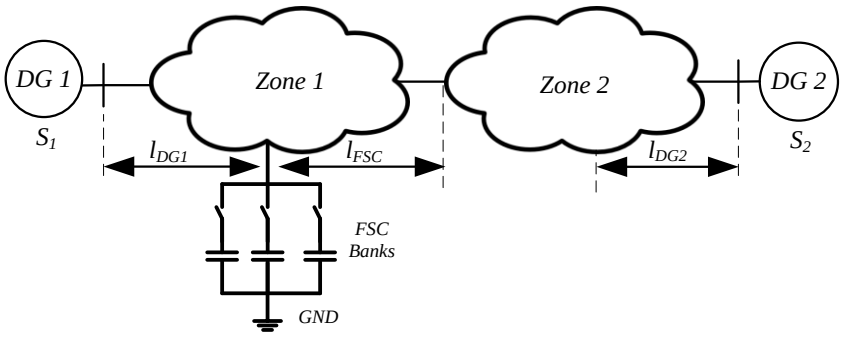

Figure 5.1 Configuration of the SC in islanded mode

In consequence, the actual compensated VARs by the SC will not be the same as the locally estimated VARs that the SC planned to compensate prior to the on-switching action. Hence in this case, if the SC has multiple switching banks, it will continue switching on the banks in a sequential manner trying to attain the estimated required VARs.This operation interference between SCs and DG units can be demonstrated from Figure 5.1. As shown in the figure, when a capacitor bank is switched on, it compensates not only the reactive power from its neighbor DG unit (i.e. DG1), but also a sharing amount from the downstream DG unit (i.e. DG2). Given that both DG 1 and DG 2 share any change in the islanded microgrid reactive power according to their droop settings, the SC locally detects that the required reactive power compensation has not been achieved. As such, it sequentially switches the banks on until it either reaches the maximum capacity or achieves the required VAR. This conflict will be even worse if there is a DG installed downstream from the reactive power direction of the SC node and if the

downstream DG (e.g. DG2) has higher rating than the DG that supplies the capacitor zone (e.g. DG1). Firstly, the SC always detects that its switching action does not compensate its specified VAR. For this reason, it will continue switching on until it reaches the maximum capacity. Secondly, the SC will be responsible for supplying the reduced reactive power by DG2 to zone #2. Accordingly, the distance of the reactive power flow will increase and in consequence the total system losses will increase. The change of the active power losses due to the switching operation of the SC can be formulated as:

$$P_{saved} = \left(\left| \frac{Q_{G1\_R}}{V_{G1}} \right|^2 \times l_{DG1} \times X \right) + \left(\left| \frac{Q_{G2\_R}}{V_{G2}} \right|^2 \times l_{DG2} \times X \right) \tag{5.1}$$

$$P_{added} = \left(\left| \frac{Q_{G2\_R}}{V_{G1}} \right|^2 \times l_{SC} \times X \right) \tag{5.2}$$

where P_{saved} and P_{added} are the saved and the added losses due to the operation of the SCs in the islanded mode, Q_{G1_R} and Q_{G2_R} are the reduction of the reactive generation from DG1 and DG2 according to their sharing when the SC switches on, respectively. V_{G1}, V_{G2} and V_{SC} are the bus voltages of DG 1, DG 2, and the SC bus respectively. X is the line reactance per unit length, l_{DG1} is the distance between the SC and its upstream DG, l_{DG2} is the distance between the SC upstream DG to the end of the DG reactive supply point, and l_{SC} is the distance between the SC and zone 2. Moreover, the continuous and dynamic change of voltage profile

of droop-controlled IMG with the system loading, which is discussed earlier in chapter 3 and can be noted from (3.1), will significantly affect the operation of the voltage-controlled SC. This interaction will not only increase the number of the SC switchings due to the continuous changing voltage profile; however, it may cause hunting of the SC that leads to its malfunction. This conflict is shown in Figure 5.2, where two DGs are supplying a single feeder in the presence of a voltage-controlled SC. As shown in the figure, prior to the operation of the SC, the capacitor found that its local controlled voltage is not within the allowable voltage bandwidth limit, at this time the operating point of the two droop-controlled DGs is located at point *A*. To that end, the SC decides to switch on to enhance the voltage

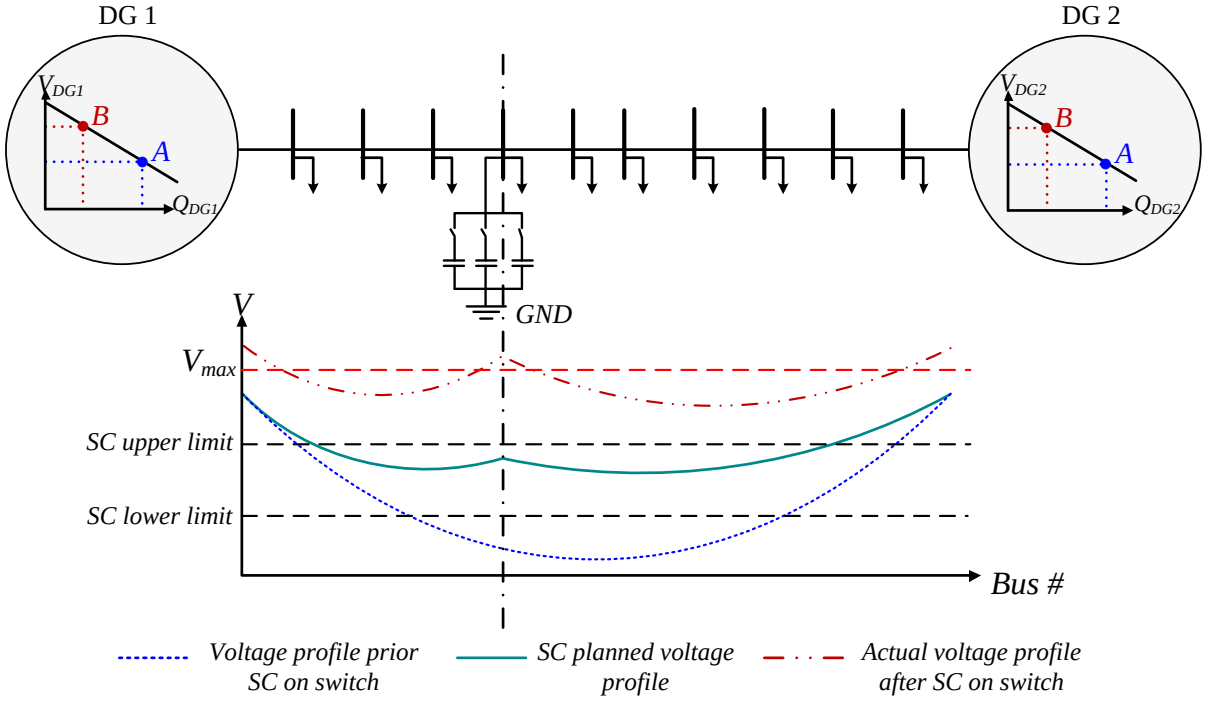

Figure 5.2 Schematic diagram for voltage-controlled SC conflict in IMG

profile. Nonetheless, after the SC switch on, both DGs sense a reduction in the system reactive power loading, thus the DGs reduce their reactive power generation and in consequence their voltage increase. Therefore, the system voltage profile experiences two voltage increment as follows; 1) enhancement from the SC; 2) reaction of the DGs to the SC enhancement, which may cause overvoltage. Additionally, in case of overvoltage, the SC will detect this voltage violation and thus will switch off, which will return the voltage profile to its original state prior to the SC turn-on. Then, the SC will detect that its voltage is out of the acceptable bandwidth, and will switch on again. Therefore, the SC will suffer from hunting (i.e. on–off loop) that will lead to the capacitor malfunction.

Furthermore, if the SC operation causes voltage rise above the no-load reference voltage $\left(V_{Gj}^{*}\right)$ at the DG node, the DG will absorb reactive power that will lead to reactive power circulation in the system and thus increase the power losses. This conflict affects both reactive power and voltage controlled SC.

5.2 Operation of SC as a Droop Control

One of the possible solutions to mitigate the operation challenges of SCs in islanded microgrids is to deal with the SC as a reactive power source with zero active power droop coefficient i.e. $n_{P,j}$ = 0. In another words, similar to the DG units, SCs would employ the same concept of the reactive power droop control. In

this case, SCs operation mechanism becomes in harmony with the islanded microgrid control philosophy (i.e. it shares the reactive power demand along with droop-controlled DG units). One advantage of the proposed droop-controlled SCs is that it can be defined as a hybrid control between Volt and VAR, as it was depicted previously in the reactive power droop characteristics in Figure 3.1. SC will thus ensure the voltage magnitude is within limits via compensating its reactive power share of the system as follows:

$$Q_{SC} = \frac{1}{n_{SC}}\left(V_{SC}^{*} - V_{SC}\right) \tag{5.3}$$

$$n_{SC} = \frac{V_{\max} - V_{\min}}{SC_{\max}} \tag{5.4}$$

where $V_{\max}$, $V_{\min}$ are the maximum and minimum allowable voltage, respectively; V_{SC} and Q_{SC} are the output voltage and reactive power at the SC node, respectively; n_{SC} and V_{SC}^{*} are the static droop gain and the no-load reference voltage, respectively; $SC_{\max}$ is the maximum SC banks rating.

However, the SC can generate only discrete reactive power according to the available number and size of its SC banks. The discrete reactive power can be controlled according to an error coefficient by approximating the SC reactive power sharing to the nearest number of banks that will fulfill the required VARs settings. Hence, the capacitor-injected VARs can be calculated as follows:

$$Q_{SC,I} = floor\left(\frac{Q_{SC}}{SCBs}\right) \tag{5.5}$$

$$If\ \ Q_{SC} - Q_{SC,I} > e \times SCB \tag{5.6}$$

$$Q_{SC,I} = Ceil\left(\frac{Q_{SC}}{SCBs}\right) \tag{5.7}$$

where Q_{SC} is the SC actual droop sharing of the loads reactive power, $Q_{SC,I}$ is the actual injected VARs, SCB is the shunt capacitor bank size, and e is the error coefficient. As shown in 1(5.5), a floor function has been applied to avoid excessive reactive power injection during light load conditions. However, an error coefficient is used to indicate how far the deviation of the selected setting from the required value. Hence, (5.7) is typically applied according to the error coefficient in order to minimize the system losses in heavy loading conditions.

5.3 Simulation and Results

In this case study five identical DGs are located across the 33-bus distribution test system operate in islanded mode, the system and its data is shown in the Appendix in Figure A.1 and Table A-1. This section presents the simulation results for a 12.66 kV 33-bus distribution feeder that operates in islanded mode of operation. The system and its data are shown in the Appendix in Figure A.1 and Table A-1. The distribution system has 5 DG units with ω^* equals one per unit.

Table 5-1 DG's droop parameter and bus location

	Rating (MVA)	Bus connection, Bus location	Connection-location Impedance [93]	ω_{Gj}^{*}	n_P	n_q	V_{Gj}^{*}
DG 1	2	Bus 5, Bus 34	0.012453+0.012453j	0.0014	0.00135	0.025	1.02
DG 2	1	Bus 9, Bus 35	0.012453+0.012453j	0.0027	0.0027	0.05	1.02
DG 3	0.5	Bus 12, Bus 36	0.012453+0.012453j	0.0054	0.0054	0.01	102
DG 4	0.5	Bus 18, Bus 37	0.003113+0.003113j	0.0054	0.0054	0.01	1.02
DG 5	1	Bus 25, Bus 38	0.003113+0.003113j	0.0027	0.0027	0.05	1.02

Table 5-1 shows the rating, location, and droop parameters of each DG unit. The load demand is represented by a real weekend normalized load profile [106]. It is assumed that the demand profile for all load points is uniform. In order to minimize the system losses there are three SCs that have been optimally placed in the conventional grid-tied configuration on buses 12, 23, and 29 [41]. The sizes for the installed SCs have been selected to be 5 × 100 kVAr, 5 × 150 kVAr and 5 × 200 kVAr, respectively. Three case studies have been conducted to investigate the operation challenges of SC in the islanded mode of operation. The case studies are classified according to the control scheme of SCs: Volt, VAR, and droop-controlled respectively. The voltage settings of the SCs have been selected to be within ± 5% of the nominal voltage. Further, the droop coefficients of SCs when they operate in droop-controlled mode are set to 0.01, 0.0667, and 0.05 for buses 12, 23, and 29 respectively. Each case study consists of two scenarios. In the first scenario, it is assumed that all DG units are droop-based dispatchable units. In the

second scenario, DG2 in Table 5-1 is replaced by a wind-based DG unit with 0.75 MVA rating and 0.8 leading PF.

Figure 5.3, Figure 5.4, and Figure 5.5 show the generated reactive power of the DG units when SCs are Volt, VAR, and droop controlled, respectively for the first scenario. The figures show that the reactive power sharing of the DG units doesn't follow the designed equal power sharing mechanism. For instance, DG5 with 1 MVA rating delivers more reactive power compared with DG1 that has a capacity of 2 MVA. Also the figures show that the amount of reactive power generated from each droop-controlled DG unit varies with the applied control scheme of SC.

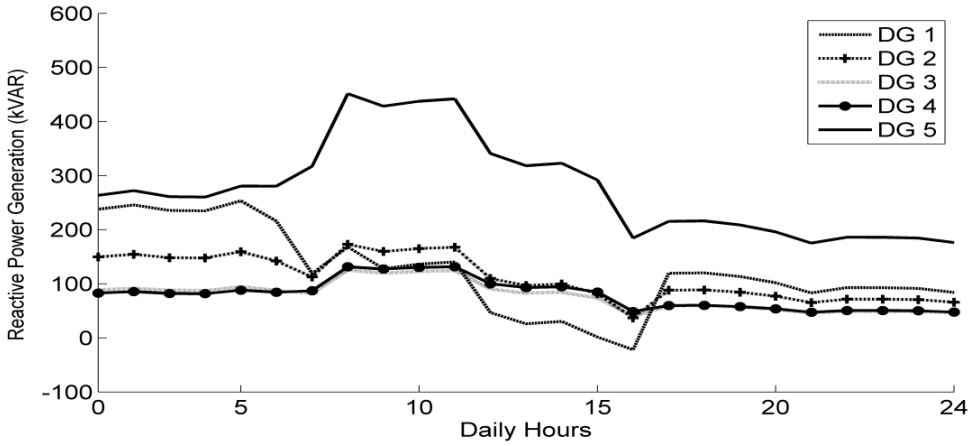

Figure 5.3 DG reactive power generation with volt-controlled SC

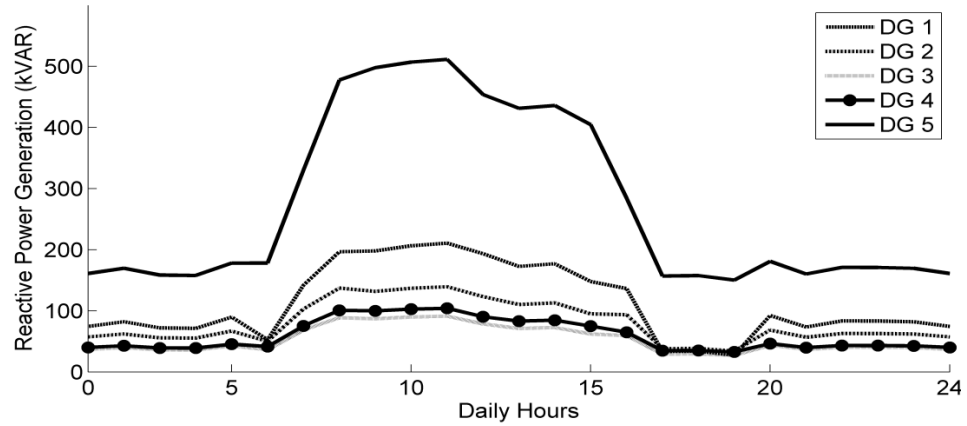

Figure 5.4 DG reactive power generation with VAR-controlled SC

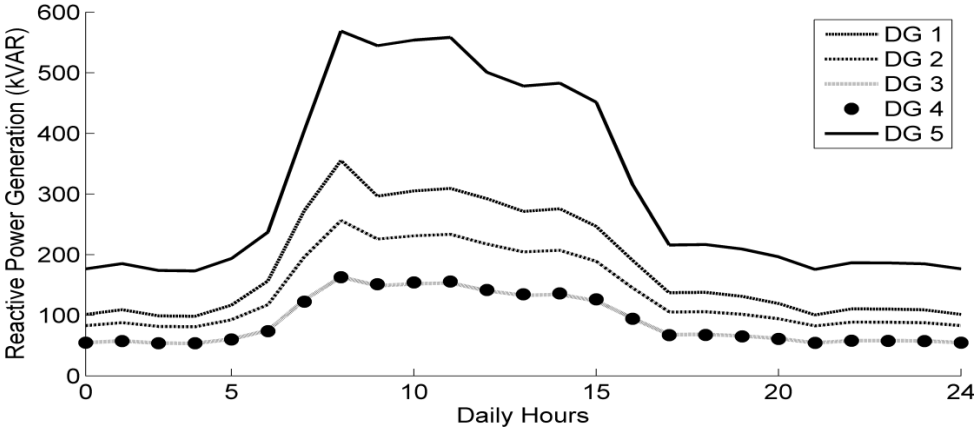

Figure 5.5 DG reactive power generation with droop-controlled SC

Figure 5.6, Figure 5.7, and Figure 5.8 present the daily SC switching operation during the studied period. As shown in Figure 5.6, the Volt-controlled SC at bus 12 is off all the day, as it is implemented close by DG3, which maintains the voltage limit. In contrast, when the SC is VAR-controlled, it switches on almost all the day, as shown in Figure 5.7. It is noteworthy that the settings of Volt-controlled SCs should be selected to ensure that the upper SC voltage limit is lower than the nominal DG's droop voltage V^*. Otherwise the SC will raise the voltage

above the nominal V^* and in consequence the DG will be enforced to absorb reactive power, as previously depicted in (3.2).

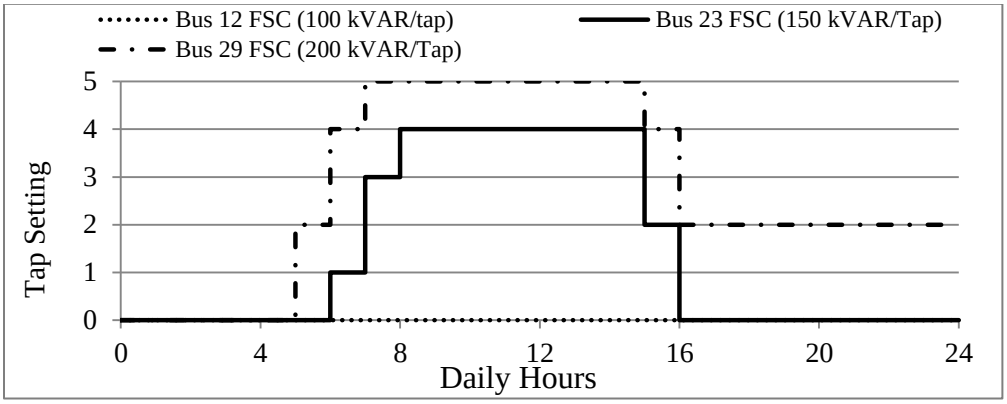

Figure 5.6 Switching operation of volt-controlled SC

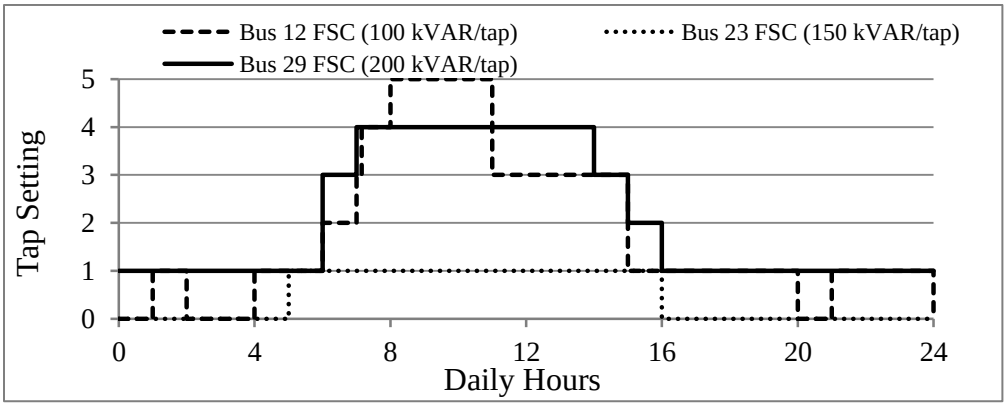

Figure 5.7 Switching operation of VAR-controlled SC controlled SC

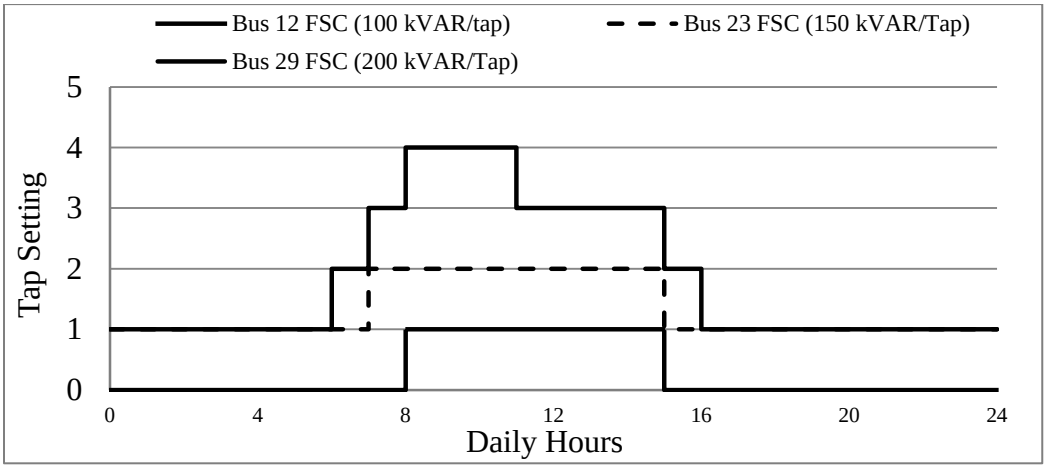

Figure 5.8 Switching operation of droop-controlled SC

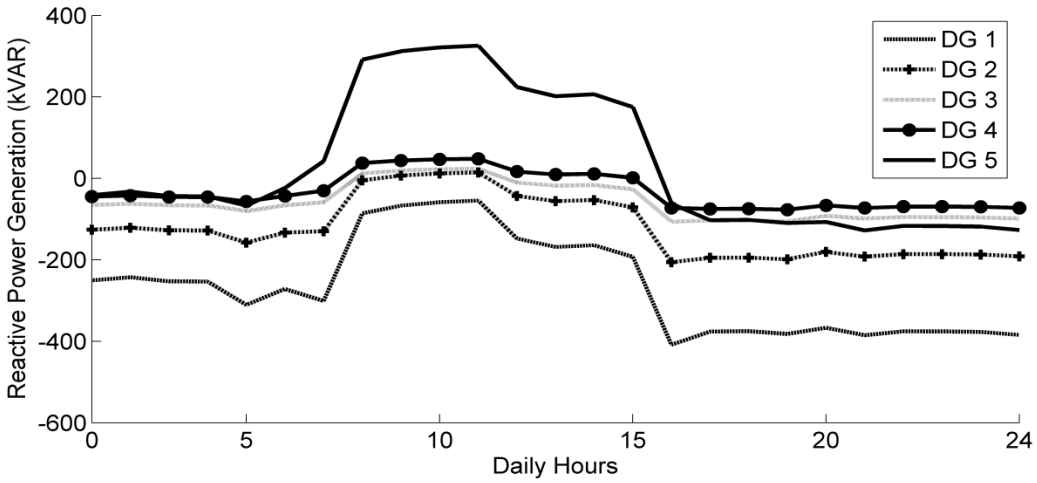

Figure 5.9 DG reactive power generation when SCs are volt-controlled and V^*=1 p.u.

Figure 5.9 shows the reactive power of the droop controlled DG units when V^* is set to 1 per unit (p.u.). As shown in the figure, most of the DG units absorb reactive power, which in turn increases the total system losses.

Figure 5.10, Figure 5.11, and Figure 5.12 show the generated reactive power of the DG units when SCs are Volt, VAR, and Droop controlled, respectively for the second scenario (i.e. a wind-based DG unit is installed). As shown in the figures, DG1, DG3, and DG4 absorb reactive power during peak wind time and light load demand in the time interval of 15–24 hours. The results show that the absorption of reactive power when SCs are droop-controlled is the lowest compared with Volt and VAR-controlled. Given that the ability of DGs to absorb reactive power is not ensured by all DG types, a circulating reactive power in the system might occur. This in turn might increase power dissipations.

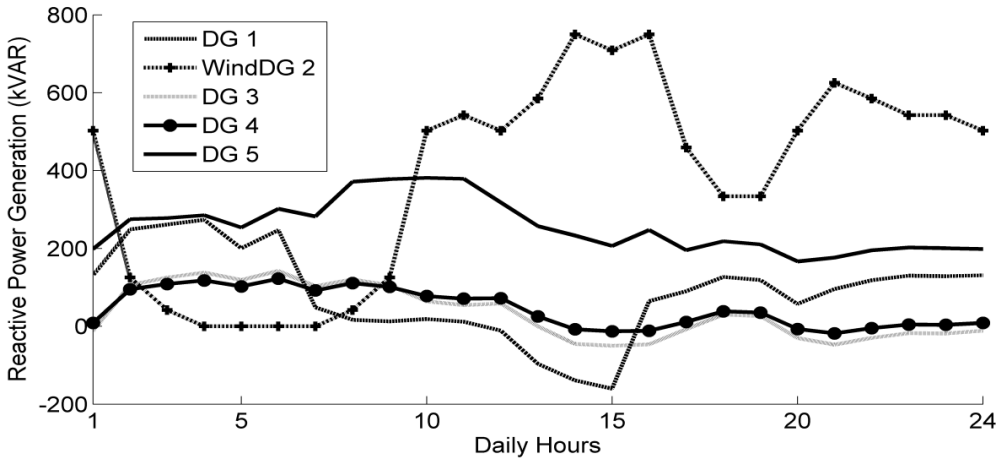

Figure 5.10 DG reactive power generation with SC volt-controlled

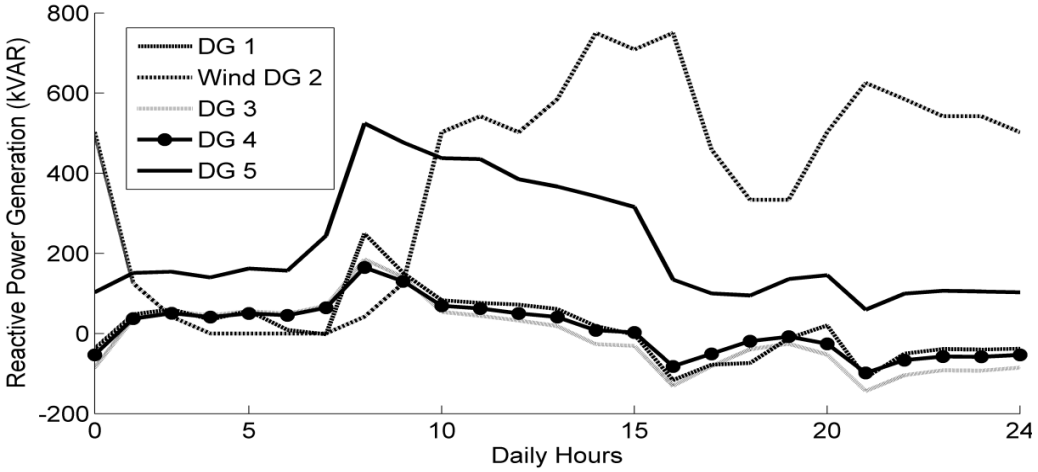

Figure 5.11 DG reactive power generation with SC VAR control

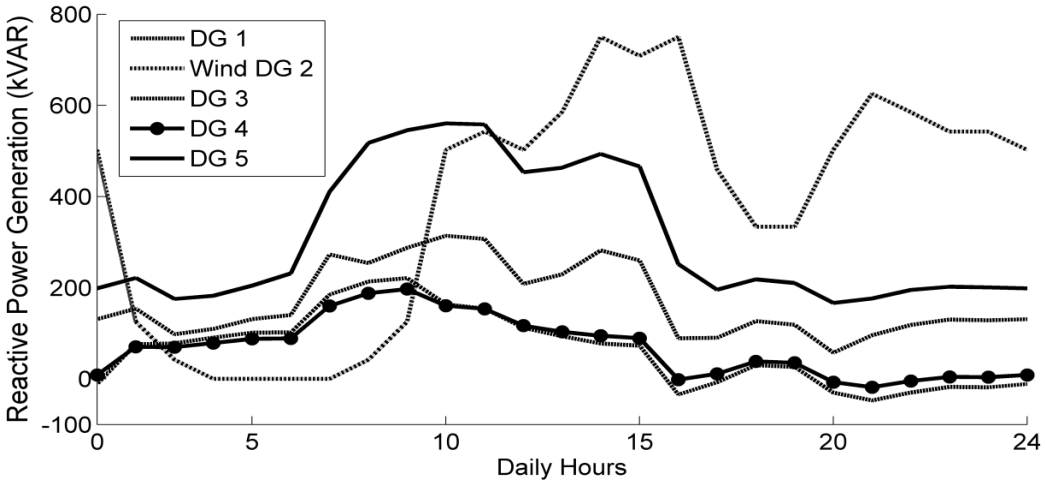

Figure 5.12 DG reactive power generation with SC droop control

The SC switching operation with the installation of wind-based DG unit is shown in Figure 5.13, Figure 5.14, and Figure 5.15 for Volt, VAR, and droop-controlled, respectively. As depicted in the figures, the proposed SC droop-controlled scheme has the lowest number of switchings during the studied period compared with Volt and VAR-controlled schemes. As such, the lifetime of the SCs will be improved significantly. Hence, the economic feasibility of installing SCs for islanded microgrids will be increased when the proposed droop-controlled SCs is applied.

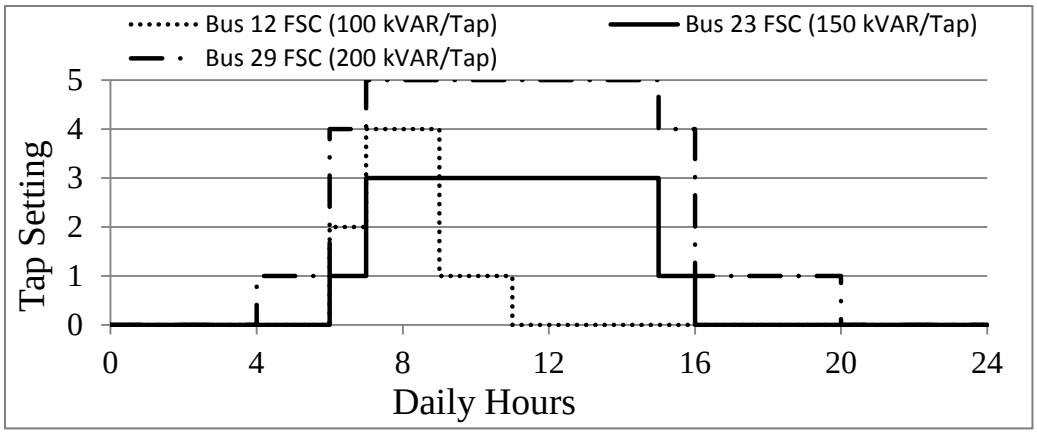

Figure 5.13 Volt SC control switching operation

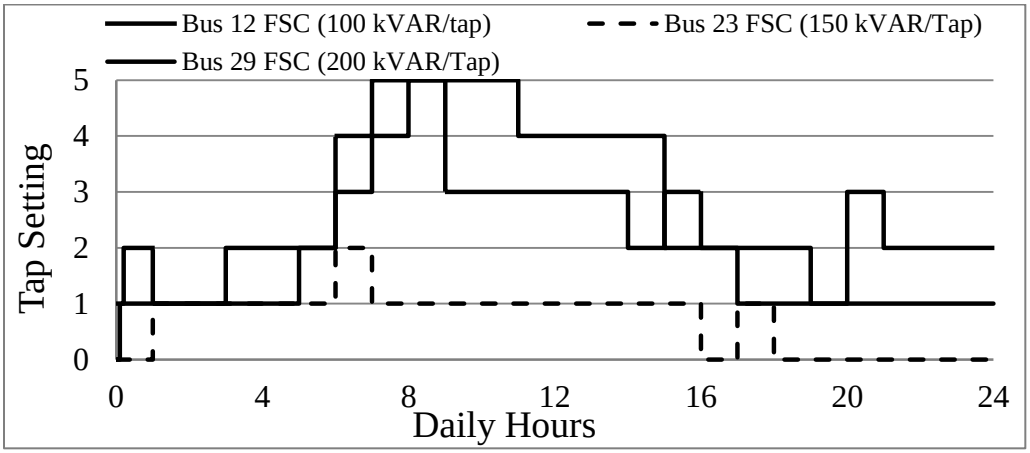

Figure 5.14 VAR SC control switching operation

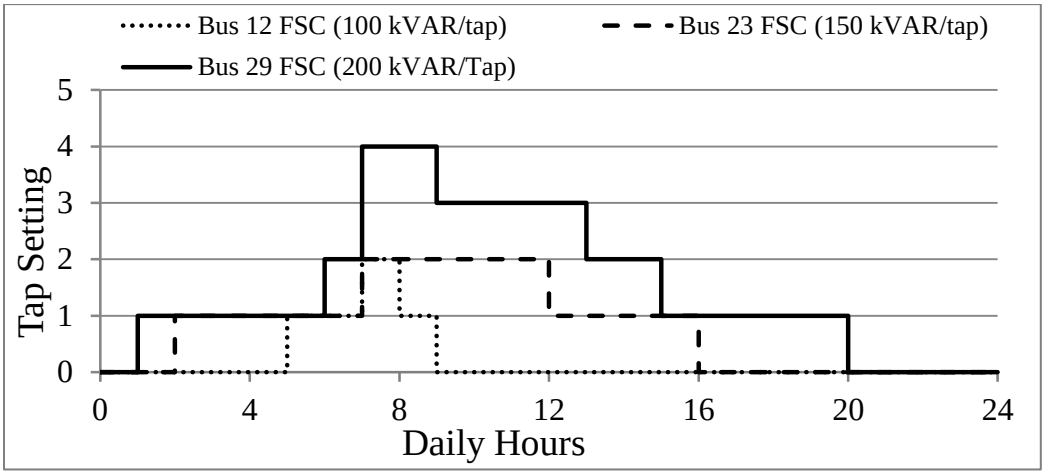

Figure 5.15 Droop SC control switching operation

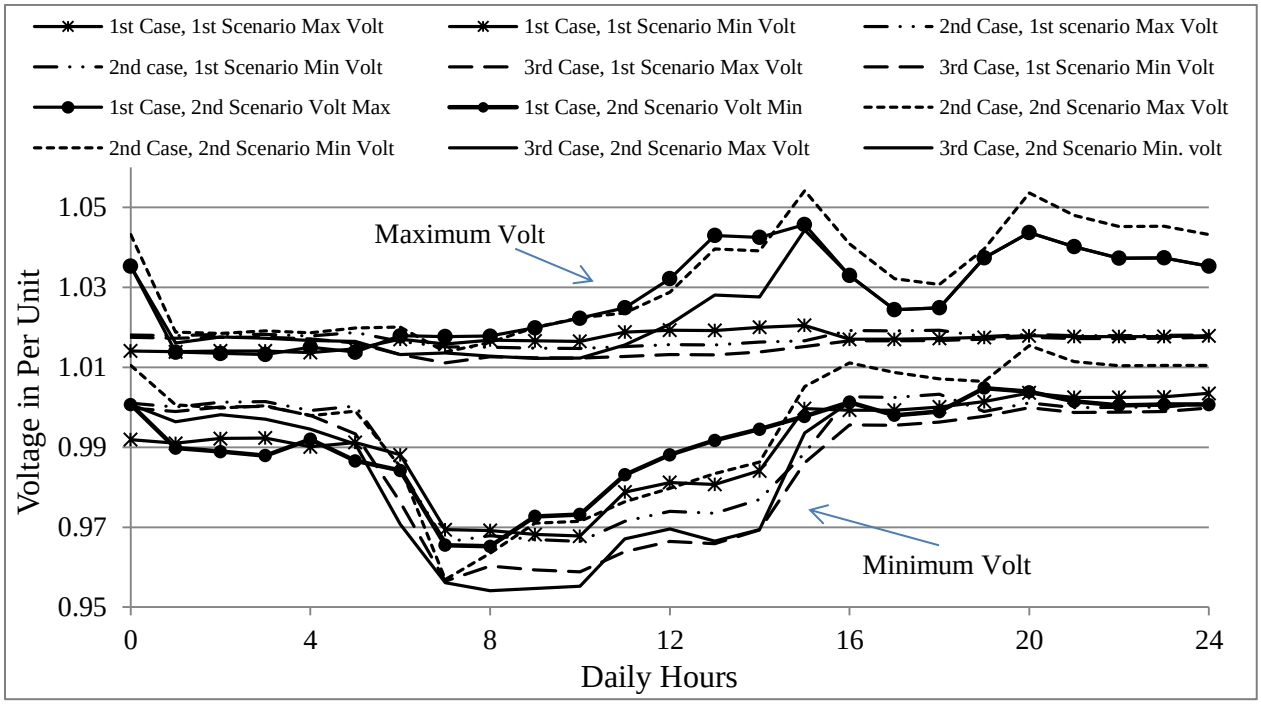

Figure 5.16 Maximum and minimum voltage in the daily profile

Figure 5.16 shows the minimum and maximum voltage magnitudes of the test system during the period of study for the two scenarios at different SCs control schemes. As shown in the figure, unlike other control schemes, Droop-controlled

SCs are capable of maintaining the voltage magnitude within its specified limits under all operating conditions.

Chapter 6

INCORPORATION OF THE LRT MODEL IN THE IMG AND INVESTIGATION OF ITS CONFLICT INTERACTION

The LRT is one of the main devices traditionally used in distribution system for voltage regulation. It consists of an autotransformer with a mechanical load tap changer. According to the ANSI/IEEE C57.15 standard, SVRs can be configured in a type-A or type-B connection. The position of the tap setting is controlled either remotely using the distribution network operator or locally via a compensation circuit called line drop compensator (LDC) [24]. The LDC circuit tends to estimate the voltage drop between the SVR and the target remote point in a secondary circuit and determine the required taps to maintain the voltage within a specified range. The relation between the SVR primary and secondary side voltage and current for each phase *ph* of a three-phase grounded wye connected SVR is given as follows [24]:

$$V_S^{ph} = \left(1 \pm T_{ph}\Delta T\right)V_P^{ph} \tag{6.1}$$

$$I_S^{ph} = \frac{1}{1 \pm T_{ph}\Delta T} I_P^{ph} \tag{6.2}$$

where V_S^{ph} and I_S^{ph} are the voltage and current at the secondary side; V_P^{ph} and I_P^{ph} are the voltage and current at the primary side; T_{ph} is the phase tap setting, and ΔT

is the change of voltage per tap setting. The SVR model described in (6.1) and (6.2) has been incorporated in the droop-based three phase power flow algorithm described in the chapter 3, where the active and reactive power at the secondary and primary side of the LRT can be obtained using (3.25) and (3.26).

The incorporation of LRTs in three-phase droop controlled IMGs has been tested using the well-known IEEE 34-bus unbalanced radial distribution feeder as shown in the Appendix in Figure A.2 and Table A-2 to Table A-5. Two identical droop-controlled DGs of 2 MVA are located at buses 2 and 4, respectively, with interconnection impedance of $0.003113 + 0.003113j$. It is assumed that the two DG units have 0.7 minimum power factor, 0.05 and 0.005 active and reactive power static droop gains respectively, ω^* are set at 1.0 per unit, and the reference voltage at no-load is set at 1.04 pu. Figure 6.1 shows the voltage profile of the feeder backbone from buses 1 to 19 at the base case scenario, where the SVRs are deactivated.

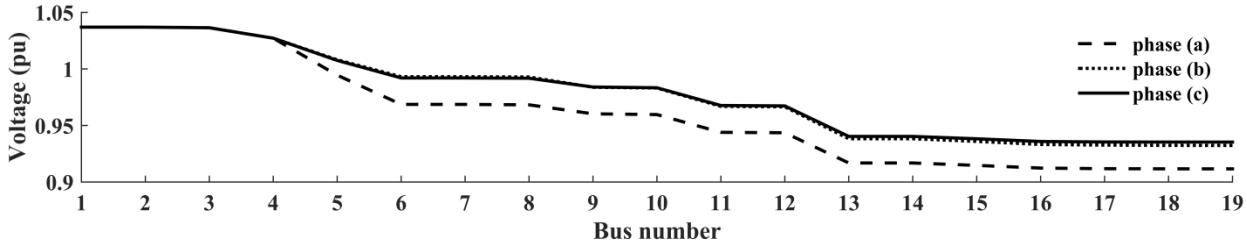

Figure 6.1 Voltage profile of the 34-bus system backbone feeder at base case

Figure 6.2 shows the voltage profile when SVRs are activated. As shown in the figure, the voltage profile of the feeder has been improved. It has been observed in the simulation that the SVRs took three consequence settings using the LDC to converge to the final tap setting, as shown in Table 6-1. This phenomenon is due to the dependency of the reactive power generation of droop-controlled DG units on their local voltage magnitudes. As shown in Table 6-2, the reactive power sharing of DG units is changed with the change of the SVRs tap settings. This in turn caused changes in the required tap settings of SVRs calculated by the LDC. Other scenarios have been conducted with different locations of droop-controlled DG units. The results show that SVRs can help DG units meeting the voltage regulation limits, especially when they are connected downstream the DG units. However, they might interfere with the operation of droop-controlled DG units based on their locations.

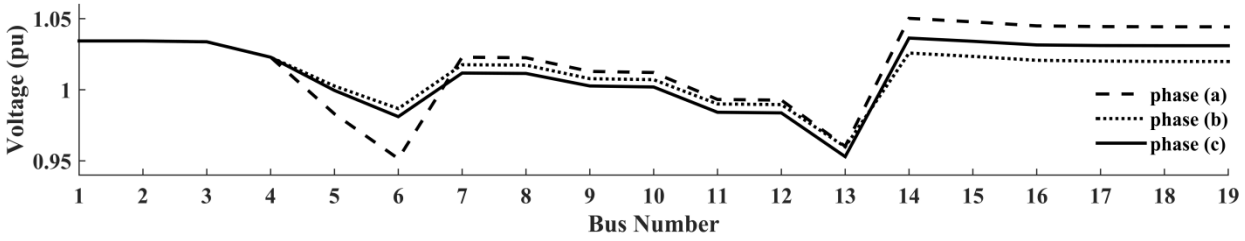

Figure 6.2 Voltage profile of the 34-bus system backbone feeder after LRTs tap setting convergence

Table 6-1 Change of LRT tap setting until convergence

Steps	*LRT 1 Tap setting*			*LRT 2 Tap Setting*		
	a	*b*	*c*	*a*	*b*	*c*
1	9	5	5	12	11	11
2	9	5	5	15	11	14
3	12	5	5	15	11	14

Table 6-2 Change of system voltage and reactive power generation until LRT convergence

Steps	*DG 1Reactive Generation*			*DG 1 Voltage*	*DG 2Reactive Generation*			*DG 2 Voltage*
	a	*b*	*c*	*a, b ,c*	*a*	*b*	*c*	*a, b, c*
Base	–0.005	0.037	0.029	1.036	0.17	0.071	0.015	1.0272
1	0.008	0.054	0.043	1.0348	0.213	0.086	0.029	1.0236
2	0.009	0.056	0.045	1.0345	0.22	0.083	0.033	1.0232
3	0.011	0.057	0.046	1.0343	0.23	0.081	0.031	1.0229

6.1 Conflict Investigation of the LRT Interaction in IMG

Several case studies were conducted by changing the location of the DGs across the three phase IEEE 34-bus system, to study the conflict interaction between the drooped control IMG and the operation of the LRTs.

Case I. ***<u>Undervoltage Problem Due to Reverse Power Flow</u>***

In this case study, two identical droop-based DG units of 2 MVA are placed at buses 8 and 11, respectively, where both DGs are between the system LRTs. The static droop n_q and m_p parameters are designed to be 0.05 and 0.005, respectively;

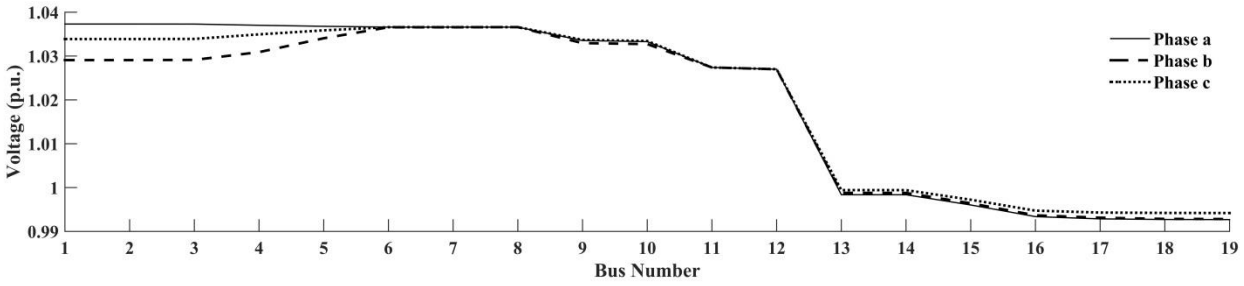

Figure 6.3 Voltage profile of the 34-bus system backbone feeder before LRTs settings

Table 6-3 DGs voltage and reactive power and LRTs tap setting and primary side voltage in case *I*

	DG 1		DG 2		LRT 1		LRT 2	
	Voltage	Generated Reactive Power	Voltage	Generated Reactive Power	Voltage	Decision	Voltage	Decision
Phase a	1.0366	0.057	1.0274	0.118	1.0366	–3	0.9984	6
Phase b		0.015		0.088	1.0366	–3	0.9988	6
Phase c		–0.004		0.046	1.0366	–3	0.9994	6

the no-load reference frequency and voltage are selected to be 1 and 1.02 per unit, respectively. As shown in Figure 6.3, LRT 2 detect that its target bus voltage is out of the acceptable range, thus it decides to regulate the voltage by +6 tap setting to all its three phase settings as shown in Table 6-3. However, due to the reverse power flow across LRT 1, it measures that the voltage exceeds the upper bandwidth voltage limit, thus decides to lower its tap setting by –3 for all its three phase lines. After, applying the two LRTs setting, LRT 2 satisfies its target bus voltage and didn't require any further tap setting. Nonetheless, LRT 1 settings lead

to an overvoltage at the upstream buses at phases *a* and *c*, due to the reverse power flow as shown in Figure 6.4. The cause of this conflict is that LRT 1 always detects that the voltage at the target point exceeds the dead bandwidth and try to reduce the tap setting; at the same time it will not be able to decrease its target bus voltage. Because, there is a DG near the target bus that holds its voltage and cause revers power flow according to the DG shared reactive power. Therefore, LRT 1 will undergo consecutive tap reduction in its tap setting until reaching the maximum reduction, which is –16 tap setting; thus, an extreme overvoltage will result at the upstream side of the network as shown in Figure 6.5.

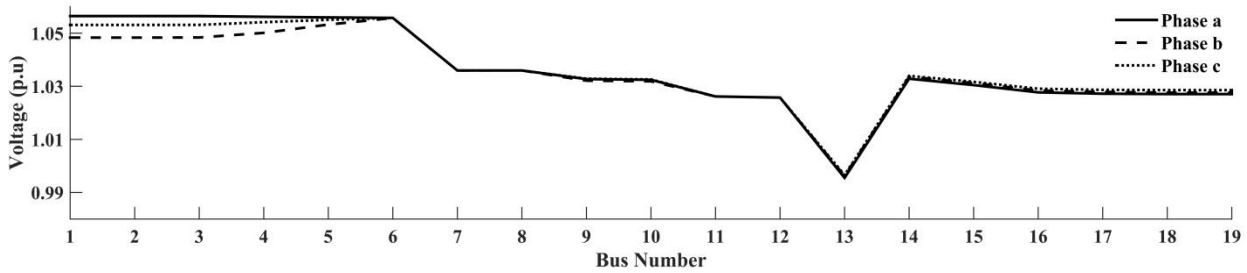

Figure 6.4 Overvoltage at the upstream side of the network due to reverse power flow

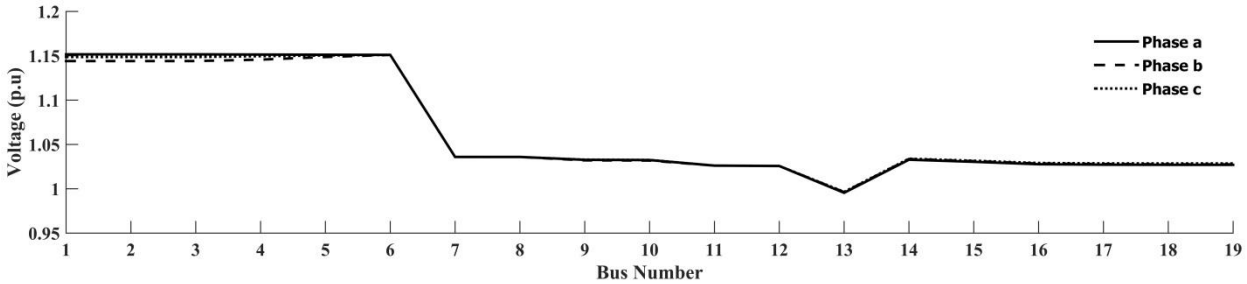

Figure 6.5 Extreme overvoltage at the upstream side of the network due to reverse power flow and conflict interaction of the LRTs in the IMG

Case II. ***Overvoltage Problem Due to Reverse Power Flow***

In this case study, two identical droop-based DG units of 2 MVA are placed at buses 15 and 17, respectively, their droop setting are similar to the previous case I setting. Similar to the aforementioned case study, LRT 1 measures that the voltage at the target point phase (a) is below the dead bandwidth as shown in Figure 6.6, and try to adjust it by increasing the tap setting to +3 as depicted in Table 6-4.

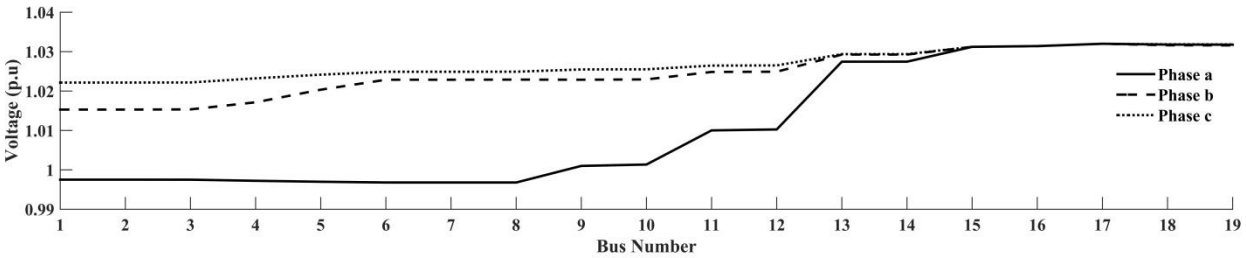

Figure 6.6 Base case voltage profile when both DGs are located downstream and after both LRTs

Table 6-4 DGs voltage and reactive power and LRTs tap setting and primary side voltage in case *II*

	DG 1		DG 2		LRT 1		LRT 2	
	Voltage	Generated Reactive Power	Voltage	Generated Reactive Power	Voltage	Decision	Voltage	Decision
Phase a	1.0312	0.0112	1.0322	0.073	0.9968	3	1.0275	0
Phase b		0.046		0.061	1.0229	0	1.0293	0
Phase c		0.018		0.027	1.0249	0	1.0294	0

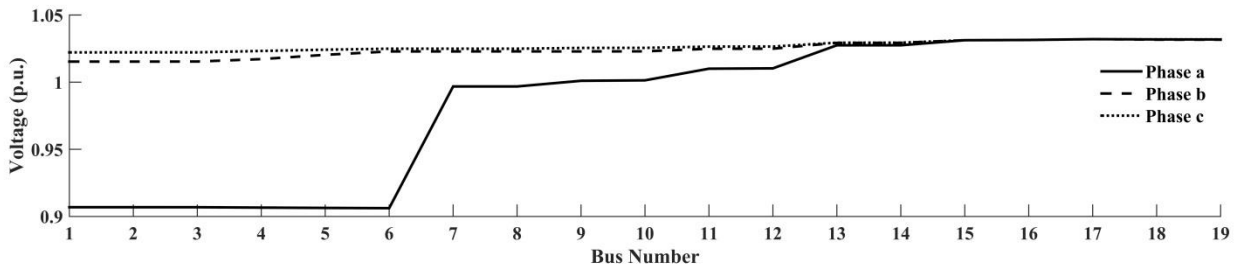

Figure 6.7 Extreme undervoltage at phase (a) due to revers power flow and conflict interaction of the LRTs in the IMG

However, after applying the new tap setting, the voltage at the target point will be the same as it is held by the downstream DG's voltage, as they have the same sharing (i.e. no change in the loading condition). Inconsequence, due to the reverse power flow the new tap setting will cause more voltage drop toward LRT 1 upstream buses, and the LRT 1 will keep trying to adjust the target point voltage by another +3 tap setting at phase (a) until reaching the maximum +16 tap setting causing an undervoltage at the upstream buses as shown in Figure 6.7.

6.2 Mitigation of LRT operation Conflicts in IMG

According to the previous simulation results, the conventional local control of the LRT fails shortly in case of reverse power flow, because the LRT can't properly estimate the voltage drop when the DG is between the LRT and the target point. Moreover, if the LRT can estimate properly the target point voltage when the DG is downstream the target point, it can't affect the downstream voltage as it is held by the downstream DGs.

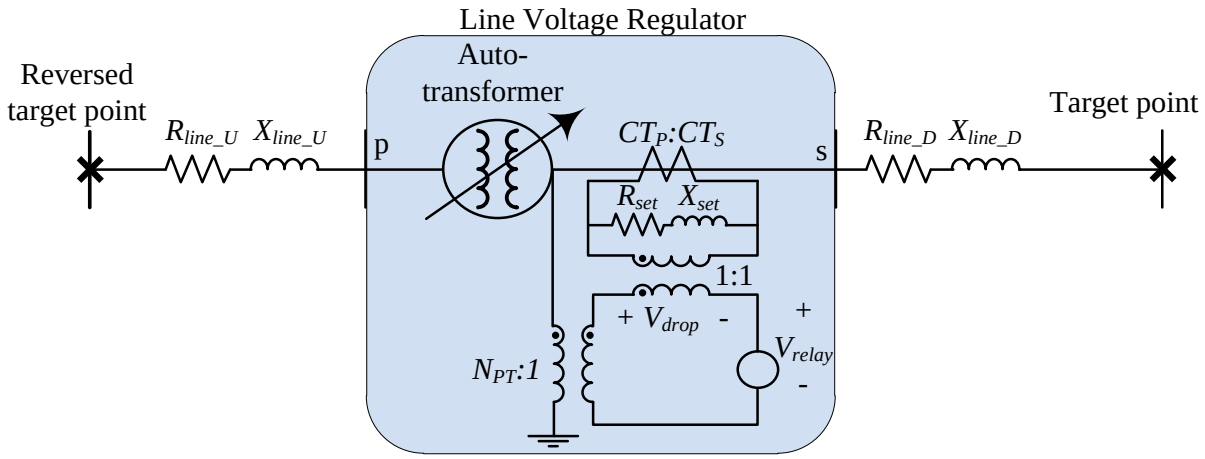

Figure 6.8 Local LRT with reversed line drop compensator target point

The local LRT conflict mitigation relies on enabling the LRT to change its target point between the traditional downstream regulating point and a new upstream regulating point depending on the direction of the power flow as shown in Figure 6.8. The proposed mitigation doesn't need any costly current transformer (CT) or potential voltage transformer (PT) to be added to the LRT primary side at node (p).

The reverse power flow will be detected by the LRT based on comparing the estimated downstream target point voltage with the regulator voltage at node(s) after performing the normal conventional estimation as shown in (2.8)–(2.10).

If the target point voltage is bigger than node(s) voltage, this means a reverse power flow. The local regulator voltage and line compensator current will be converted to the primary side of the LRT using the auto transformer ratio *aR* as follows:

$$If\ V_{reg} - V_{relay} < 0,\ Apply\ LRT\ algorithm\ given\ in\ (2.5) - (2.10) \tag{6.3}$$

$$If\ V_{reg} - V_{relay} > 0,\ (i.e.\ Reverse\ power\ \ flow\ is\ detected) \tag{6.4}$$

$$V_{reg} = \frac{V_{reg}}{aR} \tag{6.5}$$

where $$aR = 1 + 0.00625 \times Tap_t$$

$$V_{drop} = \left(I_{comp} \times aR\right) \times \left(R_{set\_U} + jX_{set\_U}\right) \tag{6.6}$$

$$V_{relay} = V_{reg} - V_{drop} \tag{6.7}$$

$$if\ \ V_{lb} \le V_{relay} \le V_{ub} \qquad Tap_t = -\left(Tap_{t-1}\right) \tag{6.8}$$

$$if\ \ V_{relay} \le V_{lb} \qquad Tap_t = -\left(Tap_{t-1} + Round\left(\frac{V_{set} - V_{relay}}{0.75}\right)\right) \tag{6.9}$$

$$if\ \ V_{relay} \ge V_{ub} \qquad Tap_t = -\left(Tap_{t-1} - Round\left(\frac{V_{relay} - V_{set}}{0.75}\right)\right) \tag{6.10}$$

where R_{set_U} and X_{set_U} are the new impedance settings that simulate the new reversed target point.

Now by repeating case *I* and case *II* in Section 5.2.2 with the proposed local LRT algorithm, where the reverse power flow conflicts occur in these case studies the new impedance setting R_{set} and X_{set} as shown in (2.10) was considered the same as the downstream setting.

Case III. ***Mitigation of Case I Reverse Power Flow Problem***

After applying the reverse LRT algorithm as given in (6.3)–(6.10) when reverse power flow is detected, LRT 1 reverses its target point and decides to have a +3 tap setting as shown in Table 6-5 instead of –3, however, as shown in Table 6-3, before applying the proposed algorithm. It is worth noting that LRT 2 has +6 tap setting similar to Case *I*. Figure 6.9 shows that the voltage profile is within the acceptable limit by applying the reverse LRT algorithm, which shows the robustness of the proposed solution.

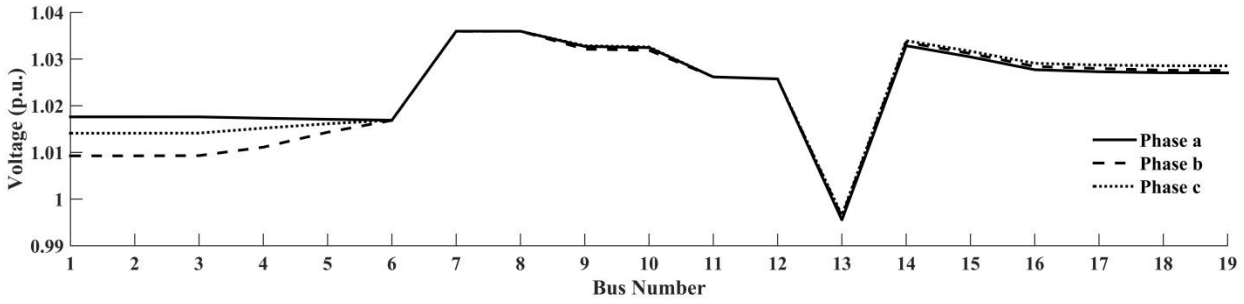

Figure 6.9 Backbone voltage profile of the 34-bus system during reverse power flow after applying the reverse target point algorithm

Table 6-5 DGs voltage and reactive power and LRTs tap setting and primary side voltage in case *III*

	DG 1		DG 2		LRT 1		LRT 2	
	Voltage	Generated Reactive Power	Voltage	Generated Reactive Power	Voltage	Decision	Voltage	Decision
Phase a	1.0366	0.057	1.0274	0.118	1.0366	3	0.9984	6
Phase b		0.015		0.088	1.0366	3	0.9988	6
Phase c		–0.004		0.046	1.0366	3	0.9994	6

Case IV. Mitigation of Case II Reverse Power Flow Problem

Similarly to the previous case study, once the LRT 1 detect a reverse power flow, it revers its target point toward its upstream and decide to have –3 tap setting at its phase (a) as shown in Table 6-6. Figure 6.10 shows the backbone voltage profile of the 34-bus system after applying the reverse local control algorithm of the LRT during revers power flow; as depicted in the figure the LRT was able to achieve appropriate voltage profile without causing under- or overvoltage.

Table 6-6 DGs voltage and reactive power and LRTs tap setting and primary side voltage in case IV

	DG 1		DG 2		LRT 1		LRT 2	
	Voltage	Generated Reactive Power	Voltage	Generated Reactive Power	Voltage	Decision	Voltage	Decision
Phase a	1.0312	0.0112	1.0322	0.073	0.9968	–3	1.0275	0
Phase b		0.046		0.061	1.0229	0	1.0293	0
Phase c		0.018		0.027	1.0249	0	1.0294	0

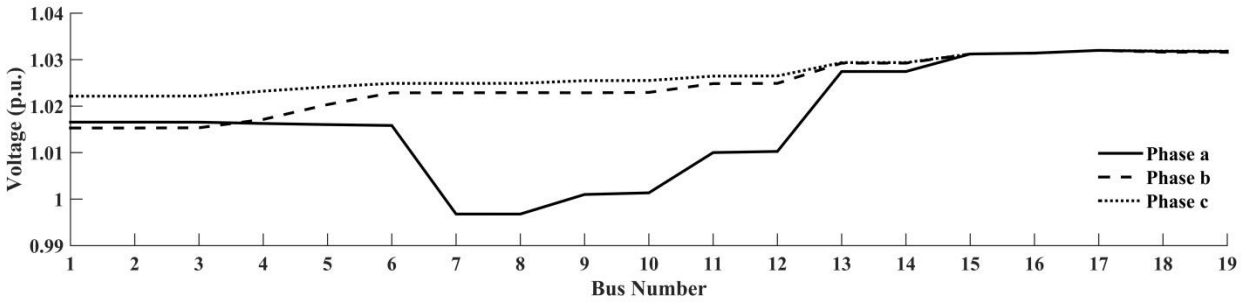

Figure 6.10 Backbone voltage profile of the 34-bus system during reverse power flow after applying the reverse target point algorithm

Chapter 7
CONCLUSION AND FUTURE WORK

This chapter summarize the thesis research work challenges, contribution, and the direction of future work.

7.1 Summary and Conclusion

The main goal and contribution of this thesis is to present a distributed control scheme to achieve voltage regulation and equal reactive power sharing in a IMG distribution system, to study the operation conflict of the conventional Volt/Var controllers such as LRTs and SCs in the IMG, and propose a local mitigation for the conventional regulator devices.

In chapter 2, a literature survey is presented for the conventional Volt/Var regulators in distribution power systems in conventional, active, and islanded modes of operation. Furthermore, the IMG mode of operation and utilization of distributed multi-agent in power systems state of art are discussed.

In chapter 3, a detailed analysis of the behaviour of the droop-controlled DG units is presented, which simplifies the causes of the droop control challenges in IMG. Moreover, two case studies are presented to study the challenges of voltage regulation and achieving equal reactive power sharing in IMGs.

In chapter 4, a distributed voltage regulation scheme for droop-controlled IMGs has been proposed. The proposed control obviates the need for a MGCC, where the centralized methods may face serious challenges with respect to the scalability and reliability of the IMG system due to the complex communication requirements and the single point-of-failure. Furthermore, allocating a MGCC for each identified microgrid in large-scale distribution systems is costly and impractical [15]. The proposed distributed control aims to periodically adjust the voltage droop parameter settings based on a peer-to-peer cooperative protocol among the DGs control units. Moreover, in such distributed control technique, it will be easier to modify and upgrade the local control of DGs without disturbing other parts of the control process. Whereas, the proposed algorithm adopts a distributed constraint satisfaction approach to formulate the problem of voltage regulation and reactive power control in a multi-agent environment. An asynchronous weak commitment technique is proposed to solve the formulated problem. The proposed algorithm takes into account the dynamic changes and variability associated with the output power of renewable DG units, as well as the variability of IMG loads. Several case studies are simulated to test the effectiveness and performance of the proposed algorithm under different operating conditions. In this chapter, two main problems in IMGs were mitigated. Firstly, voltage regulation across the entire IMG using the multi-agent environment has been achieved, and the simulation results show that

the proposed algorithm can effectively mitigate the challenges of voltage regulation in droop-controlled IMGs and thus obviates the need for a central secondary controller. Secondly, achieving equal reactive power sharing among the dispatchable droop based DGs in IMG challenge was mitigated. The reactive power sharing has been formulated as a distributed constraint satisfaction (DCS) problem. Several case studies have been carried out to test the effectiveness of the proposed algorithm. The results show that the proposed approach can achieve accurate reactive power sharing and appropriate voltage regulation in IMG systems.

In chapter 5, the operational challenges of SC in islanded microgrids have been addressed and mitigated. Different conventional local control schemes of SCs have been tested during islanded microgrid mode of operation at different operating conditions. The study shows that 1) the settings of SCs affect significantly the reactive power sharing mechanism of the droop-controlled DG units. 2) Inappropriate settings of Volt-controlled SC might cause droop-controlled DG units to absorb reactive power even during heavy loading conditions. This in turn will cause significant increase in the total system losses and undervoltage. 3) Excessive number of SC switchings occurs when either Volt or VAR-control is applied due to the interference between droop-controlled DG units and SCs. To mitigate the aforementioned challenges, a droop-based SC control has been

proposed. The results show that the proposed control scheme is capable of mitigating the conventional SC local control challenges and facilitating seamless integration of SCs in islanded microgrids operation.

In chapter 6, LRTs have been incorporated in droop-based three-phase power flow algorithms of IMG systems to provide a tool for investigating their future role in the operation of IMGs. Several case studies have been carried out to study the interaction between SVRs and droop-controlled DG units. The studies showed that SVRs could still play a key role to meet the voltage regulation requirements. However, the LRTs are strongly affected by the reverse power flow, which cause inappropriate tap settings that may lead to over- or undervoltage. A reverse algorithm has been proposed to mitigate the reverse power flow problem. The case studies reveal that the algorithm can mitigate the reverse power flow challenge.

7.2 Direction of Future Work

Based on the results of this research work, several research points came up to mind. The following subjects are suggested for future work:

1. Develop a distributed constraint optimization (DCO) algorithm to optimize the operation of microgrid. The objective function of the optimization could be minimizing the power losses or on a cost-saving basis.

2. Develop a full multi-agent control considering all IMG technologies such as Volt/Var devices, ESS, and PEV.
3. Formulate an optimization problem for small microgrid considering all IMG technologies such as Volt/Var devices, ESS, and PEV.

BIBLIOGRAPHY

[1] I. El-Samahy and E. El-Saadany, "The effect of DG on power quality in a deregulated environment," in *IEEE Power Engineering Society General Meeting, 2005*, 2005, p. 2969–2976 Vol. 3.

[2] H. E. Farag, M. M. A. Abdelaziz, and E. F. El-Saadany, "The effects of renewable energy resources on the implementation of Distributed Resources Islanded Systems," in *2013 IEEE Power and Energy Society General Meeting (PES)*, 2013, pp. 1–5.

[3] M. E. Elkhatib, R. E. Shatshat, and M. M. A. Salama, "Decentralized reactive power control for advanced distribution automation systems," *IEEE Trans. Smart Grid*, vol. 3, no. 3, pp. 1482–1490, Sep. 2012.

[4] "IEEE Guide for Design, Operation, and Integration of Distributed Resource Island Systems with Electric Power Systems," *IEEE Std 15474-2011*, pp. 1–54, Jul. 2011.

[5] Y. Wang, Y. Tan, Z. Chen, X. Wang, and Y. Tian, "A communication-less distributed voltage control strategy for a multi-bus AC islanded microgrid," in *Power Electronics Conference (IPEC-Hiroshima 2014 - ECCE-ASIA), 2014 International*, 2014, pp. 3538–3545.

[6] M. M. A. Abdelaziz, M. F. Shaaban, H. E. Farag, and E. F. El-Saadany, "A multistage centralized control scheme for islanded microgrids with pevs," *IEEE Trans. Sustain. Energy*, vol. 5, no. 3, pp. 927–937, Jul. 2014.

[7] M. M. A. Abdelaziz, H. E. Farag, E. F. El-Saadany, and Y. A. R. I. Mohamed, "A novel and generalized three-phase power flow algorithm for islanded microgrids using a newton trust region method," *IEEE Trans. Power Syst.*, vol. 28, no. 1, pp. 190–201, Feb. 2013.

[8] M. M. A. Abdelaziz, H. E. Farag, and E. F. El-Saadany, "Optimum droop parameter settings of islanded microgrids with renewable energy resources," *IEEE Trans. Sustain. Energy*, vol. 5, no. 2, pp. 434–445, Apr. 2014.

[9] H. E. Farag, M. M. A. Abdelaziz, and E. F. El-Saadany, "Voltage and reactive power impacts on successful operation of islanded microgrids," *IEEE Trans. Power Syst.*, vol. 28, no. 2, pp. 1716–1727, May 2013.

[10] J. M. Guerrero, N. Berbel, J. Matas, L. G. de Vicuna, and J. Miret, "Decentralized control for parallel operation of distributed generation inverters in microgrids using resistive output impedance," in *IECON 2006 - 32nd Annual Conference on IEEE Industrial Electronics*, 2006, pp. 5149–5154.

[11] W. Yao, M. Chen, J. Matas, J. M. Guerrero, and Z. M. Qian, "Design and analysis of the droop control method for parallel inverters considering the

impact of the complex impedance on the power sharing," *IEEE Trans. Ind. Electron.*, vol. 58, no. 2, pp. 576–588, Feb. 2011.

[12] J. M. Guerrero, J. C. Vasquez, J. Matas, L. G. de Vicuña, and M. Castilla, "Hierarchical control of droop-controlled ac and dc microgrids #x2014;a general approach toward standardization," *IEEE Trans. Ind. Electron.*, vol. 58, no. 1, pp. 158–172, Jan. 2011.

[13] A. Micallef, M. Apap, C. S. Staines, and J. M. Guerrero Zapata, "Secondary control for reactive power sharing and voltage amplitude restoration in droop-controlled islanded microgrids," in *2012 3rd IEEE International Symposium on Power Electronics for Distributed Generation Systems (PEDG)*, 2012, pp. 492–498.

[14] S. Conti, R. Nicolosi, S. A. Rizzo, and H. H. Zeineldin, "Optimal dispatching of distributed generators and storage systems for mv islanded microgrids," *IEEE Trans. Power Deliv.*, vol. 27, no. 3, pp. 1243–1251, Jul. 2012.

[15] P. H. Divshali, S. H. Hosseinian, and M. Abedi, "A novel multi-stage fuel cost minimization in a VSC-based microgrid considering stability, frequency, and voltage constraints," *IEEE Trans. Power Syst.*, vol. 28, no. 2, pp. 931–939, May 2013.

[16] H. E. Z. Farag and E. F. El-Saadany, "A Novel cooperative protocol for distributed voltage control in active distribution systems," *IEEE Trans. Power Syst.*, vol. 28, no. 2, pp. 1645–1656, May 2013.

[17] A. Bidram, A. Davoudi, F. L. Lewis, and Z. Qu, "Secondary control of microgrids based on distributed cooperative control of multi-agent systems," *IET Gener. Transm. Distrib.*, vol. 7, no. 8, pp. 822–831, Aug. 2013.

[18] A. Bidram, A. Davoudi, F. L. Lewis, and J. M. Guerrero, "Distributed cooperative secondary control of microgrids using feedback linearization," *IEEE Trans. Power Syst.*, vol. 28, no. 3, pp. 3462–3470, Aug. 2013.

[19] J. W. Simpson-Porco, F. Dorfler, and F. Bullo, "Synchronization and power sharing for droop-controlled inverters in islanded microgrids," *Automatica*, vol. 49, no. 9.

[20] Q. Sun, R. Han, H. Zhang, J. Zhou, and J. M. Guerrero, "A multiagent-based consensus algorithm for distributed coordinated control of distributed generators in the energy internet," *IEEE Trans. Smart Grid*, vol. 6, no. 6, pp. 3006–3019, Nov. 2015.

[21] X. Fang, S. Misra, G. Xue, and D. Yang, "Smart Grid-2014; The new and improved power grid: a survey," *IEEE Commun. Surv. Tutor.*, vol. 14, no. 4, pp. 944–980, Fourth 2012.

[22] M. K. K. S. Reddy, "A review of integration, control, communication and metering (ICCM) of renewable energy based smart grid," *Renew. Sustain. Energy Rev.*, vol. 38, pp. 180–192, 2014.
[23] I. Džafić, R. A. Jabr, E. Halilovic, and B. C. Pal, "A sensitivity approach to model local voltage controllers in distribution networks," *IEEE Trans. Power Syst.*, vol. 29, no. 3, pp. 1419–1428, May 2014.
[24] W. H. Kersting, "Distribution feeder voltage regulation control," *IEEE Trans. Ind. Appl.*, vol. 46, no. 2, pp. 620–626, Mar. 2010.
[25] M. I. Marei, E. F. El-Saadany, and M. M. A. Salama, "An efficient control of the series compensator for sag mitigation and voltage regulation," in *Power Electronics Specialist Conference, 2003. PESC '03. 2003 IEEE 34th Annual*, 2003, vol. 3, pp. 1242–1247 vol.3.
[26] M. I. Marei, E. F. El-Saadany, and M. M. A. Salama, "A new approach to control dvr based on symmetrical components estimation," *IEEE Trans. Power Deliv.*, vol. 22, no. 4, pp. 2017–2024, Oct. 2007.
[27] "American national standard for electric power systems and equipment-voltage ratings (60 hertz), ANSI Standard C84.1," Dec. 2006.
[28] Z. Wang, J. Wang, B. Chen, M. M. Begovic, and Y. He, "MPC-based voltage/var optimization for distribution circuits with distributed generators and exponential load models," *IEEE Trans. Smart Grid*, vol. 5, no. 5, pp. 2412–2420, Sep. 2014.
[29] A. Padilha-Feltrin, D. A. Q. Rodezno, and J. R. S. Mantovani, "Volt-VAR multiobjective optimization to peak-load relief and energy efficiency in distribution networks," *IEEE Trans. Power Deliv.*, vol. 30, no. 2, pp. 618–626, Apr. 2015.
[30] J. J. Grainger and S. Civanlar, "Volt/Var control on distribution systems with lateral branches using shunt capacitors and voltage regulators part I: the overall problem," *IEEE Trans. Power Appar. Syst.*, vol. PAS-104, no. 11, pp. 3278–3283, Nov. 1985.
[31] H. E. Farag and E. F. El-Saadany, "Voltage regulation in distribution feeders with high DG penetration: From traditional to smart," in *2011 IEEE Power and Energy Society General Meeting*, 2011, pp. 1–8.
[32] S. Yoshizawa, Y. Yamamoto, J. Yoshinaga, Y. Hayashi, S. Sasaki, T. Shigetou, and H. Nomura, "Novel voltage control of multiple step voltage regulators in a distribution system," in *Innovative Smart Grid Technologies Conference (ISGT), 2014 IEEE PES*, 2014, pp. 1–5.
[33] F. A. Viawan and D. Karlsson, "Voltage and reactive power control in systems with synchronous machine-based distributed generation," *IEEE Trans. Power Deliv.*, vol. 23, no. 2, pp. 1079–1087, Apr. 2008.

[34] N. A. El-Taweel and H. E. Farag, "Operation challenges of feeder shunt capacitors in islanded microgrids," in *2015 IEEE Electrical Power and Energy Conference (EPEC)*, 2015, pp. 191–196.
[35] P. Brady, C. Dai, and Y. Baghzouz, "Need to revise switched capacitor controls on feeders with distributed generation," in *Transmission and Distribution Conference and Exposition, 2003 IEEE PES*, 2003, vol. 2, pp. 590–594 vol.2.
[36] S. F. Mekhamer, M. E. El-Hawary, M. M. Mansour, M. A. Moustafa, and S. A. Soliman, "State of the art in optimal capacitor allocation for reactive power compensation in distribution feeders," in *Power Engineering 2002 Large Engineering Systems Conference on, LESCOPE 02*, 2002, pp. 61–75.
[37] H. E. Farag, M. M. A. Abdelaziz, and E. F. El-Saadany, "Incorporating voltage regulator and load models in unbalanced power flow studies of active distribution systems," in *2012 IEEE Power and Energy Society General Meeting*, 2012, pp. 1–7.
[38] M. E. Elkhatib, R. El-Shatshat, and M. M. A. Salama, "Novel coordinated voltage control for smart distribution networks with DG," *IEEE Trans. Smart Grid*, vol. 2, no. 4, pp. 598–605, Dec. 2011.
[39] J. O. Petintin and M. Shaaban, "Voltage regulation in a smart distribution system incorporating variable renewable generation," in *2014 IEEE Innovative Smart Grid Technologies - Asia (ISGT ASIA)*, 2014, pp. 583–588.
[40] W. H. Kersting, "The modeling and application of step voltage regulators," in *Power Systems Conference and Exposition, 2009. PSCE '09. IEEE/PES*, 2009, pp. 1–8.
[41] M. H. Haque, "Capacitor placement in radial distribution systems for loss reduction," *Transm. Distrib. IEE Proc. - Gener.*, vol. 146, no. 5, pp. 501–505, Sep. 1999.
[42] A. R. Salehinia, M. R. Haghifam, M. Shahabi, and F. Mahdloo, "Energy loss reduction in distribution systems using GA-based optimal allocation of fixed and switched capacitors," in *Energy Conference and Exhibition (EnergyCon), 2010 IEEE International*, 2010, pp. 835–840.
[43] G. A. Bortignon and M. E. El-Hawary, "A review of capacitor placement techniques for loss reduction in primary feeders on distribution systems," in *Canadian Conference on Electrical and Computer Engineering, 1995*, 1995, vol. 2, pp. 684–687 vol.2.
[44] G. B. J. M. M. Aman, "Optimum shunt capacitor placement in distribution system—A review and comparative study," *Renew. Sustain. Energy Rev.*, vol. 30, pp. 429–439, 2014.

[45] H. E. Z. Farag and E. F. El-Saadany, "Optimum shunt capacitor placement in multimicrogrid systems with consideration of islanded mode of operation," *IEEE Trans. Sustain. Energy*, vol. 6, no. 4, pp. 1435–1446, Oct. 2015.
[46] Y. Y. Hsu and H. C. Kuo, "Dispatch of capacitors on distribution system using dynamic programming," *Transm. Distrib. IEE Proc. C - Gener.*, vol. 140, no. 6, pp. 433–438, Nov. 1993.
[47] C. Dai and Y. Baghzouz, "Impact of distributed generation on voltage regulation by LTC transformer," in *11th International Conference on Harmonics and Quality of Power, 2004*, 2004, pp. 770–773.
[48] R. A. Walling, R. Saint, R. C. Dugan, J. Burke, and L. A. Kojovic, "Summary of distributed resources impact on power delivery systems," *IEEE Trans. Power Deliv.*, vol. 23, no. 3, pp. 1636–1644, Jul. 2008.
[49] P. M. S. Carvalho, P. F. Correia, and L. A. F. Ferreira, "Distributed reactive power generation control for voltage rise mitigation in distribution networks," *IEEE Trans. Power Syst.*, vol. 23, no. 2, pp. 766–772, May 2008.
[50] D. N. Gaonkar, P. C. Rao, and R. N. Patel, "Hybrid method for voltage regulation of distribution system with maximum utilization of connected distributed generation source," in *2006 IEEE Power India Conference*, 2006.
[51] A. H. Rafa, O. Anaya-Lara, and J. R. Mcdonald, "Power factor control for inverter-interfaced microgeneration," in *Universities Power Engineering Conference, 2008. UPEC 2008. 43rd International*, 2008, pp. 1–5.
[52] J. C. Vasquez, R. A. Mastromauro, J. M. Guerrero, and M. Liserre, "Voltage Support Provided by a Droop-Controlled Multifunctional Inverter," *IEEE Trans. Ind. Electron.*, vol. 56, no. 11, pp. 4510–4519, Nov. 2009.
[53] M. H. J. Bollen and A. Sannino, "Voltage control with inverter-based distributed generation," *IEEE Trans. Power Deliv.*, vol. 20, no. 1, pp. 519–520, Jan. 2005.
[54] C. L. Masters, "Voltage rise: the big issue when connecting embedded generation to long 11 kV overhead lines," *Power Eng. J.*, vol. 16, no. 1, pp. 5–12, Feb. 2002.
[55] R. Tonkoski and L. A. C. Lopes, "Voltage regulation in radial distribution feeders with high penetration of photovoltaic," in *IEEE Energy 2030 Conference, 2008. ENERGY 2008*, 2008, pp. 1–7.
[56] A. W. K De Brabandere, "Prevention of inverter voltage tripping in high density PV grids," *19th EU-PVSEC Paris Fr.*, 2004.
[57] R. Tonkoski, L. A. C. Lopes, and T. H. M. El-Fouly, "Coordinated active power curtailment of grid connected PV inverters for overvoltage prevention," *IEEE Trans. Sustain. Energy*, vol. 2, no. 2, pp. 139–147, Apr. 2011.

[58] Y. Ueda, K. Kurokawa, T. Itou, K. Kitamura, K. Akanuma, M. Yokota, H. Sugihara, and A. Morimoto, "Advanced analysis of grid-connected PV system's performance and effect of batteries," *Elect Eng Jpn.*, vol. 164, pp. 247–258, 2008.
[59] M. A. Kashem and G. Ledwich, "Multiple distributed generators for distribution feeder voltage support," *IEEE Trans. Energy Convers.*, vol. 20, no. 3, pp. 676–684, Sep. 2005.
[60] A. E. Kiprakis and A. R. Wallace, "Maximising energy capture from distributed generators in weak networks," *Gener. Transm. Distrib. IEE Proc.-*, vol. 151, no. 5, pp. 611–618, Sep. 2004.
[61] V. Calderaro, G. Conio, V. Galdi, and A. Piccolo, "Reactive power control for improving voltage profiles: A comparison between two decentralized approaches," *Electr. Power Syst. Res.*, vol. 83, no. 1, pp. 247–254, Feb. 2012.
[62] S. Paudyal, C. A. Canizares, and K. Bhattacharya, "Optimal operation of distribution feeders in smart grids," *IEEE Trans. Ind. Electron.*, vol. 58, no. 10, pp. 4495–4503, Oct. 2011.
[63] M. E. Elkhatib, R. El Shatshat, and M. M. A. Salama, "Optimal control of voltage regulators for multiple feeders," *IEEE Trans. Power Deliv.*, vol. 25, no. 4, pp. 2670–2675, Oct. 2010.
[64] J.-H. Choi and J.-C. Kim, "Advanced voltage regulation method of power distribution systems interconnected with dispersed storage and generation systems," *IEEE Trans. Power Deliv.*, vol. 16, no. 2, pp. 329–334, Apr. 2001.
[65] S. Deshmukh, B. Natarajan, and A. Pahwa, "Voltage/VAR control in distribution networks via reactive power injection through distributed generators," *IEEE Trans. Smart Grid*, vol. 3, no. 3, pp. 1226–1234, Sep. 2012.
[66] N. Daratha, B. Das, and J. Sharma, "Coordination between OLTC and svc for voltage regulation in unbalanced distribution system distributed generation," *IEEE Trans. Power Syst.*, vol. 29, no. 1, pp. 289–299, Jan. 2014.
[67] A. Borghetti, M. Bosetti, S. Grillo, S. Massucco, C. A. Nucci, M. Paolone, and F. Silvestro, "Short-term scheduling and control of active distribution systems with high penetration of renewable resources," *IEEE Syst. J.*, vol. 4, no. 3, pp. 313–322, Sep. 2010.
[68] M. A. Azzouz and E. F. El-Saadany, "Optimal coordinated volt/var control in active distribution networks," in *2014 IEEE PES General Meeting | Conference Exposition*, 2014, pp. 1–5.
[69] T. Senjyu, Y. Miyazato, A. Yona, N. Urasaki, and T. Funabashi, "Optimal distribution voltage control and coordination with distributed generation," *IEEE Trans. Power Deliv.*, vol. 23, no. 2, pp. 1236–1242, Apr. 2008.

[70] J. Zhao, L. Ju, W. Luo, and J. Zhao, "Reactive power optimization considering dynamic reactive power reserves," in *2014 International Conference on Power System Technology (POWERCON)*, 2014, pp. 97–102.
[71] M. A. Azzouz, M. F. Shaaban, and E. F. El-Saadany, "Real-time optimal voltage regulation for distribution networks incorporating high penetration of PEVs," *IEEE Trans. Power Syst.*, vol. 30, no. 6, pp. 3234–3245, Nov. 2015.
[72] A. Sajadi, H. E. Farag, P. Biczel, and E. F. El-Saadany, "Voltage regulation based on fuzzy multi-agent control scheme in smart grids," in *2012 IEEE Energytech*, 2012, pp. 1–5.
[73] M. E. Baran and I. M. El-Markabi, "A Multiagent-based dispatching scheme for distributed generators for voltage support on distribution feeders," *IEEE Trans. Power Syst.*, vol. 22, no. 1, pp. 52–59, Feb. 2007.
[74] X. Liu, A. Aichhorn, L. Liu, and H. Li, "Coordinated control of distributed energy storage system with tap changer transformers for voltage rise mitigation under high photovoltaic penetration," *IEEE Trans. Smart Grid*, vol. 3, no. 2, pp. 897–906, Jun. 2012.
[75] H. E. Z. Farag, E. F. El-Saadany, and R. Seethapathy, "A two ways communication-based distributed control for voltage regulation in smart distribution feeders," *IEEE Trans. Smart Grid*, vol. 3, no. 1, pp. 271–281, Mar. 2012.
[76] M. A. Azzouz, H. E. Farag, and E. F. El-Saadany, "Fuzzy-based control of on-load tap changers under high penetration of distributed generators," in *2013 3rd International Conference on Electric Power and Energy Conversion Systems (EPECS)*, 2013, pp. 1–6.
[77] M. A. Azzouz, H. E. Farag, and E. F. El-Saadany, "Real-time fuzzy voltage regulation for distribution networks incorporating high penetration of renewable sources," *IEEE Syst. J.*, vol. PP, no. 99, pp. 1–10, 2014.
[78] A. Bidram, A. Davoudi, and F. L. Lewis, "A multiobjective distributed control framework for islanded ac microgrids," *IEEE Trans. Ind. Inform.*, vol. 10, no. 3, pp. 1785–1798, Aug. 2014.
[79] J. M. Guerrero, L. Garcia De Vicuna, J. Matas, M. Castilla, and J. Miret, "A wireless controller to enhance dynamic performance of parallel inverters in distributed generation systems," *IEEE Trans. Power Electron.*, vol. 19, no. 5, pp. 1205–1213, Sep. 2004.
[80] J. M. Guerrero, L. Garcia De Vicuna, J. Matas, M. Castilla, and J. Miret, "Output impedance design of parallel-connected ups inverters with wireless load-sharing control," *IEEE Trans. Ind. Electron.*, vol. 52, no. 4, pp. 1126–1135, Aug. 2005.

[81] Y. A.-R. I. Mohamed and E. F. El-Saadany, "Adaptive decentralized droop controller to preserve power sharing stability of paralleled inverters in distributed generation microgrids," *IEEE Trans. Power Electron.*, vol. 23, no. 6, pp. 2806–2816, Nov. 2008.
[82] Y. W. Li and C.-N. Kao, "An accurate power control strategy for power-electronics-interfaced distributed generation units operating in a low-voltage multibus microgrid," *IEEE Trans. Power Electron.*, vol. 24, no. 12, pp. 2977–2988, Dec. 2009.
[83] A. R. Salehinia, M. R. Haghifam, and M. Shahabi, "Volt/Var control in a microgrid with consideration of uncertainty of generation in both grid-connected and islanded modes of operation," in *Integration of Renewables into the Distribution Grid, CIRED 2012 Workshop*, 2012, pp. 1–4.
[84] J. M. Guerrero, L. Hang, and J. Uceda, "Control of distributed uninterruptible power supply systems," *IEEE Trans. Ind. Electron.*, vol. 55, no. 8, pp. 2845–2859, Aug. 2008.
[85] A. Tuladhar, H. Jin, T. Unger, and K. Mauch, "Control of parallel inverters in distributed AC power systems with consideration of line impedance effect," *IEEE Trans. Ind. Appl.*, vol. 36, no. 1, pp. 131–138, Jan. 2000.
[86] J. He and Y. W. Li, "An enhanced microgrid load demand sharing strategy," *IEEE Trans. Power Electron.*, vol. 27, no. 9, pp. 3984–3995, Sep. 2012.
[87] M. Savaghebi, A. Jalilian, J. C. Vasquez, and J. M. Guerrero, "Secondary control scheme for voltage unbalance compensation in an islanded droop-controlled microgrid," *IEEE Trans. Smart Grid*, vol. 3, no. 2, pp. 797–807, Jun. 2012.
[88] H. Han, Y. Liu, Y. Sun, M. Su, and J. M. Guerrero, "An improved droop control strategy for reactive power sharing in islanded microgrid," *IEEE Trans. Power Electron.*, vol. 30, no. 6, pp. 3133–3141, Jun. 2015.
[89] M. Tahir and S. K. Mazumder, "Self-triggered communication enabled control of distributed generation in microgrids," *IEEE Trans. Ind. Inform.*, vol. 11, no. 2, pp. 441–449, Apr. 2015.
[90] J. W. Simpson-Porco, Q. Shafiee, F. Dorfler, J. C. Vasquez, J. M. Guerrero, and F. Bullo, "Secondary frequency and voltage control of islanded microgrids via distributed averaging," *IEEE Trans. Ind. Electron.*, vol. 62, no. 11, pp. 7025–7038, Nov. 2015.
[91] J.-H. Teng, "A direct approach for distribution system load flow solutions," *IEEE Trans. Power Deliv.*, vol. 18, no. 3, pp. 882–887, Jul. 2003.
[92] H. H. Zeineldin and J. L. Kirtley, "Islanding operation of inverter based Distributed Generation with static load models," in *2008 IEEE Power and*

Energy Society General Meeting - Conversion and Delivery of Electrical Energy in the 21st Century, 2008, pp. 1–6.
[93] D. Singh, R. K. Misra, and D. Singh, "effect of load models in distributed generation planning," *IEEE Trans. Power Syst.*, vol. 22, no. 4, pp. 2204–2212, Nov. 2007.
[94] M. M. A. Abdelaziz, "Effect of detailed reactive power limit modeling on islanded microgrid power flow analysis," *IEEE Trans. Power Syst.*, vol. 31, no. 2, pp. 1665–1666, Mar. 2016.
[95] S. A. Arefifar, Y. A. R. I. Mohamed, and T. El-Fouly, "Optimized multiple microgrid-based clustering of active distribution systems considering communication and control requirements," *IEEE Trans. Ind. Electron.*, vol. 62, no. 2, pp. 711–723, Feb. 2015.
[96] T. Luo, M. J. Dolan, E. M. Davidson, and G. W. Ault, "Assessment of a new constraint satisfaction-based hybrid distributed control technique for power flow management in distribution networks with generation and demand response," *IEEE Trans. Smart Grid*, vol. 6, no. 1, pp. 271–278, Jan. 2015.
[97] M. Yokoo, E. H. Durfee, T. Ishida, and K. Kuwabara, "The distributed constraint satisfaction problem: formalization and algorithms," *IEEE Trans. Knowl. Data Eng.*, vol. 10, no. 5, pp. 673–685, Sep. 1998.
[98] A. Meisels, *Distributed Search by Constrained Agents*. London: Springer London, 2008.
[99] Y. Deng, Y. He, and B. Zhang, "A branch-estimation-based state estimation method for radial distribution systems," *IEEE Trans. Power Deliv.*, vol. 17, no. 4, pp. 1057–1062, Oct. 2002.
[100] W. Zhang and V. Sorge, *Distributed Constraint Problem Solving and Reasoning in Multi-agent Systems*. IOS Press, 2004.
[101] N. A. Lynch, "Distributed Algorithms - Nancy A. Lynch - Google Books." .
[102] M. Yokoo and K. Hirayama, "Distributed constraint satisfaction algorithm for complex local problems." in *International Conference on Multi Agent Systems, 1998. Proceedings*, pp. 372–379, 1998.
[103] P. J. Modi, W.-M. Shen, M. Tambe, and M. Yokoo, "An asynchronous complete method for distributed constraint optimization," in *In AAMAS*, 2003, pp. 161–168.
[104] S. A. Arefifar and Y. A. R. I. Mohamed, "DG mix, reactive sources and energy storage units for optimizing microgrid reliability and supply security," *IEEE Trans. Smart Grid*, vol. 5, no. 4, pp. 1835–1844, Jul. 2014.
[105] M. E. Nassar and M. M. A. Salama, "Adaptive self-adequate microgrids using dynamic boundaries," *IEEE Trans. Smart Grid*, vol. 7, no. 1, pp. 105–113, Jan. 2016.

[106] “Load Profiles.” [Online]. Available: https://www.aepohio.com/account/service/choice/cres/LoadProfiles.aspx. [Accessed: 10-May-2016].
[107] “Distribution Test Feeders - Distribution Test Feeder Working Group - IEEE PES Distribution System Analysis Subcommittee.” [Online]. Available: https://ewh.ieee.org/soc/pes/dsacom/testfeeders/. [Accessed: 07-Jun-2016].

APPENDIX

A.1 The 33-bus distribution test system data [93]

Table A-1 33-bus distribution system data

From	To	Line Impedance in per unit	Loads at To-node	
			Active power	Reactive power
1	2	0.000574+0.000293j	0.1	0.06
2	3	0.00307+0.001564j	0.09	0.04
3	4	0.002279+0.001161j	0.12	0.08
4	5	0.002373+0.001209j	0.06	0.03
5	6	0.0051+0.004402j	0.06	0.02
6	7	0.001166+0.003853j	0.2	0.1
7	8	0.00443+0.001464j	0.2	0.1
8	9	0.006413+0.004608j	0.06	0.02
9	10	0.006501+0.004608j	0.06	0.02
10	11	0.001224+0.000405j	0.045	0.03
11	12	0.002331+0.000771j	0.06	0.035
12	13	0.009141+0.007192j	0.06	0.035
13	14	0.003372+0.004439j	0.12	0.08
14	15	0.00368+0.003275j	0.06	0.01
15	16	0.004647+0.003394j	0.06	0.02
16	17	0.008026+0.010716j	0.06	0.02
17	18	0.004558+0.003574j	0.09	0.04
2	19	0.001021+0.000974j	0.09	0.04
19	20	0.009366+0.00844j	0.09	0.04
20	21	0.00255+0.002979j	0.09	0.04
21	22	0.004414+0.005836j	0.09	0.04
3	23	0.002809+0.00192j	0.09	0.05
23	24	0.005592+0.004415j	0.42	0.2
24	25	0.005579+0.004366j	0.42	0.2
6	26	0.001264+0.000644j	0.06	0.025
26	27	0.00177+0.000901j	0.06	0.025
27	28	0.006594+0.005814j	0.06	0.02
28	29	0.005007+0.004362j	0.12	0.07
29	30	0.00316+0.00161j	0.2	0.6
30	31	0.006067+0.005996j	0.15	0.07
31	32	0.001933+0.002253j	0.21	0.1
32	33	0.002123+0.003301j	0.06	0.04

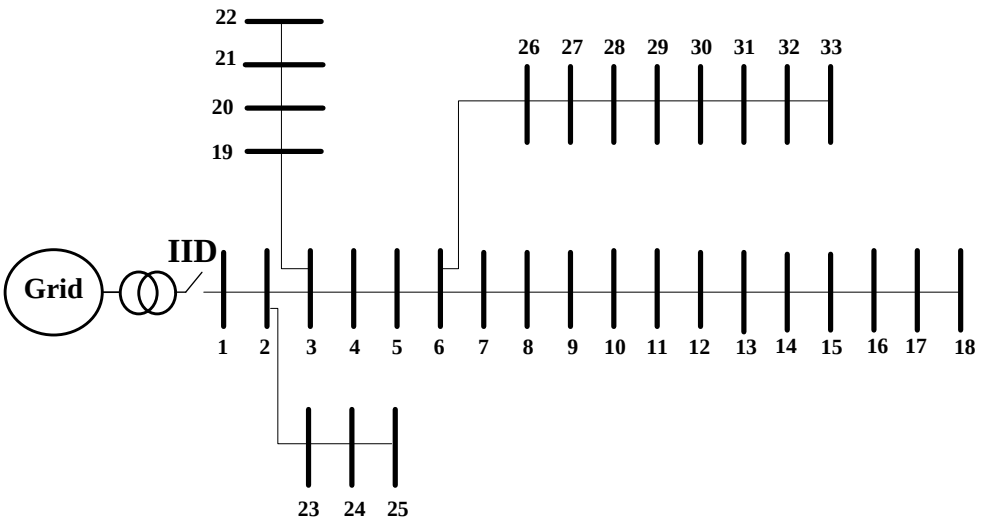

Figure A.1 The 33-bus distribution test system

A.2 The unbalanced three phase 34-bus distribution test system data [107]

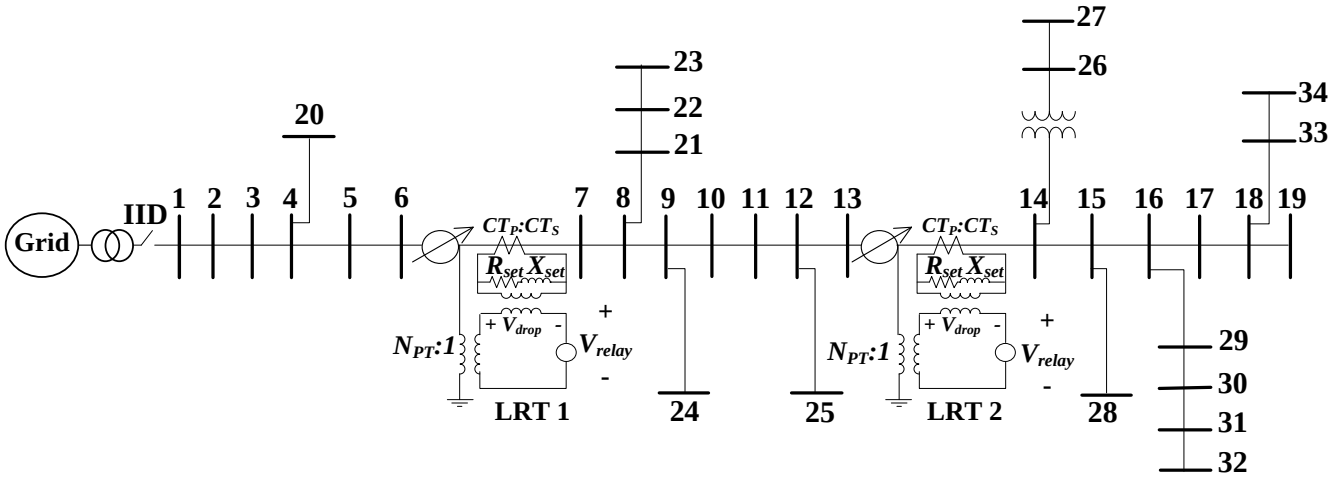

Figure A.2 The unbalanced 34-bus distribution test system

Table A-2 The unbalanced IEEE 34-bus distribution test system distributed load data and feeder lengths

Distributed Loads										
From Bus	*To* Bus	*Load* Model	*Ph-(a)* kW	*Ph-(a)* kVAr	*Ph-(b)* kW	*Ph-(b)* kVAr	*Ph-(c)* kW	*Ph-(c)* kVAr	*Length (ft.)*	*Impedance configuration*
800	802	-	0	0	0	0	0	0	2580	0
802	806	Y-PQ	0	0	30	15	25	14	1730	0
806	808	-	0	0	0	0	0	0	32230	0
808	810	Y-I	0	0	16	8	0	0	5804	3
808	812	-	0	0	0	0	0	0	37500	0
812	814	-	0	0	0	0	0	0	29730	0
814	850	-	0	0	0	0	0	0	10	1
816	818	-	0	0	0	0	0	0	1710	2
816	824	D-I	0	0	5	2	0	0	10210	1
818	820	Y-Z	34	17	0	0	0	0	48150	2
820	822	Y-PQ	135	70	0	0	0	0	13740	2
824	826	Y-I	0	0	40	20	0	0	3030	3
824	828	Y-PQ	0	0	0	0	4	2	840	1
828	830	Y-PQ	7	3	0	0	0	0	20440	1
830	854	-	0	0	0	0	0	0	520	1
832	858	D-Z	7	3	2	1	6	3	4900	1
832	888	-	0	0	0	0	0	0	0	-
834	860	D-Z	16	8	20	10	110	55	2020	1
834	842	-	0	0	0	0	0	0	280	1
836	840	D-I	18	9	22	11	0	0	860	1
836	862	-	0	0	0	0	0	0	280	1
842	844	Y-PQ	9	5	0	0	0	0	1350	1
844	846	Y-PQ	0	0	25	12	20	11	3640	1
846	848	Y-PQ	0	0	23	11	0	0	530	1
850	816	-	0	0	0	0	0	0	310	1
852	832	-	0	0	0	0	0	0	10	1
854	856	Y-PQ	0	0	4	2	0	0	23330	3
854	852	-	0	0	0	0	0	0	36830	1
858	864	Y-PQ	2	1	0	0	0	0	1620	2
858	834	D-PQ	4	2	15	8	13	7	5830	1
860	836	D-PQ	30	15	10	6	42	22	2680	1
862	838	Y-PQ	0	0	28	14	0	0	4860	4
888	890	-	0	0	0	0	0	0	10560	0
Total			262	133	240	120	220	114		

Table A-3 The unbalanced IEEE 34-bus distribution test system spot load data

Bus	Load Model	*Ph-(a)* kW	*Ph-(a)* kVAr	*Ph-(b)* kW	*Ph-(b)* kVAr	*Ph-(b)* kW	*Ph-(c)* kVAr
860	Y-PQ	20	16	20	16	20	16
840	Y-I	9	7	9	7	9	7
844	Y-Z	135	105	135	105	135	105
848	D-PQ	20	16	20	16	20	16
890	D-I	150	75	150	75	150	75
830	D-Z	10	5	10	5	25	10
Total		344	224	344	224	359	229

Table A-4 The unbalanced IEEE 34-bus distribution test system impedance (p.u.)

Impedance Configuration #	R_{aa}	X_{aa}	R_{ab}	X_{ab}	R_{ac}	X_{ac}	R_{bb}	X_{bb}	R_{bc}	X_{bc}	R_{cc}	X_{cc}
0	1.3368	1.3343	0.2101	0.5779	0.2130	0.5015	1.3238	1.3569	0.2066	0.4591	1.3294	1.3471
1	1.93	1.4115	0.2327	0.6442	0.2359	0.5691	1.9157	1.4281	0.2288	0.5238	1.9219	1.4209
2	2.7995	1.4855	0	0	0	0	0	0	0	0	0	0
3	0	0	0	0	0	0	2.7995	1.4855	0	0	0	0

Table A-5 The IEEE 34-bus distribution test system LRTs settings and location

ID	*Line Segment*	*Location*	*PT Ratio*	*CT Rating*	*Band-width*	*Ph-(a) Settings*			*Ph-(b) Settings*			*Ph-(c) Settings*		
						R_{set}	X_{set}	*Voltage level*	R_{set}	X_{set}	*Voltage level*	R_{set}	X_{set}	*Voltage level*
LRT 1	814-850	814	120	100	2 *volt*	2.7	1.6	122	2.7	1.6	122	2.7	1.6	122
LRT 2	852-832	852	120	100	2 *volt*	2.5	1.5	124	2.5	1.5	124	2.5	1.5	124